AFRPL-TR-70-62

APPLICATION OF FRACTURE MECHANICS TO PREDICTING FAILURES IN SOLID PROPELLANTS

(Final Report)

J. D. Burton

B. C. Harbert

TECHNICAL REPORT AFRPL-TR-70-62

May 1970

AIR FORCE ROCKET PROPULSION LABORATORY

AIR FORCE SYSTEMS COMMAND

EDWARDS AIR FORCE BASE, CALIFORNIA

Rocketdyne
North American Rockwell
SOLID ROCKET DIVISION
P.O. Box 548
McGregor, Texas 76657

AFRPL-TR-70-62

APPLICATION OF FRACTURE MECHANICS TO PREDICTING FAILURES IN SOLID PROPELLANTS

(Final Report)

J. D. Burton

B. C. Harbert

TECHNICAL REPORT AFRPL-TR-70-62

May 1970

AIR FORCE ROCKET PROPULSION LABORATORY

AIR FORCE SYSTEMS COMMAND

EDWARDS AIR FORCE BASE, CALIFORNIA

Rocketdyne
North American Rockwell

SOLID ROCKET DIVISION
P O Box 548
McGregor, Texas 76657

FOREWORD

This report documents the effort accomplished at Rocketdyne under Contract No. F04611-69-C-0035 for the period 1 January 1969 to 27 February 1970. The report carries the contractor's library serial number R-4608. The program was sponsored by the Air Force Rocket Propulsion Laboratory, Air Force Systems Command, United States Air Force, Edwards, California. Air Force Project Engineers were Mr. Donald Saylak and Captain Scott Beckwith.

This technical report has been reviewed and is approved.

Donald Saylak (RPMCB)
Project Engineer

ABSTRACT

This report documents a 14-month program conducted at Rocketdyne, Solid Rocket Division, to study the parameters of crack growth in viscoelastic materials. Tests conducted on Solithane and on a filled propellant are described, and results of the experimental effort are presented. Analysis of data through the concepts of viscoelastic fracture mechanics is discussed. The behavior of cracks in solid rocket motor geometries and of propellant/liner unbonds was monitored in unique test situations. Basic analytic concepts were compared with test data and found to show promise of applicability. Recommendations for expansion of this study are presented.

ACKNOWLEDGEMENTS

Many people contributed to this effort. Special gratitude is expressed by the authors for the assistance and contributions of Mr. Don Saylak and Captain Scott Beckwith, the AFRPL project engineers for this program; of Mr. C. E. Bryant, Rocketdyne Program Manager; of Drs. J. S. Noel, W. B. Jones, and M. L. Williams, who served as technical consultants; of Mr. H. T. Faria, who assisted in the experimental effort; of Mrs. T. Y. Park, who assisted in the computer analysis; and of Mmes. M. C. Raper, J. A. Symank, and S. S. Brewton, who edited and typed this report.

CONTENTS

CONTENTS
(Continued)

FIGURES

FIGURES

(Continued)

FIGURES

(Continued)

TABLES

SECTION 1, INTRODUCTION AND SUMMARY

This report describes the experimental work, the analytical calculations, and the resulting conclusions of that portion of the Fracture Mechanics Program conducted at Rocketdyne, Solid Rocket Division. The program was sponsored and directed by the Air Force Rocket Propulsion Laboratory, Edwards Air Force Base, on Contract F04611-69-C-0035.

The need to incorporate the concepts of fracture mechanics in the evaluation of solid propellant rocket motor grain structural integrity under service life conditions becomes more urgent as requirements for motor performance and reliability are advanced. The approach, based on a balance of energy in the propellant grain, is applicable to both cohesive failure analysis (grain cracking) and adhesive failure studies (grain/liner or liner/case unbonding). Failures may be induced by thermal cycling, vibration and acceleration, and ignition pressurization or by combinations of these loadings. Since the grain is normally restrained against the stiff case, tensile loads induced by thermal cycling of the motor and those resulting from different coefficients of thermal expansion for the grain, liner, and case are often the loads responsible for grain failures.

Structural integrity assessments are currently based on failure initiation. Predictions are based on elastic or, at best, quasi-viscoelastic analyses, and a maximum principal strain failure criterion is applied to the grain cracking evaluation. The bond-line failure problem is usually treated with a maximum principal stress criterion. In either case, initiation of a flaw is the limit of consideration; but the effect of a small flaw on motor performance cannot be predicted by conventional analyses.

Fracture mechanics appears to be a greatly improved technique for structural analysis. Determination of flaw initiation may still result from a strain or stress criterion, but energy balance offers a means of predicting the rate at which a flaw will grow and the path it is likely to take under a given motor loading. With this capability, it becomes possible to determine whether or not a flaw will occur, where it is likely to occur, and how it will propagate if it does occur. The ultimate goal is to prevent ignition of a motor which might have excessive burning surface due to cracking or have a short flame path to the case wall causing premature case burnthrough. This program represents a step in developing the tools required to make the necessary structural analysis to accomplish this goal.

The main objective of the program was to advance current understanding of solid rocket grain fracture. Specific task objectives included the development and application of experimental and analytical techniques to account for loadings, material characteristics, environments, and stress rates encountered in realistic solid rocket motor designs and to predict the propagation of fractures and separations in these motors. Within the framework of these goals, experimental effort was emphasized

through the development of a test to permit analog studies of propellant grain cross-sectional geometries. Exploratory investigations to develop a test for successfully evaluating the bond strength of propellant/liner systems were also conducted. Analytical effort centered on the analysis of data generated during the experimental phase. The approach to evaluating crack initiation and growth was based on the concept of balancing energy in the specimen (or motor). Total energy input at the boundary is weighed against that stored elastically in the specimen, that dissipated through viscous flow (in viscoelastic material), and that released through the creation of additional surface (by crack growth). The analytical theory used and the experimental program are summarized in the following paragraphs.

PROGRAM ADMINISTRATION

The Fracture Mechanics Program sponsored by AFRPL was originally intended to be a 12-month technical effort culminating in a final report issued in the fourteenth month. Delays in processing specimens resulted in a 2-month program extension with the final report draft being issued 1 month following as indicated in the summary schedule below.

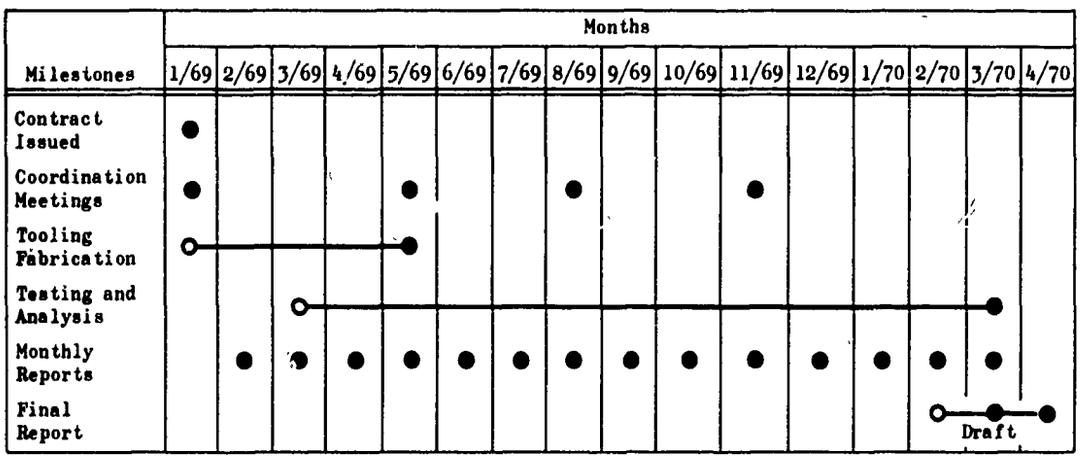

Amended Fracture Mechanics Program Summary Schedule

Associate contractors (Thiokol Chemical, Wasatch; and UTC, Sunnyvale) and the AFRPL monitors, Mr. Don Saylak and Captain Scott Beckwith, maintained close contact throughout the program via monthly reports, on-site visits, and regular coordination meetings (as indicated on the schedule summary). Technical presentations at these meetings formed the basis for discussion and evaluation of program progress and led to appropriate redirection of efforts where such redirection enhanced the value of the experimental data or the analytical effort.

The analysis relied, in part, on a finite element computer code obtained from Thiokol Chemical Corp., Wasatch Division. This computer code

was adapted to the IBM 360/65 computer available to Rocketdyne and was used in computing energy changes in the blister peel and disc specimens. Thiokol's computer code was not modified nor were any new computer codes generated at Rocketdyne on the Fracture Mechanics Program.

Basic test data in their original and reduced form are to be retained at Rocketdyne, Solid Rocket Division, for at least 2 years and will be available for further study as required by follow-on or related efforts.

SUMMARY OF THEORY

The essence of the theory of fracture as originally demonstrated by A. A. Griffith (Ref. 1) and extended to linear viscoelastic materials by M. L. Williams (Ref. 2 and 3) is in the concept of a balance of energy. In particular, the rate of release of stored energy is compared to the energy used as new surface is created in the body. The criterion for flaw growth in an elastic material is expressed mathematically by

$$\frac{d}{dA}(V + A\gamma) = 0 \tag{1}$$

where V is the potential energy of the system, A the free surface area, and γ the surface energy per unit of new surface area. For the elementary case of an infinite, thin elastic sheet subject to uniform constant tension, σ, and with a crack of length 2c, Eq. 1 becomes

$$\frac{d}{dc}\left(-\frac{\sigma^2 \pi c^2}{E} + 4\gamma c\right) = 0 \tag{2}$$

Performing the indicated derivation,

$$\frac{2\sigma^2 \pi c}{E} = 4\gamma \tag{3}$$

becomes the basis for determining the critical stress, σ_{cr}, as a function of the half-crack length, c.

$$\sigma_{cr} = \sqrt{\frac{2E\gamma}{\pi c}} \tag{4}$$

Equation 2 is better understood by schematically plotting the two individual terms as in Fig. 1. The regions in which, for a given applied stress σ, the crack will or will not become unstable are indicated. This approach to failure analysis circumvents the problem encountered with the conventional local stress or strain criteria of failure--namely the presence of an infinity (singularity) in the magnitude of the calculated stress or strain at the tip of the crack.

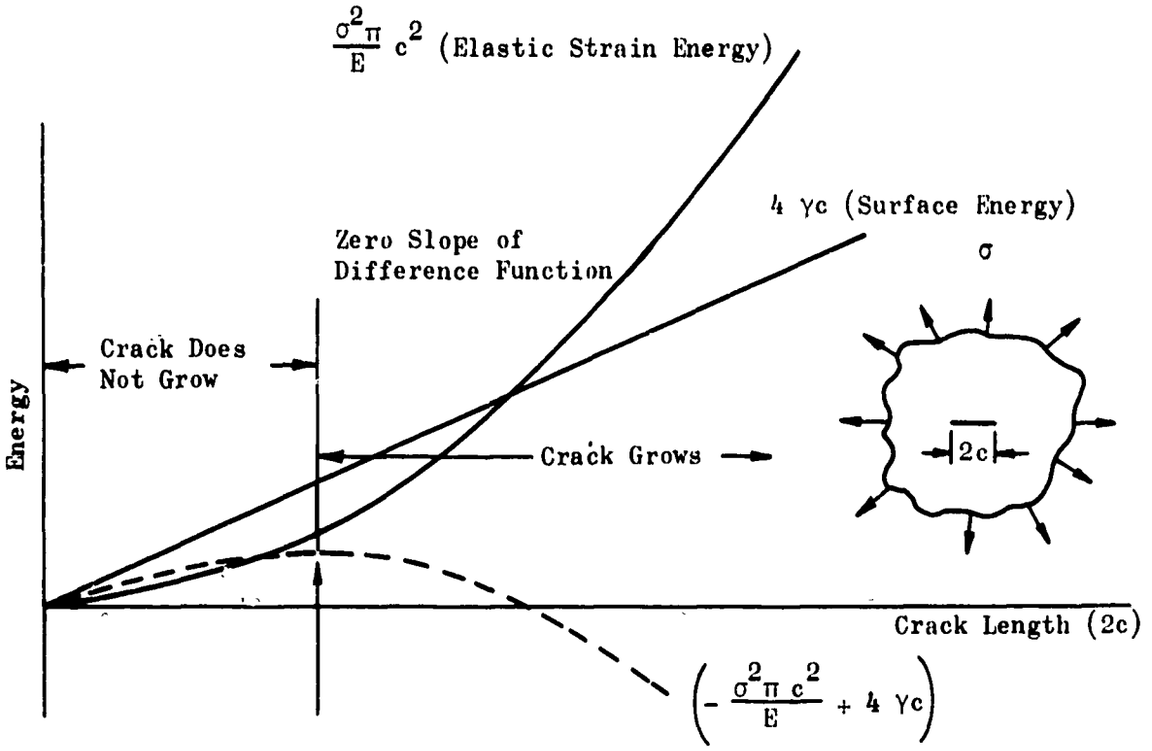

Figure 1. Energy Balance--Elastic Thin Sheet

The generalization of the energy balance concept to the prediction of crack type failures in viscoelastic materials is based on analysis of simplified flaw geometries. Because of the time-dependent nature of the material properties, a balance of the rate of change of energy (as opposed to energy) is required. As shown in Ref. 3 and 4, balance of the energy rate change (power) leads to identical criticality criteria as those for elastic materials with the exception that the viscoelastic properties replace the constant Young's modulus. The basic equations of criticality for several useful geometries and loading histories are given in Ref. 5.

Beyond initiation of failure, that is, when the flaw itself interferes with the overall stress field, the simplifications in the analysis discussed above limit the adequacy of that analysis. O. L. Bowie has addressed a geometric problem of practical interest to rocket motor analysts in Ref. 6 by developing equations of criticality for the problem of radial cracks originating at the boundary of an internal circular hole. For general cases of specimen and flaw geometries, elastic analysis is available in the form of finite element computer techniques (Ref. 7) combined with energy computations (Ref. 8). Utilizing these approaches, the effects of loading history and specimen geometry may be evaluated, correlated with experiment, and extended to analysis of the initiation and growth of propellant grain cracks and propellant/liner debonds.

SUMMARY OF THE TESTING

The experimental effort deals with the development of test techniques which, when applied to Solithane and to propellant materials, can be used to evaluate the theoretical concepts of fracture mechanics applied to viscoelastic materials. A compendium of the test conditions and specimen characteristics is presented in Table I. Propellant for these experiments was furnished by Thiokol Chemical Corporation, Wasatch Division, Brigham City, Utah. The Solithane was cast by the United Technology Corporation, Sunnyvale, California. These companies participated in the overall Fracture Mechanics Program and are directly involved in analytical effort corollary to the experimental testing.

TABLE I

SUMMARY OF EXPERIMENTAL EFFORT

SOLITHANE (50/50)

Radial Planar Loading (RPL) Disc Test - All at 77 F	
3	Circular Port - As Cast - Constant Displacement Rate to Failure-Initiation, Rate, Trajectory
3	Star Port - As Cast - Constant Displacement Rate to Failure Initiation, Rate, Trajectory
3	Circular Port - Constant Displacement - Induced Crack - Crack Rate
3	Star Port - Constant Displacement - Induced Crack - Crack Rate
1	Circular Part - Photoelastic Isoclinic Survey
1	Star Port - Photoelastic Isoclinic Survey
TPH-1011 PROPELLANT	
Biaxial Strip	
9	As-Cast Specimens - 1 Rate - 3 Temp (20 F, 77 F, 140 F) Relaxation Modulus, Cohesive Characteristic Energy Release Rate, γ_c
9	Milled Specimens - 1 Rate - 3 Temp (20 F, 77 F, 140 F), Relaxation Modulus, Ultimate Tensile Properties
Blister Peel - All at 77 F	
10	Propellant/Liner/Steel Specimens - Varied Pressurization Rates - Adhesive Characteristic Energy Release Rate, γ_a
RPL Disc Test - All at 77 F - All loaded at ~ Constant Displacement Rate	
16	Test total - 6 had Bond Failure - 2 Additional Loss of Data Acquisition During Test
2	Low Web Circular Port - As Cast - Crack Initiation, Rate, Trajectory
2	Star Port - As Cast - Crack Initiation, Rate, Trajectory
3	Low Web Circular Port - Precracked - Crack Growth Initiation, Rate
1	Star Port - Precracked - Crack Growth Initiation, Rate

The tests fall into two regimes: first, those dealing with the adhesive fracture between propellant and liner and, second, those dealing with cohesive failure (cracking) in the propellant (or Solithane) material itself. Variations in imposed loadings were restricted to relatively narrow ranges since major emphasis was on evaluation of the test itself. Nonetheless, practical loadings were applied, and the resulting data are of interest in the assessment of the features of viscoelastic fracture mechanics techniques.

The blister peel test was studied to establish the characteristics of debond growth at the propellant-liner interface. The blister test was used because of some indicated advantages over the more conventional peel tests described in the ICRPG Solid Propellant Mechanical Behavior Manual. These conventional tests--90^0 peel, "Brouser's leg" or joint peel and non-instrumented poker chip--present technical difficulties for evaluating the rate of change in energy with growth in unbond area. The problems include modeling of the imposed boundary and monitoring of the unbond growth. Similitude of local stress-state with that found in a motor is closely observed in the blister test. By maintaining a simplified geometry, it is feasible to compute the stored energy in the body. The test method requires a minimum of equipment, and the results are directly related to motor unbond growth. A three-layer specimen (Fig. 2)--steel base, liner material interface, and propellant body--is

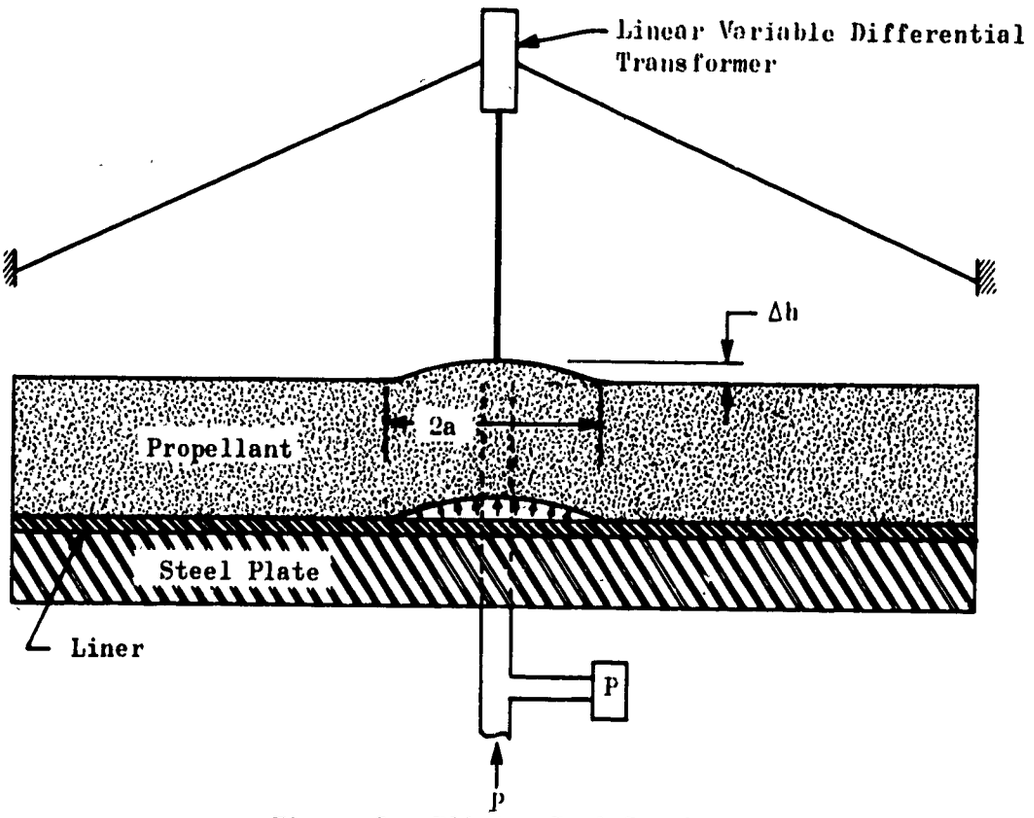

Figure 2. Blister Peel Specimen

tested by pressurizing the cavity formed at the initial unbond between the propellant and liner (Ref. 9). The pressure in the cavity rises as a $P_f(1-e^{-kt})$ function; and for times such that P is about 20% of P_f, this function is nearly linear. If the cavity begins to grow (through debonding) the k coefficient changes, resulting in a new slope for the cavity pressure-time trace. This shift is readily observed in most instances. Several tests are obtainable on a single specimen, and post-test examination shows the initial unbond area for each test in the sequence. The data thus collected are reduced to give the characteristic energy release rate for adhesion, γ_a, for the propellant/liner interface.

Cohesive failure was investigated using a device specially developed to simulate uniform two-dimensional tension in a thin sheet. The loading boundary in this test is analogous to that found in a case-bonded propellant grain undergoing thermal cycling. The test apparatus, labeled the Radial Planar Loading (RPL) device, was evolved from a bicycle wheel concept. The essentially rigid rim provides a base for inducing tension in the spokes. By uniformly tightening the spokes a state of nearly axisymmetric tension is induced at the hub. The load is distributed more uniformly when the hub is replaced by a less rigid ring. Thus, the RPL device consists of 18 radial arms which, by virtue of their stiffness, provide a rigid displacement to a rubber collar which has the thin disc specimen bonded inside (Fig. 3). For the tests on this program, the collar was displaced at a rate intended to be linear with time until flaw growth occurred. In some of the Solithane tests, the displacement was held constant, a flaw induced, and the flaw growth recorded.

Photographic records of the RPL tests are an integral part of the data. These provide the displacement measurements and crack length data. A separate analog record of the time each photograph was taken and load measured in 9 of the 18 arms completes the data package. Supporting data for analysis of the disc response comes from characterization of the disc material to give tensile relaxation modulus, $E_{rel}\ (t/a_T)$, and characteristic energy release rate for cohesion, γ_c. Results of the tests may then be compared with those predicted analytically to provide the basis for evaluating the analysis. Specimens of propellant and Solithane with both circular and star geometry ports were used for these tests.

The tests, test results, theory used in the analysis, and the comparison of test results with analysis, are discussed in the following sections. Conclusions drawn from this study concerning the significance of the test techniques explored and the adequacy of the analytical techniques applied are also discussed. Recommendations for exploitation of the results of this program are given.

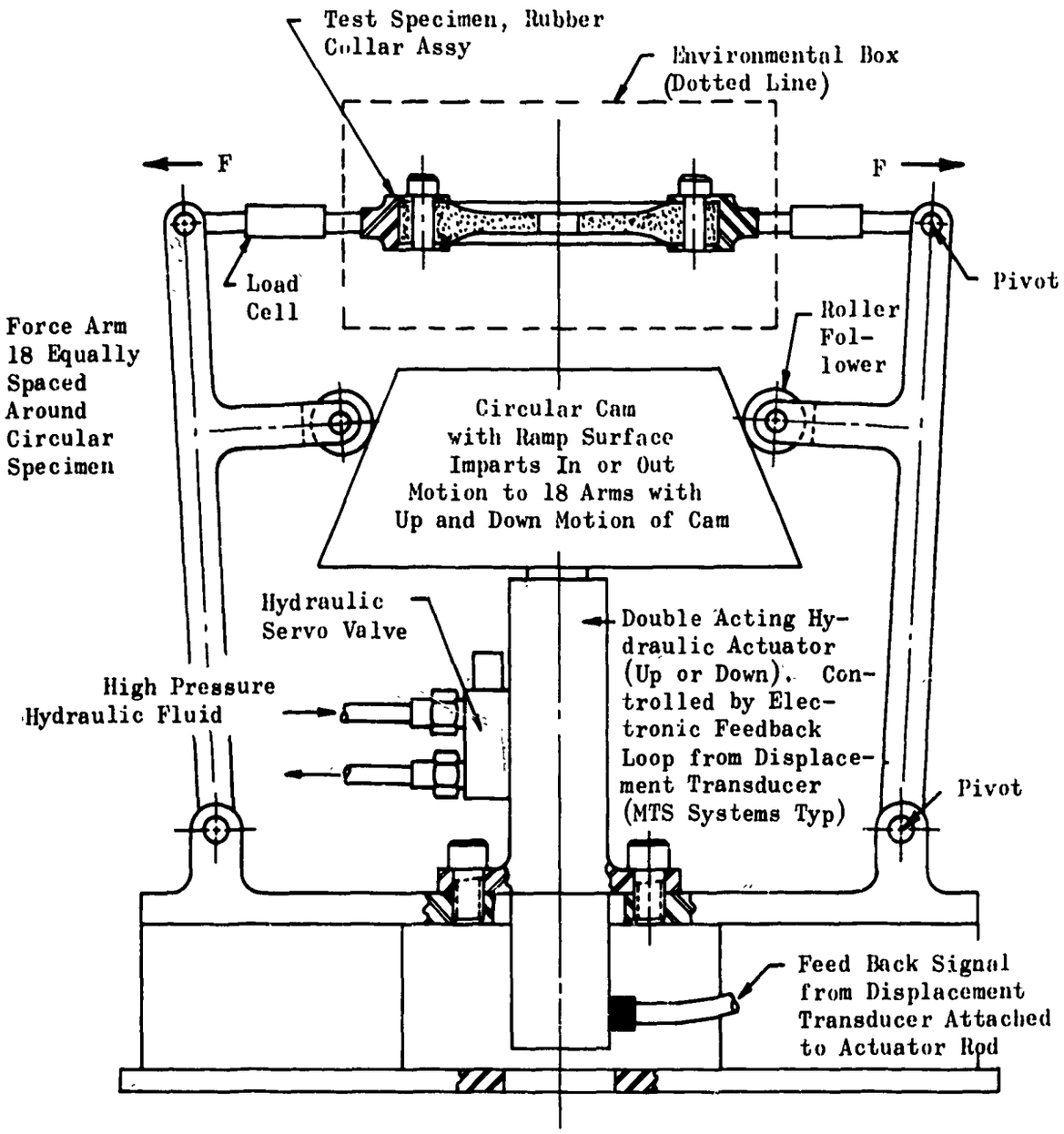

Figure 3. Radial Planar Loading Device

SECTION II, A BRIEF REVIEW OF THE THEORY OF FRACTURE MECHANICS AS APPLIED TO VISCOELASTIC MATERIALS

The history of the development of fracture mechanics concepts for brittle elastic materials; the application of those concepts to metals, rubbers, and finally viscoelastic materials; and studies of the feasibility of applying fracture mechanics to solid propellant rocket motor structural analysis is well documented (Ref. 5 and 10--13). Following the qualitative idea of the Griffith critical stress formulation, extended to account for various dissipative mechanisms, the critical stress is written as

$$\sigma_{cr} = k \sqrt{\frac{f(E)}{2c} (\gamma_b + \gamma_d + \gamma_v + \cdots)} \tag{5}$$

where k is a geometric constant; 2c, the crack length; f(E), the material property (modulus function); subscripts b, v, and d, the components of brittle, ductile, and viscoelastic dissipative mechanisms, respectively. For subsequent discussion of the viscoelastic fracture response in the disc and blister peel specimens, it is pertinent to examine Eq. 5 for the geometries and the materials tested.

GRIFFITH FRACTURE IN LINEAR VISCOELASTIC MATERIAL

A significant contribution was offered by Williams (Ref. 3) when he found, for certain simple cases, that a condition for criticality of a loaded viscoelastic body analogous to that for an elastic body existed. The difference in the two results was contained in the representation of the material property so that direct substitution of the proper relaxation modulus for Young's modulus in the elastic solution sufficed. This work was extended (Ref. 5) to include several geometries and boundary conditions. Of particular interest to the present study is the criticality for a cylindrical flaw in a plane stress body subject to uniform displacement, u(b,t), at the outer boundary, b, Fig. 4. We must first balance the power input-output:

$$\dot{I} = \dot{F} + 2\dot{D} + \dot{S}\dot{E} \tag{6}$$

where $\dot{I}$, the power input resulting from the boundary displacement is given by

$$\dot{I} = \sum_{S_e}^{\nu} T_i \dot{u}_i \tag{7}$$

or more specifically

$$\dot{I} = 2\pi b \sigma_r (b,t) \dot{u} (b,t) \tag{8}$$

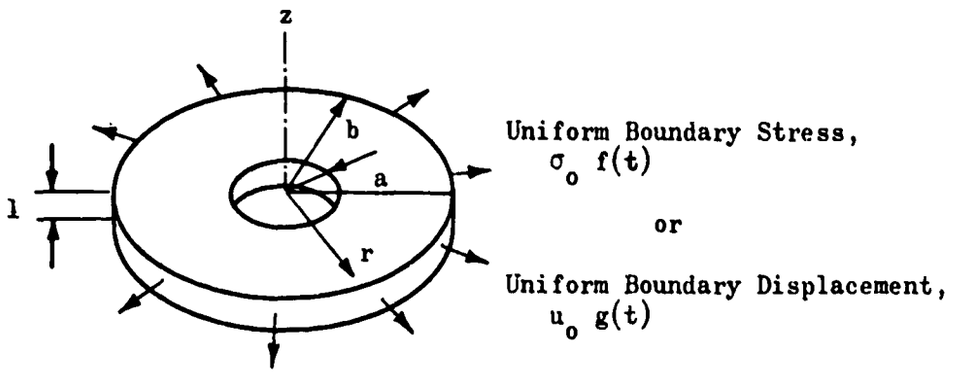

Figure 4. Plane Stress Cylindrical Flaw Model

This approach is referred to as a global energy approach inasmuch as the energy in the entire body is considered. An alternate approach giving similar results is the local energy method in which only the energy change in the vicinity of the flaw is considered.

The rate of change of surface energy, $\dot{SE}$, is

$$\dot{SE} = \frac{\partial}{\partial t} \int_S \gamma \, dS \tag{9}$$

where γ is the characteristic energy release rate at the increasing crack surface S. For our case,

$$\dot{SE} = \frac{\partial}{\partial t} \left[2\pi \, a(t) \, \gamma \right] \tag{10}$$

Finally, the combined term, $\dot{F} + 2D$, representing the rate of change of stored (strain) energy and the viscous dissipation, is given by

$$\dot{F} + 2D = \frac{\partial}{\partial t} \int_{vol} \int_o^t \sigma_i \, \dot{\epsilon}_i \, dt \, dV \tag{11}$$

Or, again for the plane stress body with a cylindrical flaw

$$\dot{F} + 2D = \frac{\partial}{\partial t} \int_{a(t)}^b \int_o^t 2\pi \, Q \, r \, dt \, dr \tag{12}$$

where Q is defined as

$$Q = \sigma_r \dot{\epsilon}_r + \sigma_\theta \dot{\epsilon}_\theta + \sigma_z \dot{\epsilon}_z \tag{13}$$

For a plane stress body subjected to uniform displacement at the outer boundary one finds (see e.g., Ref. 14) for an incompressible elastic material the displacements and strains

$$u(r,t) = u(b,t)\left(\frac{b}{r}\right)\left(\frac{r^2 + 3a^2}{b^2 + 3a^2}\right) \tag{14}$$

$$\varepsilon_r(r,t) = \frac{\partial u}{\partial r} = u(b,t)\left(\frac{b}{r^2}\right)\left(\frac{r^2 - 3a^2}{b^2 + 3a^2}\right) \tag{15}$$

$$\varepsilon_\theta(r,t) = \frac{u}{r} = u(b,t)\left(\frac{b}{r^2}\right)\left(\frac{r^2 + 3a^2}{b^2 + 3a^2}\right) \tag{16}$$

and the stresses

$$\sigma_r(r,t) = 2u(b,t)\,E\left(\frac{b}{r^2}\right)\left(\frac{r^2 - a^2}{b^2 + 3a^2}\right) \tag{17}$$

$$\sigma_\theta(r,t) = 2u(b,t)\,E\left(\frac{b}{r^2}\right)\left(\frac{r^2 + a^2}{b^2 + 3a^2}\right) \tag{18}$$

Using the elastic-viscoelastic transform analogy (Ref. 15), the inversion technique proposed by Schapery (Ref. 16), and combining the above equations we obtain Eq. 19 and 20, shown on the following page.

$$\dot{F} + 2D = 4\pi \left\{ (b^2 - a^2)\, \dot{S}(t) \left[S(t)\, E_g + \int_0^t \frac{\partial E(t-\tau)}{\partial (t-\tau)}\, S(\tau)\, d\tau \right] \right.$$

$$+ \frac{1}{3}\left(\frac{1}{a^2}\right) \dot{P}(t) \left[P(t)\, E_g + \int_0^t \frac{\partial E(t-\tau)}{\partial (t-\tau)}\, P(\tau)\, d\tau \right]$$

$$- 2a\, \dot{a} \int_0^t \dot{S}\,(\xi) \left[S\,(\xi)\, E_g + \int_0^{\xi} \frac{\partial E(\xi-\tau)}{\partial (\xi-\tau)}\, S(\tau)\, d\tau \right] d\xi$$

$$\left. - \frac{2\dot{a}}{a^3} \int_0^t \dot{P}\,(\xi) \left[P(\xi)\, E_g + \int_0^{\xi} \frac{\partial E(\xi-\tau)}{\partial (\xi-\tau)}\, P(\tau) \right] d\xi \right\} \quad (19)$$

and

$$\dot{I} = 4\pi \left\{ (b^2 - a^2)\, \dot{S}(t) \left[S(t)\, E_g + \int_0^t \frac{\partial E(t-\tau)}{\partial (t-\tau)}\, S(\tau)\, d\tau \right] \right.$$

$$\left. + \frac{1}{3}\left(\frac{1}{a^2} - \frac{1}{b^2}\right) \dot{P}(t) \left[P(t)\, E_g + \int_0^{\xi} \frac{\partial E(t-\tau)}{\partial (t-\tau)}\, P(\tau)\, d\tau \right] \right\} \quad (20)$$

where

$$S(t) = -\frac{3}{2}\, u(b,t)\, \frac{a^2 b^2}{b^2 - a^2} \quad (21)$$

$$P(t) = \frac{1}{2}\, u(b,t)\, \frac{b^2}{b^2 - a^2} \quad (22)$$

and $E(t)$ refers to the relaxation modulus. Summing Eq. 10, 19, and 20 we obtain for the power balance

$$0 = \dot{a}\left\{\gamma - 4a \int_0^t \dot{S}(\xi)\left[S(\xi)\, E_g + \int_0^\xi \frac{\partial E(\xi-\tau)}{\partial(\xi-\tau)}\, S(\tau)\, d\tau\right] d\xi\right.$$

$$\left. - \frac{4}{3a^3} \int_0^t \dot{P}(\xi)\left[P(\xi)\, E_g + \int_0^\xi \frac{\partial E(\xi-\tau)}{\partial(\xi-\tau)}\, P(\tau)\, d\tau\right] d\xi\right\} \qquad (23)$$

Equation 23 is satisfied by $\dot{a} = 0$ or, for flaw growth $(\dot{a} > 0)$

$$\gamma - 4a \int_0^t \dot{S}(\xi)\left[S(\xi)\, E_g + \int_0^\xi \frac{\partial E(\xi-\tau)}{\partial(\xi-\tau)}\, S(\tau)\, d\tau\right] d\xi$$

$$- \frac{4}{3a^3} \int_0^t \dot{P}(\xi)\left[P(\xi)\, E_g + \int_0^\xi \frac{\partial E(\xi-\tau)}{\partial(\xi-\tau)}\, P(\tau)\, d\tau\right] d\xi = 0 \qquad (24)$$

For a constant displacement rate

$$u(b,t) = u_o t \qquad (25)$$

we obtain from Eq. 24

$$\gamma = 16 \frac{u_o^2\, a}{b^2\left(1 + 3\frac{a^2}{b^2}\right)^2}\left[\frac{2}{t_o^2} \int_0^{t_o} \int_0^\xi E(\tau)\, d\xi d\tau\right] \qquad (26)$$

the time to flaw growth initiation being t_o.

The preceding analysis is somewhat limited because of assumptions concerning specimen geometry and the nature of γ and the omission of kinetic energy. A word on each of these assumptions is pertinent. The limitation to a small plane stress cylindrical flaw establishes the nature of the criticality for this basic geometry. For more realistic geometries, a combination of the above solution with a non-demensionalized elastic computer analysis provides an analogous viscoelastic fracture solution. This treatment is presented in the analytical section. Recent studies (Ref. 5, 17) have shown γ to be a time-dependent function in a manner similar to the relaxation modulus. Fortunately, for consideration of crack initiation, γ does not enter until new surface is created. Thus, $\gamma(t)$ is substituted directly into the criticality equation with its value at t_o, the time of failure. The role of the kinetic energy is perhaps less understood. Studies by Williams (Ref. 18) and Blatz (Ref. 19) indicate that this term may be significant for high-rate short-time loadings and for oscillatory (vibration) loadings. For the oscillatory input, the kinetic energy term has been shown to decrease the time (or number of cycles) to cause fracture (Ref. 20). The loadings applied in the present experimental program were of the relatively long-time slow-rate type.

FRACTURE AT A BIMATERIAL BONDLINE

A treatment, similar to that of the Griffith crack problem, has been applied to an infinite sheet of two materials with the central crack at their interface. When the material in the upper half is incompressible and the lower half rigid, the adhesive fracture energy, γ_a, can be computed (Ref. 21). A related problem of a pressurized axisymmetric two material body (blister specimen) is described by Dannenberg (Ref. 22). The adhesive energy for this type specimen when the upper material is incompressible and elastic is given in Ref. 23 as

$$\gamma_a = \frac{3}{2\pi}\left(\frac{a\, P_{cr}^2}{E}\right) \tag{27}$$

where a is the initial unbond radius and P_{cr} the applied pressure at which the unbond begins to propagate. The first order correction for viscoelastic materials is given by replacing the modulus of elasticity, E, by the relaxation modulus $E_{rel}(t)$ evaluated at the time of unbonding (Ref. 17). For more realistic testing, a three-layer specimen--rigid base, liner interlayer, propellant upper layer--is required. An analysis treating the interlayer as a Winkler (elastic) foundation has been made for the sheet (Griffith crack) problem (Ref. 24) and for the axisymmetric blister specimen (Ref. 25). A numerical analysis using elastic finite element techniques was incorporated in this program and is discussed in Section IV.

CRACK PROPAGATION

A problem equally important to determining when a flaw will begin to grow is that of finding the manner in which it will propagate. The trajectory or path it follows and the rate with which it proceeds are of interest. The trajectory problem, for other than the most simple case, is best handled by the finite element method. While this approach is tedious and time consuming, the determination of the path that will release the greatest energy in the shortest distance is straightforward for an elastic material. The assumption that the result will apply equally to a viscoelastic material is not without basis. It has been shown (e.g., Ref. 3) that fracture in certain simple geometries observes the same geometric constants whether the material is elastic or viscoelastic. Crack trajectory is essentially a problem of geometry; so elastic analysis should be applicable to viscoelastic materials.

The associated problem of crack growth rate is not so straightforward. The dissipative mechanisms of viscoelastic materials would be expected to play an important role in propagation rate analysis. Mueller (Ref. 26) gives a most useful treatise on the subject of viscoelastic crack propagation. He studied the problem of crack growth in a viscoelastic strip using a balance of energy in a control volume around the tip of the crack (local energy balance) and established a relatively simple relationship between the applied load, temperature, material properties, and the crack velocity. Crack velocity, $\dot{a}$, is implicitly determined by:

$$\dot{a}\left\{\pi K_n^2 \sigma_o^2 b\left[\frac{273}{T} D_{cr}\left(\frac{\Delta c}{\dot{a}\, a_T}\right)\right] - \gamma\right\} = 0 \qquad (28)$$

for an applied load σ_o. Equation 28 is analogous to Eq. 26 for a displacement boundary. The stress intensity factor is a non-dimensionalized characterization of the stress singularity at the crack tip defined by

$$K_n = \lim_{x \to a} \sqrt{\frac{x-a}{b}}\, \frac{\sigma(x,o)}{\sigma_o} \qquad (29)$$

The material parameter involved is the creep compliance normalized in this case to 0 Centigrade, and is indicated by $\left[\frac{273}{T} D_{cr}\left(\frac{\Delta c}{\dot{a}\, a_T}\right)\right]$. The quantity, Δc, is a characteristic of the material and may be envisioned as the width of a thread of material immediately in front of the advancing crack tip which breaks to permit crack growth. This thread represents a uniaxial stressed portion of the material which breaks as some critical load is reached as suggested in Ref. 14.

As before, when crack growth occurs ($\dot{a} > 0$) we have the criticality condition

$$\sigma_o = \frac{1}{K_n}\sqrt{\frac{1}{\pi b}\ \frac{Y}{\left(\frac{273}{T}\right)\ D_{cr}\ \left(\frac{\Delta c}{\dot{a}\ a_T}\right)}} \tag{30}$$

Application of these concepts of crack initiation and propagation are implemented in the analysis of data generated during the experimental effort.

SECTION III, EXPERIMENTAL PROGRAM

This fracture mechanics study was basically an experimental effort with emphasis on test development, test technique, and the measurement of the fracture response of linear viscoelastic and solid propellant materials. A limited number of strip biaxial tests were conducted on TPH-1011 propellant to verify the tensile relaxation and cohesive fracture properties. Several blister peel tests were run on TPH-1011/liner specimens to evaluate the feasibility for this type test on propellant-liner systems and to measure the characteristic adhesive energy for this system. Tests using the Radial Planar Loading (RPL) apparatus were conducted on TPH-1011 propellant and Solithane to evaluate this experimental approach to failure studies and yield data for correlation with analytical results. These tests are described and the data presented in the following discussions.

BIAXIAL STRIP TESTS (TPH-1011 PROPELLANT)

Tests to measure TPH-1011 propellant relaxation modulus, ultimate tensile capability, and characteristic cohesive energy release rate, γ_c, were conducted on biaxial strip specimens prepared at Thiokol-Wasatch. Eight specimens, tested at three temperatures, were made by machining a large block of propellant. Six additional specimens were made by casting propellant into a specially designed mold. The basic strip specimen geometry is shown in Fig. 5.

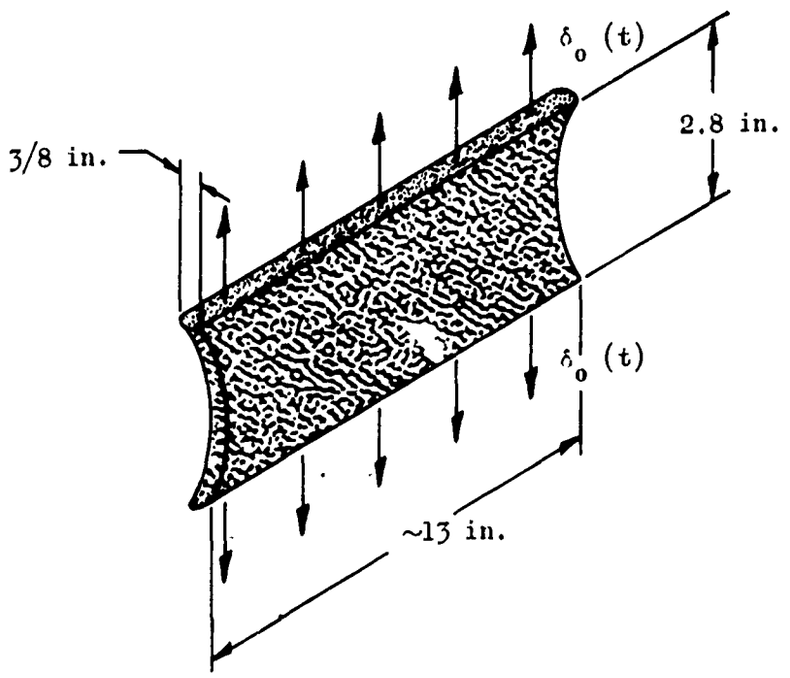

Figure 5. Biaxial Strip Specimen Geometry

The test sequence conducted on the eight machined strips consisted of the following steps:

1. Strain specimen to approximately 0.02 in./in. strain level at 20 in./min crosshead rate
2. Hold specimen at 0.02 in./in. strain level for about 2 hours while recording load response
3. At end of relaxation tests, continue straining to failure at a crosshead rate of 2.0 in./min

The ultimate failure strains measured are summarized in Table II.

TABLE II

STRAIN AT PEAK LOAD

TPH-1011 STRIP BIAXIAL TEST*

Test No.	Temperature, deg F	Strain at Peak Load, in./in.
5	140	0.20
7	20	0.13
8	20	0.12
9	77	0.23

* All tests at 2.5 in./min crosshead rate.

The relaxation modulus from the constant-strain portion of the test was reduced according to

$$E_{rel} = \frac{\text{Force Output}}{\text{Applied Displacement}} \left(\frac{2.8}{13.25 \times 0.375}\right) (1.06) \qquad (31)$$

and is shown as a function of time for each temperature in Fig. 6. Time-temperature superposition was achieved using the shift-factor

$$a_T = \left(\frac{203}{T + 123}\right)^{17} \qquad (32)$$

where T is the temperature in degrees Farenheit and the data are referenced to 80 F. The relaxation modulus reported by Thiokol for uniaxial specimens is given by

$$\log \hat{E}_{rel}(t/a_T) = 2.538 - 0.1232 \log (t/a_T) + 0.01292 \log^2 (t/a_T) - 0.0006608 \log^3 (t/a_T) \qquad (33)$$

For purposes of comparison, the shifted data measured in the tests are plotted along with Eq. 33 converted to biaxial equivalent (1.33 uniaxial) in Fig. 7. Since the comparison was within experimental scatter limits, Eq. 33 formed the basis for all data reduction and analytical effort requiring modulus as input.

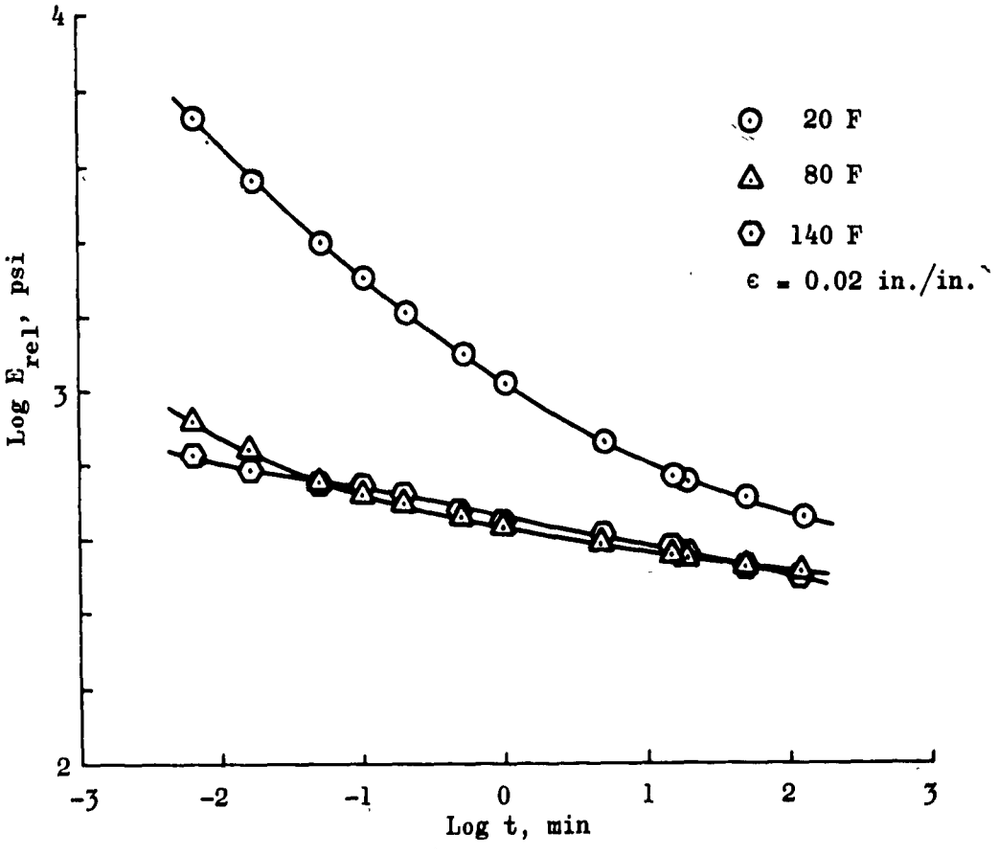

Figure 6. TPH-1011 Propellant Biaxial Relaxation Modulus

Subsequent to these tests, six biaxial strips were prepared by casting sheets of propellant and cutting them to the dimensions shown in Fig. 5. In addition, a 1-inch slit was cut through the specimen near the center and parallel to the tester grips for determination of γ_c. Two specimens were tested at each of three temperatures, the test procedure being essentially the same as that used for the machined strips. As seen in Fig. 8, the relaxation modulus compared favorably with that measured on the machined strips.

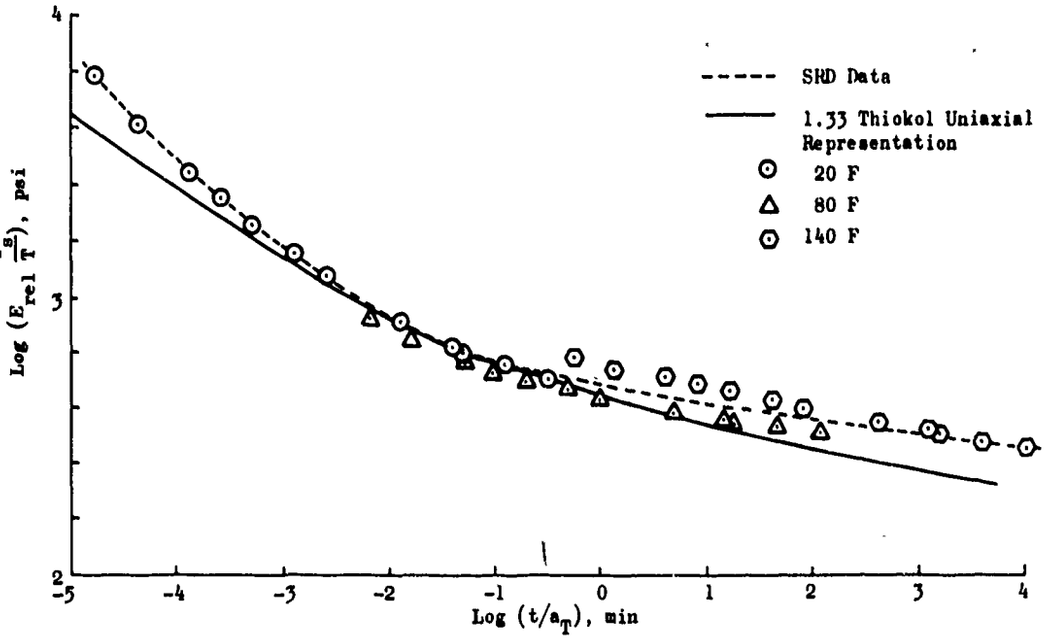

Figure 7. Biaxial Relaxation Modulus Curve, TPH-1011 Propellant

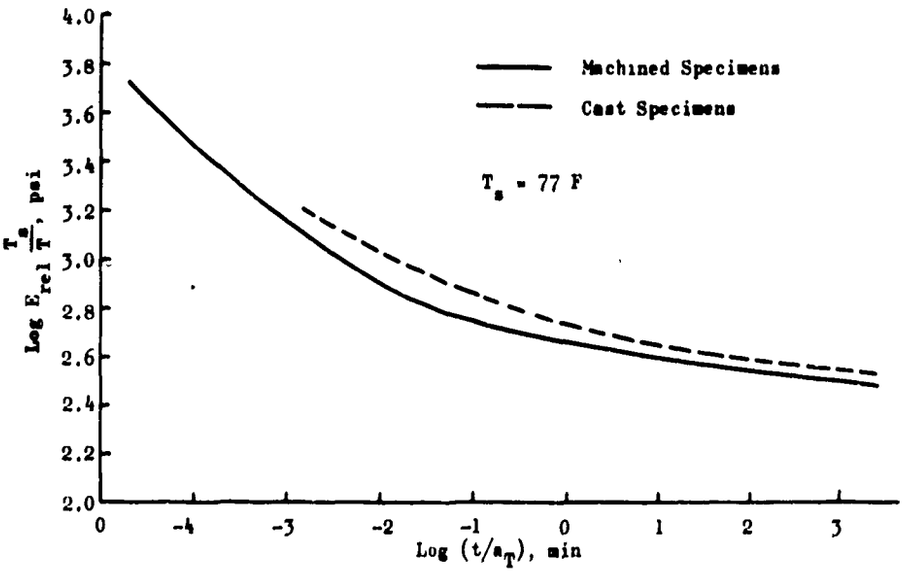

Figure 8. Biaxial Relaxation Modulus, TPH-1011 Propellant

The time and strain of crack growth initiation were used to determine γ_c. From Ref. 17,

$$\gamma_c = c_o \frac{\pi/2}{(1-\nu^2)^2} \left[F_1\left(\frac{c_o}{w}\right) F_2\left(\frac{c_o}{b}\right) \right] \left[\frac{2}{t_o^2} E_{rel}^{(2)}(t_o) \right] \left(\epsilon_y^2\right) \quad (34)$$

where c_o, b, w are geometric characteristics of the specimen, ν, the Poisson ratio; ϵ_y, the strain at flaw growth initiation; and t_o, the time to flaw growth initiation. The term in the second bracket of Eq. 34 is the 'second time-averaged' relaxation modulus and is shown in Fig. 9. The correction factors F_1 and F_2 were taken from Ref. 17, and for the present case

$$F_1\left(\frac{c_o}{w}\right) = 1.0; \quad F_2\left(\frac{c_o}{b}\right) = 0.62 \quad (35)$$

Test results for four of the six tests (two were negated because of experimental difficulties) are shown in Table III. Assuming the same temperature shift (Eq. 32) as used for the modulus the γ_c measured was plotted along that reported by Thiokol as a function of time and is shown in Fig. 10. The obvious discrepancy may be attributed to several factors:

1. Method of propellant specimen processing
2. Method of data reduction
3. Age of propellant
4. Validity of time-temperature equivalence assumption

Since a rather large difference was noted, both values were recalled at points in the analysis requiring γ_c for input. The only solution to resolving the discrepancy would be to conduct additional tests to determine more adequately the value of γ_c as a function of both time and temperature.

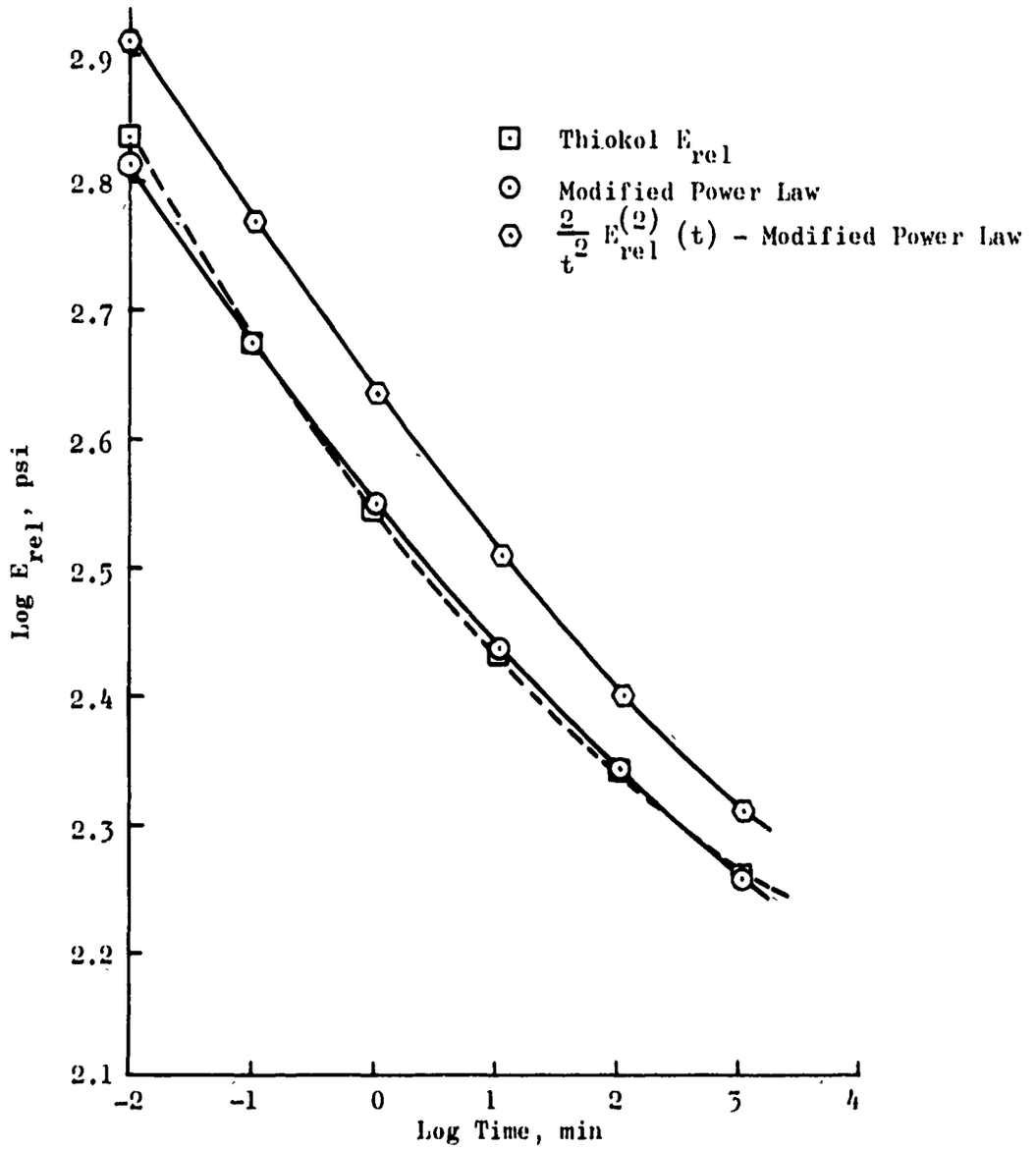

Figure 9. TPH-1011 Propellant Uniaxial Relaxation Behavior at 77 F

TABLE III

γ_c - TPH-1011

Test No.	Temperature, deg F	t_o, min	ϵ_y, in./in.	γ, in.-lb/in.^{2}
6A	80	~ 0.050	0.065	6.30
7A	80	~ 0.050	0.062	5.76
8A	140	~ 0.050	0.063	3.67
11A	20	~ 0.042	0.051	7.95

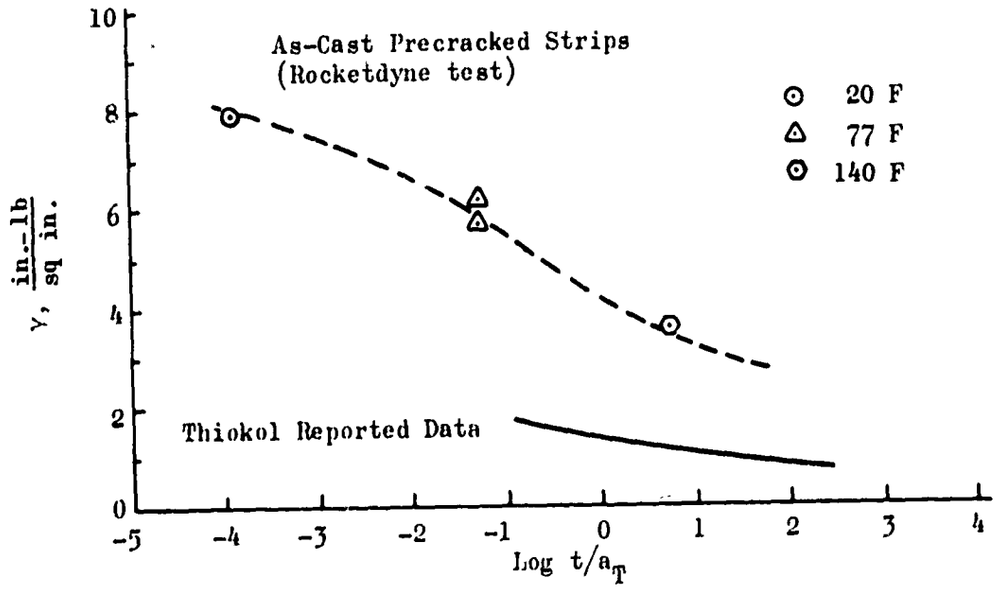

Figure 10. γ_c Measured from Strip Biaxial Specimens

BLISTER PEEL TESTS

One of the two major experimental development thrusts on the Fracture Mechanics Program is the feasibility study of the blister peel test as applied to propellant/liner/case systems. The standard "90°" peel test used throughout the industry provides a qualitative measure of the relative peel capability of several systems but says little about the capability of any system to withstand a given environmental loading. Since fracture at the bondline is an essential area of interest in structural integrity analysis, the need for an engineering test to provide quantitative measurement of bond capability is obvious. A promising approach is the blister peel test (Ref. 9, 22). The test layout for this particular application is shown schematically in Fig. 11. A photograph of the actual system is shown in Fig. 12. A view of the blister specimen is shown in the sketch in Fig. 2.

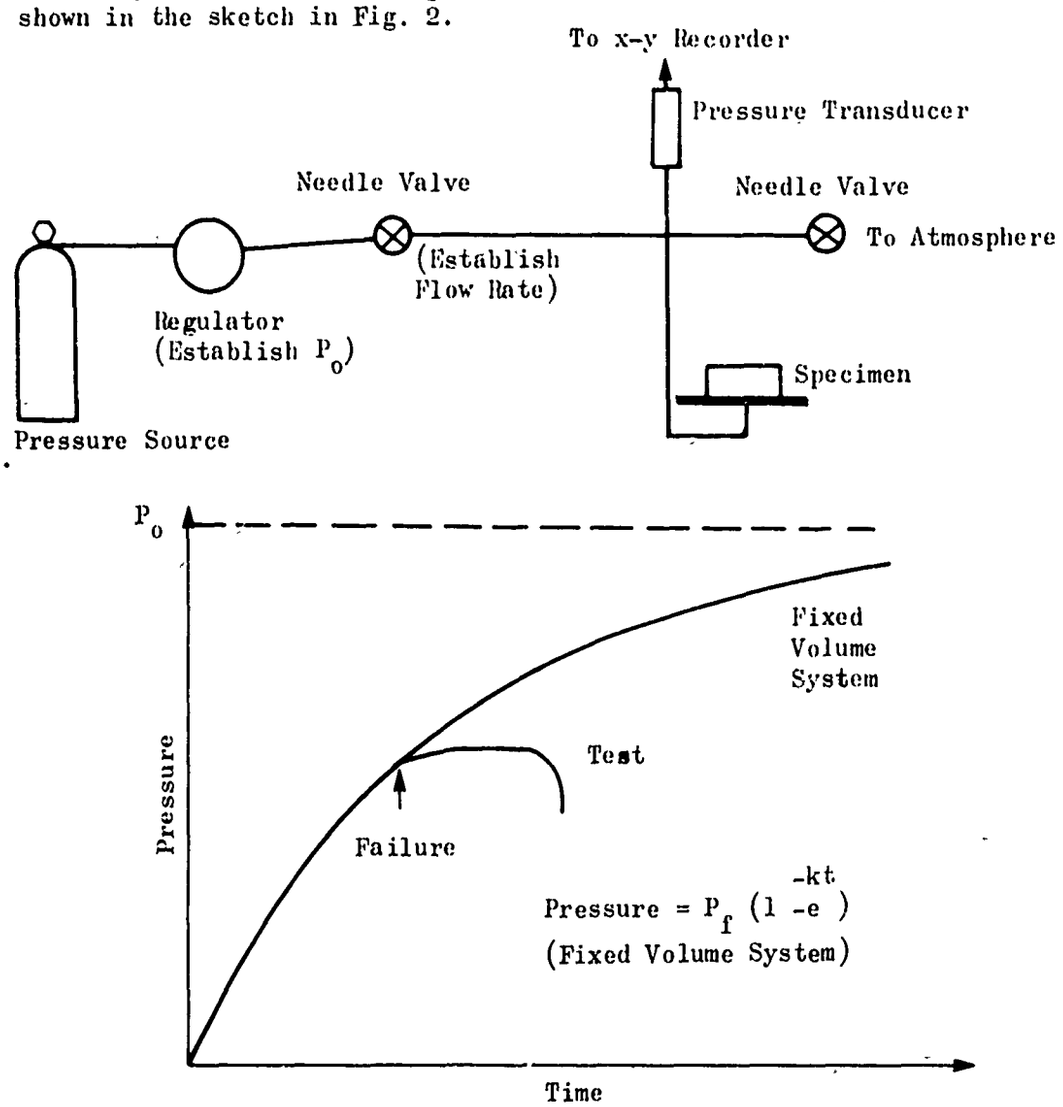

Figure 11. Blister Peel Test Arrangement

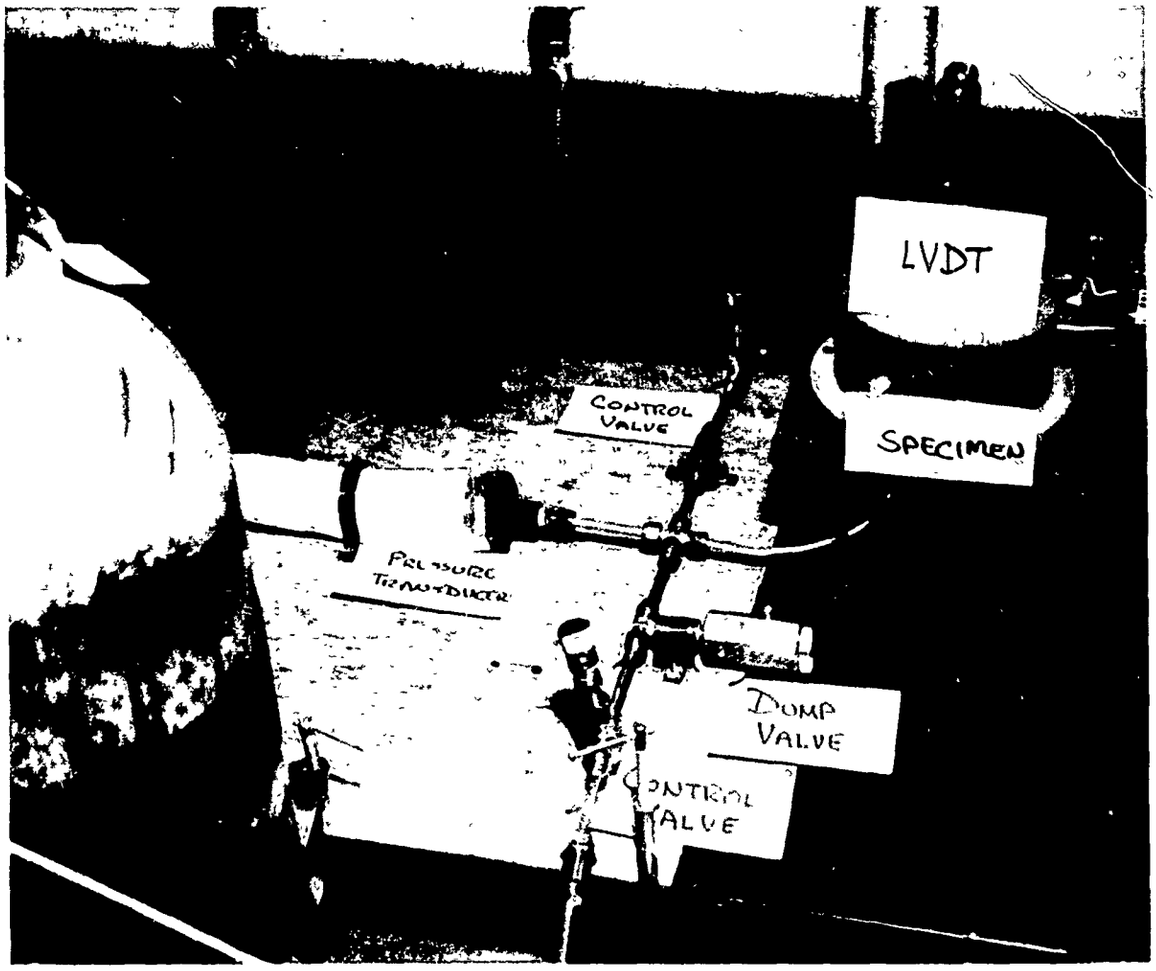

Figure 12. Blister Peel Test Apparatus

Test specimens were prepared by spreading a uniform thickness of uncured liner over the surface of a steel disc. A Teflon plug through the center of the disc protruded to the upper surface of the liner to provide a gas path to the liner-propellant interface. After the liner was partially cured, a 1-inch diameter disc of Teflon approximately 0.005 inch thick was placed over the plug to provide a known initial unbond area. Uncured TPH-1011 propellant was then cast onto the liner, and the entire assembly was cured.

Pressurization of the unbond was achieved by removing the plug and connecting the chamber to a dry nitrogen source. A pressure transducer on the line provided a record of cavity pressure as a function of time. The rate of pressurization was approximately constant, and rates of about 1.0, 3.0, and 100.0 in./min were used. Representative pressure-time plots for three of the tests are shown in Fig. 13.

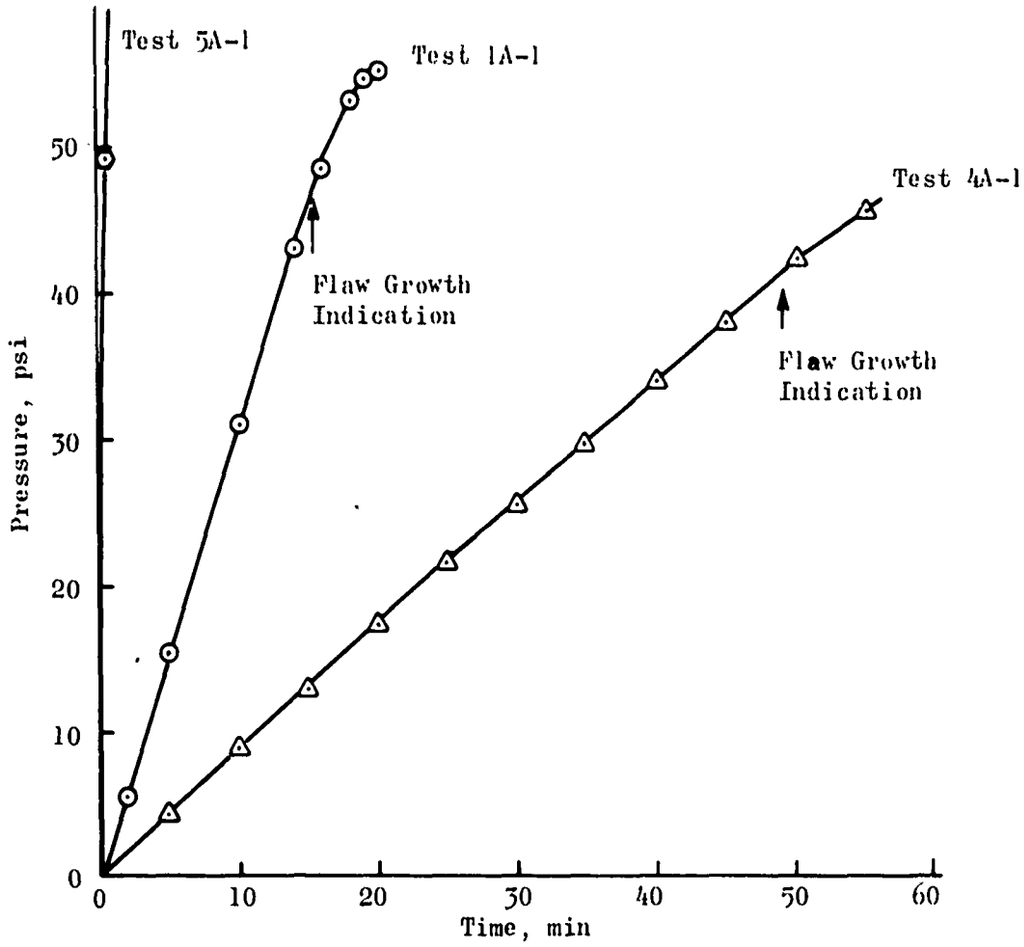

Figure 13. Representative Time-Pressure Histories TPH-1011 Propellant Blister Peel Specimen

A linear variable differential transformer (LVDT) was mounted above the propellant to record, as a function of time, the change in height of the propellant over the center of the unbond. Since the unbond was unavailable for visual observation, flaw growth had to be determined from perturbations in the pressure and deflection functions. Time intervals near failure are displayed for the first test on eight specimens in Fig. 14 through 21.

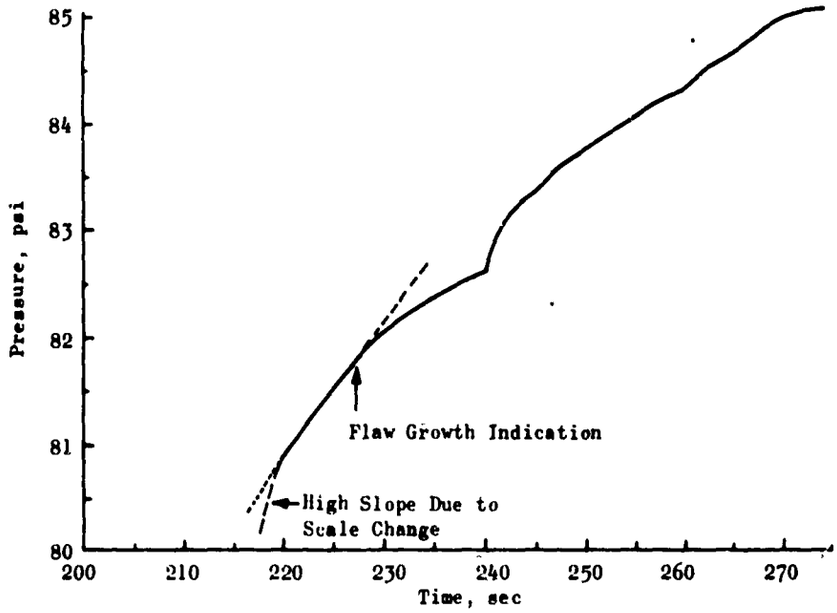

Figure 14. TPH-1011 Propellant Blister Test 1, Failure Region

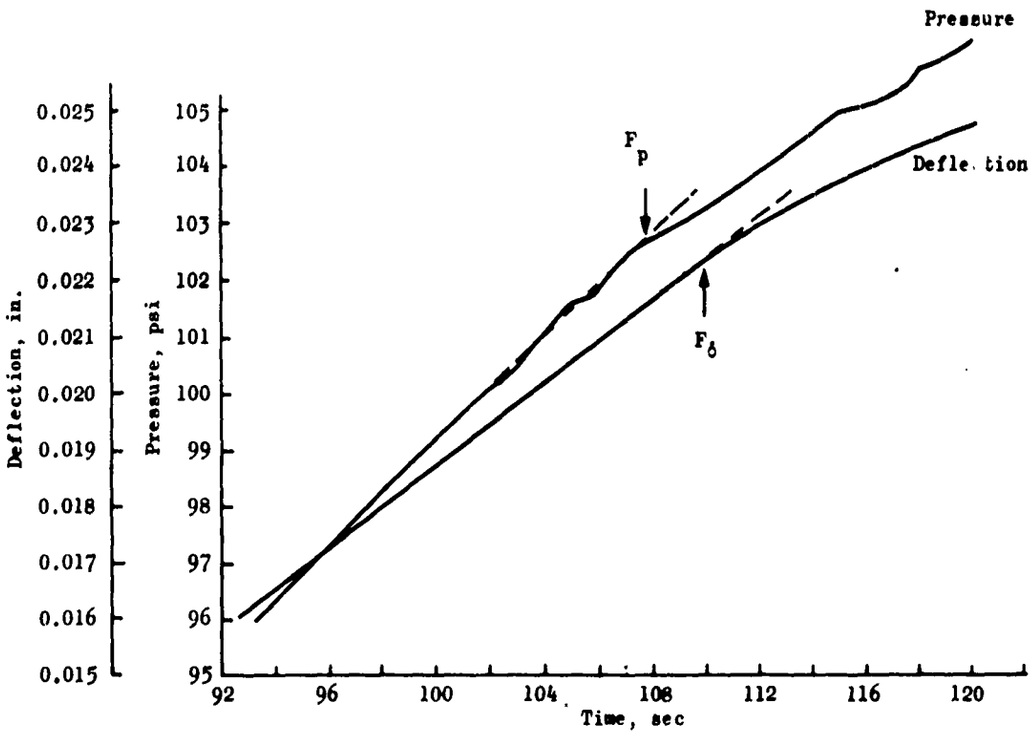

Figure 15. TPH-1011 Propellant Blister Test 4, Failure Region

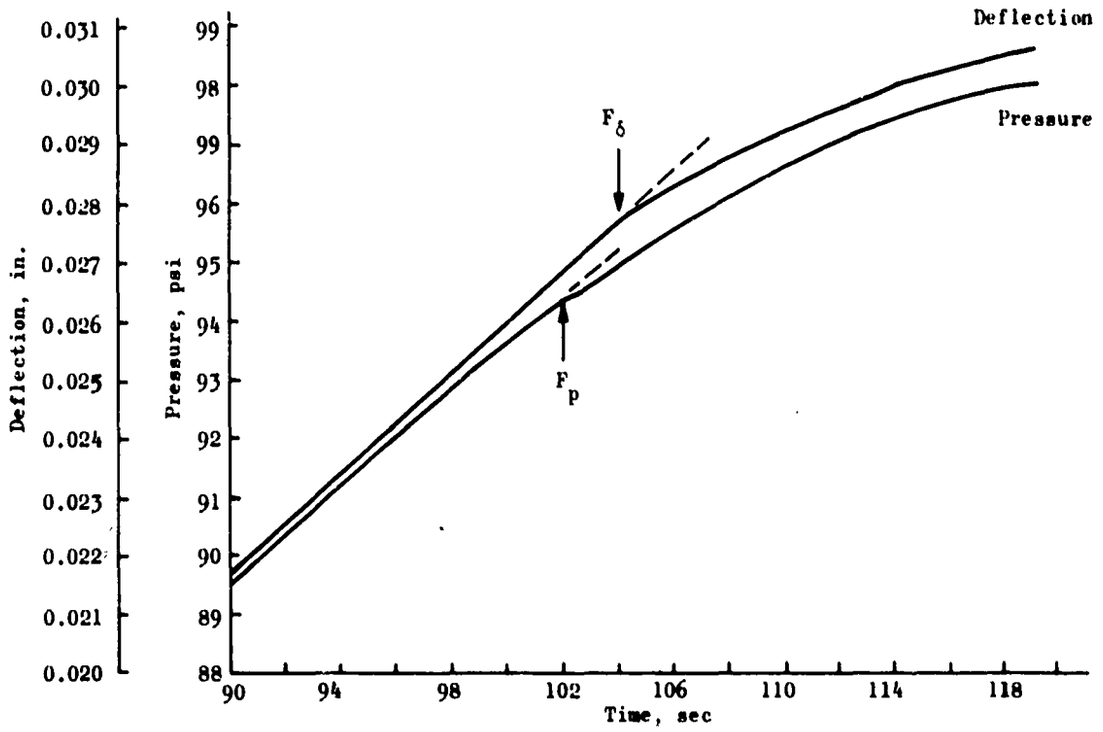

Figure 16. TPH-1011 Propellant Blister
Test 5, Failure Region

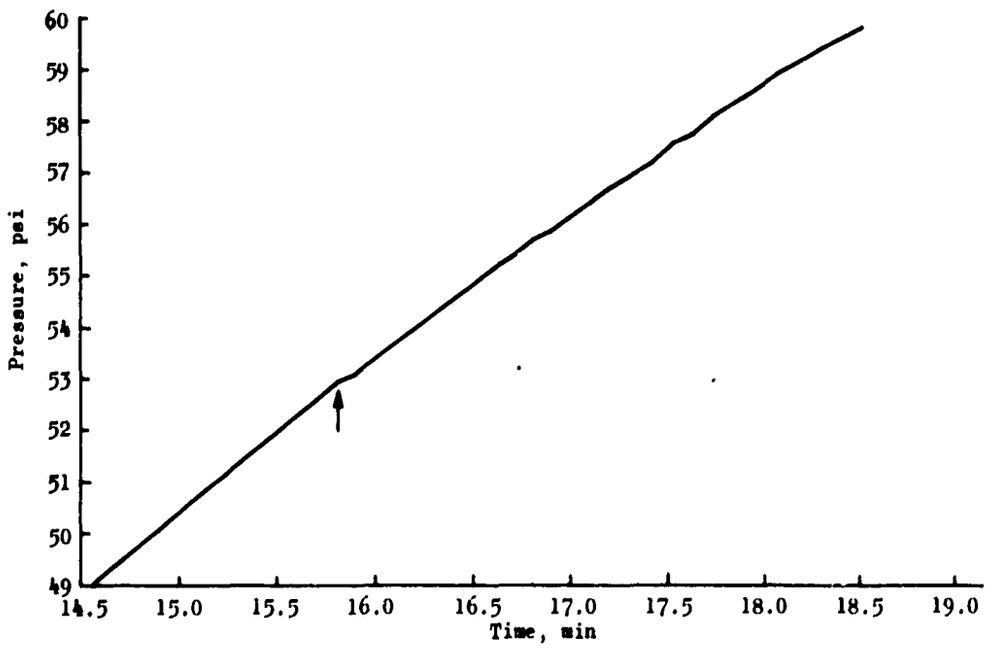

Figure 17. TPH-1011 Propellant Blister Peel
Test 1A-1, Failure Region

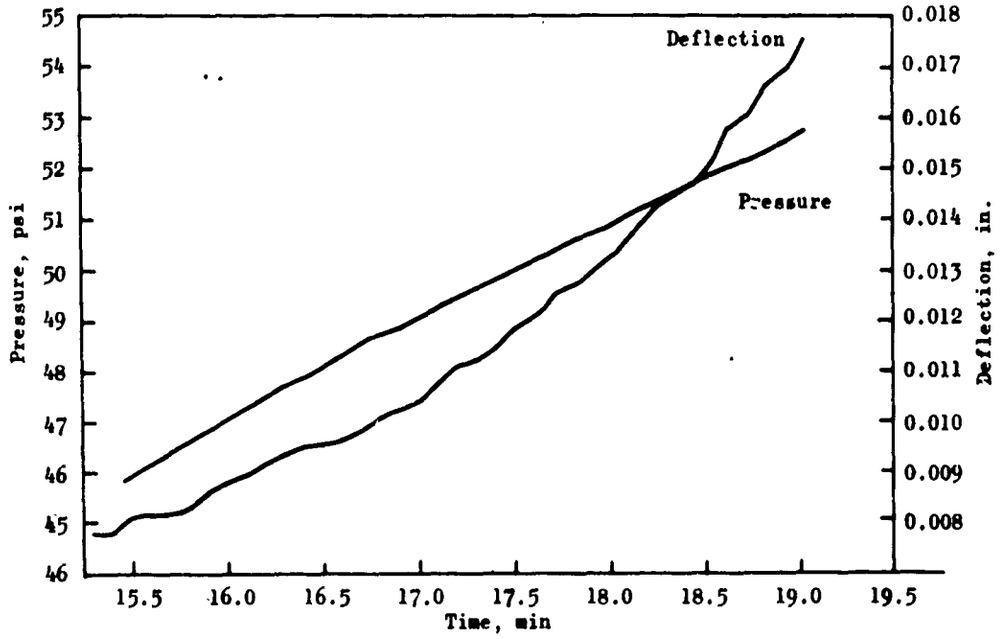

Figure 18. TPH-1011 Propellant Blister Peel
Test 2A-1, Failure Region

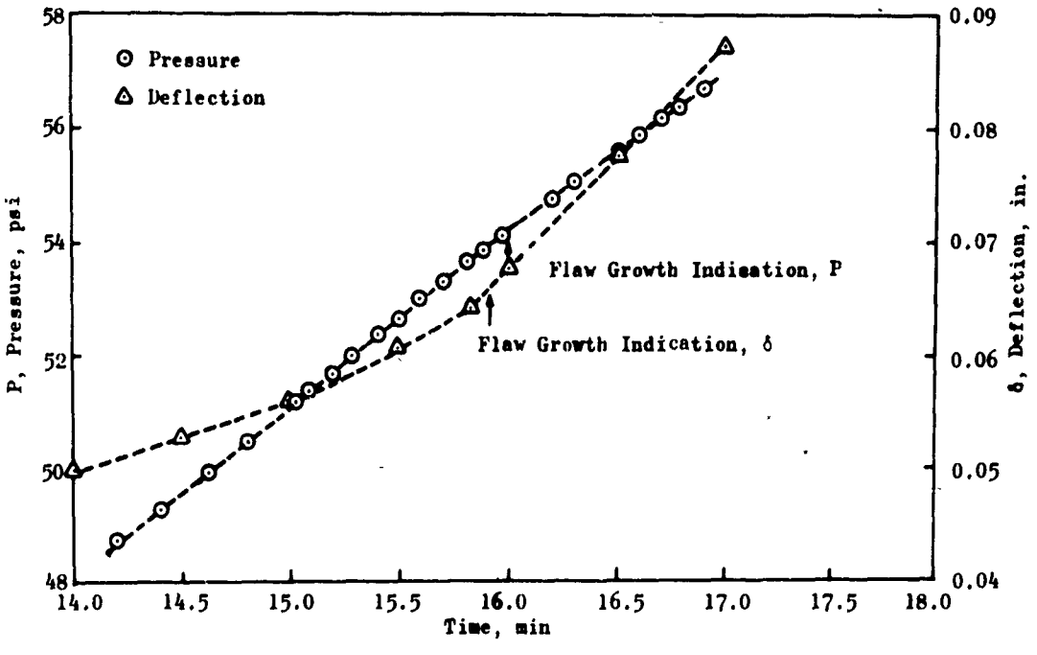

Figure 19. TPH-1011 Propellant Blister
Test 3A-1, Failure Region

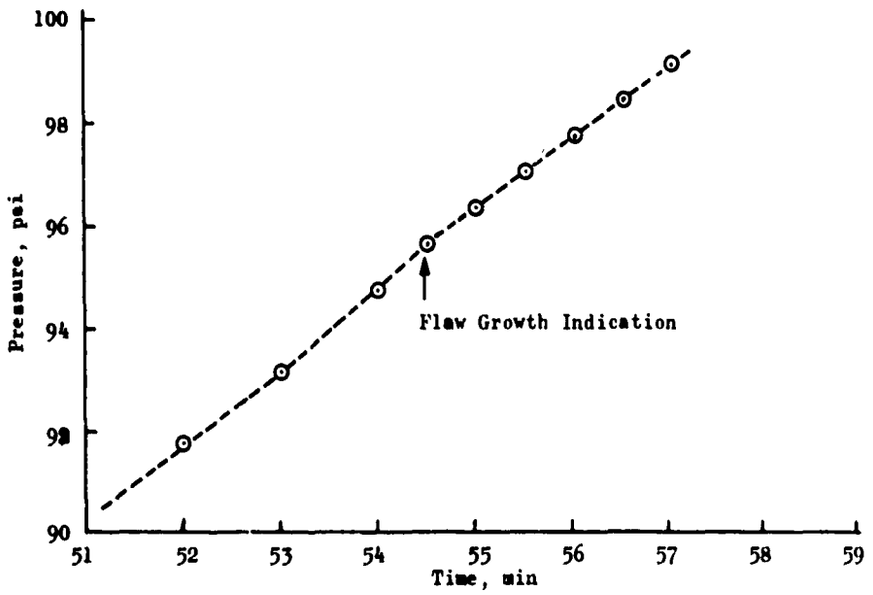

Figure 20. TPH-1011 Propellant Blister Test 4A-1 Failure Region

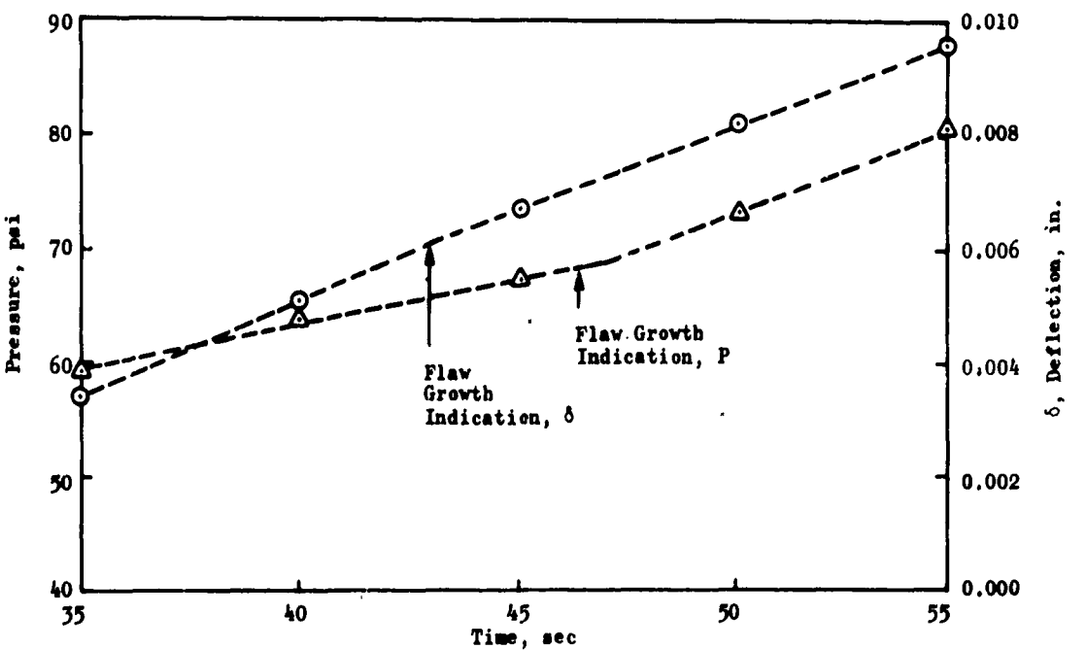

Figure 21. TPH-1011 Propellant Blister Test 5A-1, Failure Region

Repeated tests were performed on five of the specimens by relieving the pressure shortly after unbond growth was detected. The specimen was then repressurized until failure was again noted. As many as 14 tests were run on an individual specimen. Observations indicate a practical limit of about six or seven tests to achieve a desirable spacing between unbonds and stay within the center half of the specimen radius. After the final test on a specimen, the propellant was lifted off and rings, apparently coinciding with start-stop of the testing, were noted (Fig. 22). For tests subsequent to the first, the unbond radius was determined by measuring the ring diameters. The symmetry of the rings indicates the uniformity of the failures and permits analysis of the failure as axisymmetric.

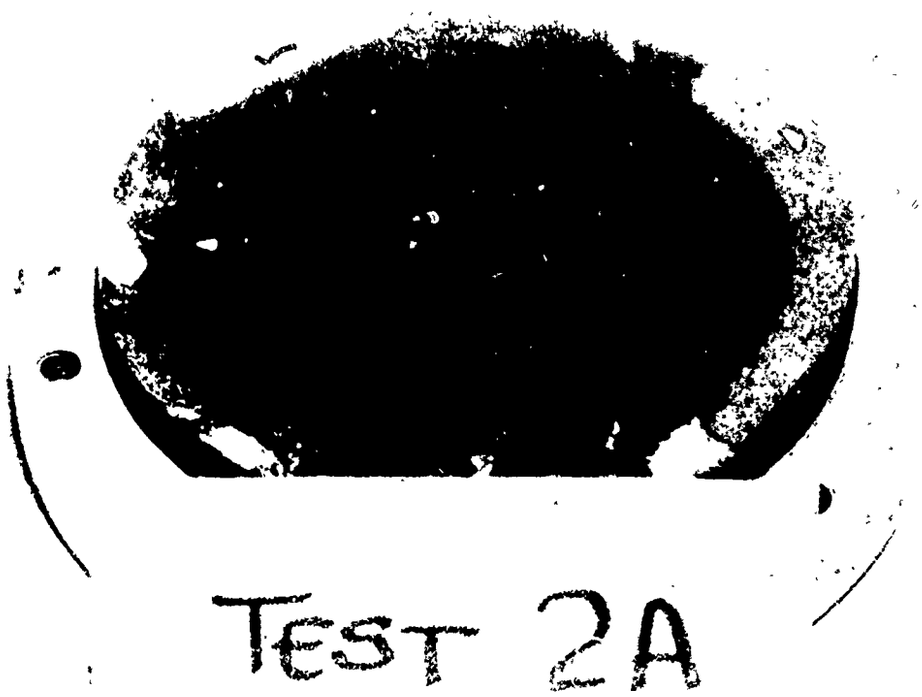

Figure 22. Postfracture Liner Surface

Data were interpreted, ignoring effects of the liner interface, according to Eq. 27 or

$$\gamma_a = 0.477 \frac{c\, P_{cr}^2}{E_{rel}(t_o)} \tag{36}$$

A finite element non-dimensionalized computer solution was also obtained in which the liner was accounted for.* This analysis and its significance is discussed in Section V. A tabulation of the test data and calculated γ_a for the eight specimens based on Eq. 36 is given in Table IV. These results are shown as γ_a vs log t in Fig. 23. The spread in data is on the order of $\pm$ 20%, but no statistical estimate of the standard deviation was attempted because of the limited number of tests. This spread is tolerable and not unexpected because of variation in propellant modulus, accuracy of initial flaw measurement, pressure reading, and assumptions in the data reduction.

RPL TEST APPARATUS

Analytical solutions to fracture behavior have been obtained for certain simple cases of uniform all-around tension. Application of these solutions to experimental data rests, to some degree, on the ability to achieve the boundary conditions assumed in the analysis. Because of the strong analogy between all-around tension models and case-bonded solid propellant grains, concepts for achieving a laboratory-scale experimental tool to bridge the gap between propellant grain and theoretical model were evaluated. From these considerations, a device to permit uniform loading of a circular disc was conceived.

The feasibility of such a device was explored using a bicycle wheel. Load was induced on a circular specimen by tightening the spokes on the wheel. It was established that a disc specimen, bonded in a rubber ring which transfers load from the individual spokes and distributes it over the specimen boundary, could be made to fail at the inner port in a manner similar to cracks obtained in solid propellant motors subjected to temperature cycling. This concept was developed on the Fracture Mechanics program and the result was the Radial Planar Loading (RPL) device, Fig. 24. Features designed into this apparatus are as follows:

1. Operating temperature range of -80 to 200 F
2. Load or displacement boundary may be applied to load distribution collar
3. Radial displacement rates from 0.002 to 0.2 in./min at the collar are attainable.

*The philosophy in using these methods of data reduction includes consideration of the surface area of only one material. This is opposed to the consideration of the dual surface created in cohesive fracture. The single surface assumption does not affect the results but must be kept in mind when comparing adhesive and cohesive energy release rates and when applying fracture mechanics to motor unbond analysis.

TABLE IV

BLISTER TEST SUMMARY

Specimen Number	Run Number	Time-to-Failure, min.	Failure Pressure, psi	Initial Unbond Radius, in.	Modulus,[5] psi	Energy Release Rate, γ, in.-lb/in.^{2}
1		1.71	82.0	0.50	322	4.98
2		....[1]	....	....	....	....
3	1	....[2]	....	....	....	....
	2	1.38[3]	76.0	0.75	330	6.26
4		1.80	103.0	0.50	320	7.91
5		1.70	94.0	0.50	322	6.54
1A	1	15.65	54.0	0.50	254	2.64
	2	16.0	48.4	0.78	253	3.44
	3	26.9	25.6	1.05[4]	243	2.51
2A	1	16.30	47.8	0.55	252	2.29
	2	16.0	36.0	0.82	253	2.00
	3	15.58	31.8	1.06	254	2.01
	4	15.0	28.4	1.32	256	1.98
	5	1.41	32.7	1.64	330	2.53
3A	1	16.60	55.7	0.51	252	3.00
	2	14.5	47.3	0.71	256	2.96
	3	13.2	40.6	0.93	259	2.82
	4	12.0	34.6	1.14	261	2.49
	5	11.5	30.8	1.34	262	2.31
	6	28.6	28.6	1.39	241	2.25
	7	27.4	25.1	1.50	242	1.86
	8	0.65	30.8	1.71	362	2.14
4A	1	51.40	44.2	0.53	228	2.17
	2	No Failure	....	....	....	....
	3	63.75	37.8	0.75	226	2.26
	4	No Failure	....	....	....	....
	5	37.60	36.0	0.89	237	2.32
	6	32.90	29.8	0.98	240	1.73
	7	42.80	27.5	1.08	234	1.66
	8	48.30	29.2	1.16	231	2.04
	9	No Failure	....	....	....	....
	10	50.5	29.2	1.22	230	2.16
	11	54.8	27.0	1.48	229	2.12
	12	96.8	25.6	1.66	219	2.37
	13	No Failure	....	....	....	....
	14	1.2	27.6	2.21	336	2.39
5A	1	0.78	76.0	0.52	352	4.07
	2	0.78	70.0	0.76	352	5.16
	3	0.72	61.9	0.88	357	4.51
	4	0.80	62.9	1.06	351	5.76
	5	0.86	60.6	1.21	350	6.06
	6	0.66	57.5	1.52	361	6.64
	7	0.80	50.1	1.87	351	6.38
	8	0.97	42.1	2.33	344	5.73

(1) Bad run, data not interpreted

(2) Failure point not apparent

(3) Dye penetrant had been introduced into system, 0.75 crack radius assumed

(4) Doubt as to the accuracy of the analysis for $c \geq 1.0$ makes these results questionable

(5) $\log E = 2.538 - 0.1232 \log t + 0.01292 \log^2 t - 0.0006608 \log^3 t$

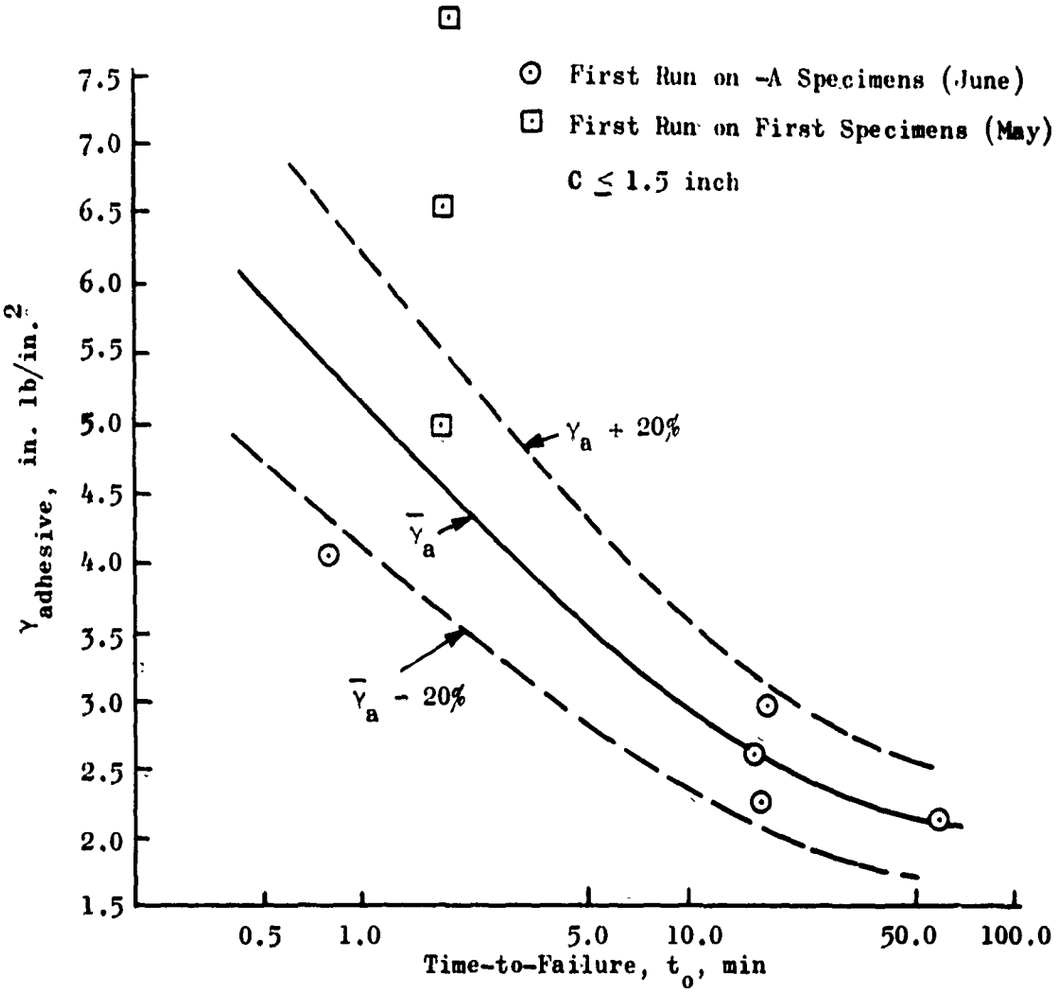

Figure 23. Summary of Blister Specimen γ_a Determination

The basis of operation of the RPL device is that of a hydraulically controlled mechanical device. A driving cam is lifted by a hydraulic pump which is controlled by an MTS electronics system. As the cam is raised, 18 arms are displaced. These 18 arms are connected through rods to a rubber load collar which distributes the load to a circular disc of the material being tested. Nine of the 18 rods are instrumented with load cells to give load applied. The driving cam is controlled to a preprogrammed rate by feedback from cam-displacement or collar-displacement (for displacement boundaries) or from load cell output (for force boundaries). Test records include analog time records of load cell outputs and cam displacement. Photographs of the specimen are made at regular intervals and correlated with the analog time record.

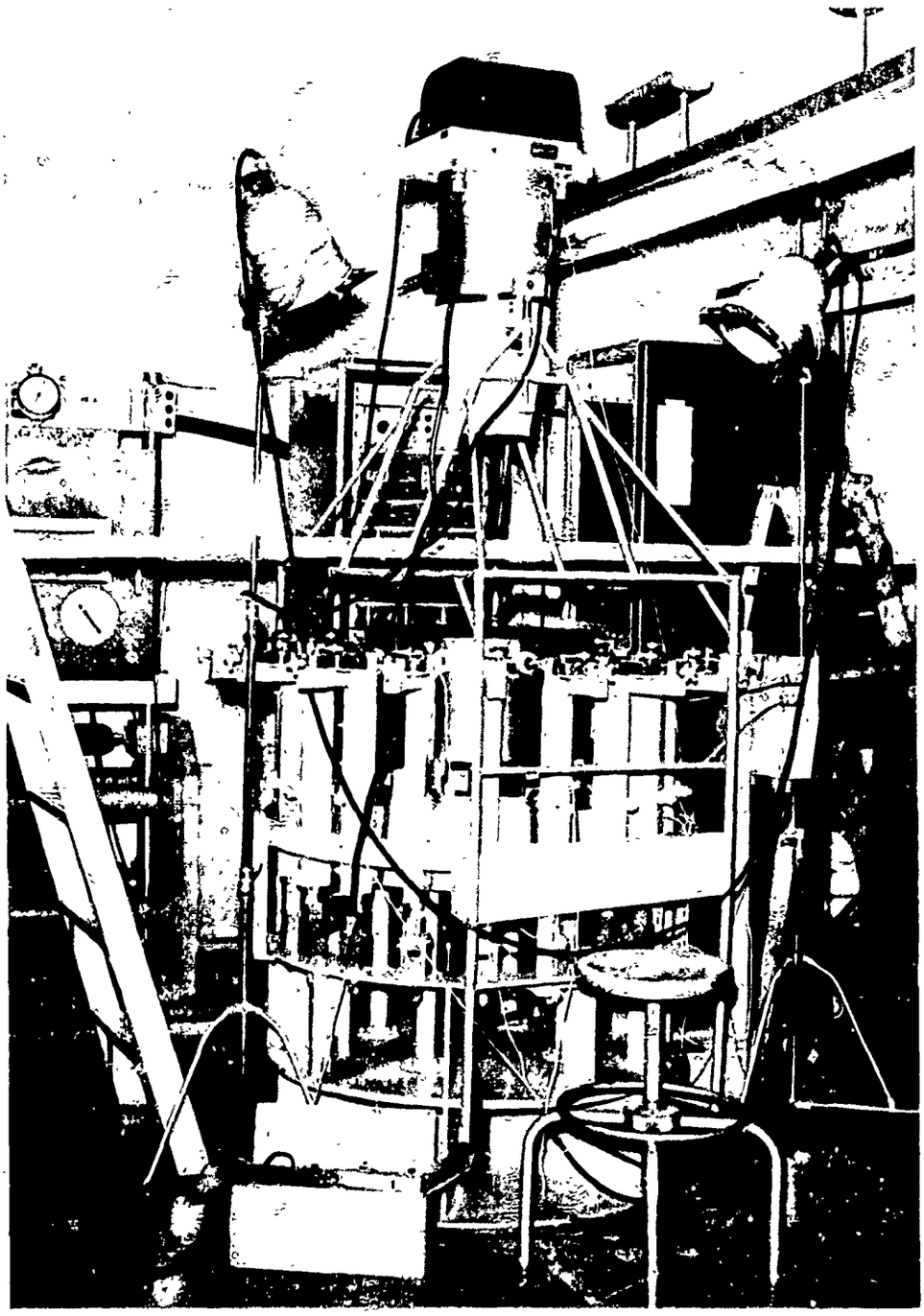

11-4-691045

Figure 24. Radial Planar Loading Device

The camera for making photographic records is a modified aerial reconnaisance camera with a 9-inch film size. The resulting photograph is 1.000 ± 0.005 times the actual specimen size. This permits direct measurement from the photo negatives of collar and specimen displacements and crack growth.

The test specimens for the RPL apparatus were cast in individual molds using Teflon plugs for the center port and barrel. After cure, the discs are bonded into the rubber load collar. The bond is then cured and the specimen mounted into the test machine. Load from the 18 rods or spokes is induced into the collar by bolts through clevices on the rod ends and through bushings in the collar. This bolt-circle diameter formed part of the initial machine setup and was set at 6.625 ± 0.025 inch. This corresponded most closely to the bolt-circle diameter of the rubber load collar following cure. To minimize initial stresses in the specimen, the collars were bolted to a base with the 6.625-inch bolt diameter, and the specimens were then bonded into the collar.

All tests performed on this program used a displacement boundary. As outlined in Table I, a variety of tests were performed on both Solithane and TPH-1011 propellant specimens. These tests are described on the following pages.

SOLITHANE DISC TESTS

Twelve Solithane discs were tested in the RPL device. Of these, six had circular ports of about 1.36-inch diameter, Fig. 25. The other six were six-point stars with a high radius base as shown in Fig. 26. Three of each type specimen were tested at a nearly constant displacement rate until a crack initiated at the inner port

After the crack had run to a depth of about 0.2 inch, the specimen was unloaded, rested, then retested until crack growth started again. This allowed measurement of crack growth initiation as a function of crack depth. The data from the six tests are summarized in Table V and presented graphically in Fig. 27 and 28 for the circular port and star port specimens, respectively. The general shape of the curves are as expected from analytical studies, e.g., Ref. 6.

The remaining six specimens were tested to measure flaw growth rate at constant displacement for three displacement levels. The specimens were displaced radially about 0.026, 0.032, and 0.036 inch, respectively. Cracks approximately 0.15 inch deep were initiated using a razor after the specimen stress had relaxed from the application of displacement. The cracks were allowed to grow to the collar with a record of specimen load. Photographs of the crack were made throughout the test. A photographic record of the crack growth from one of these tests is shown in Fig. 29. The radial displacement, crack length, and average load measured in the loading rods are shown in Fig. 30--35 for the six specimens tested in this manner.

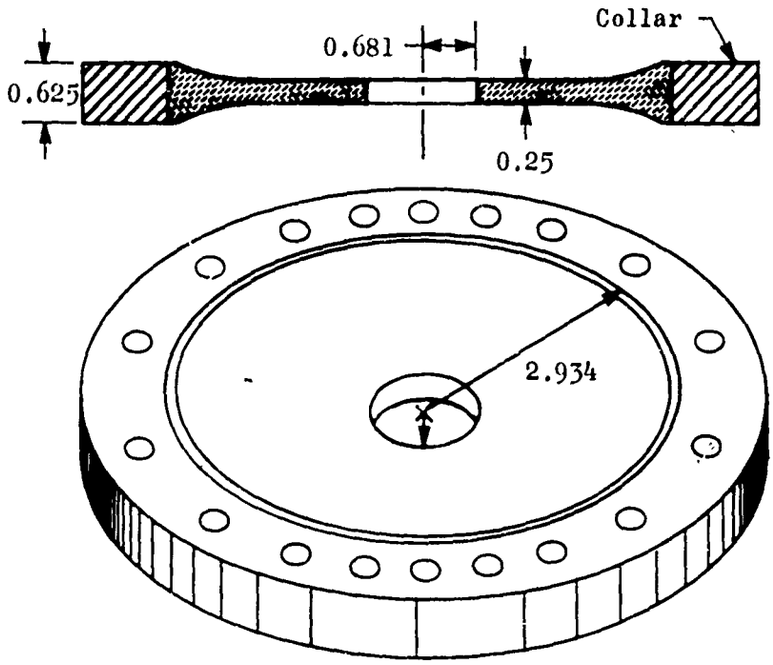

Figure 25. Biaxial Disc Cross Section
Low Web Circular Port

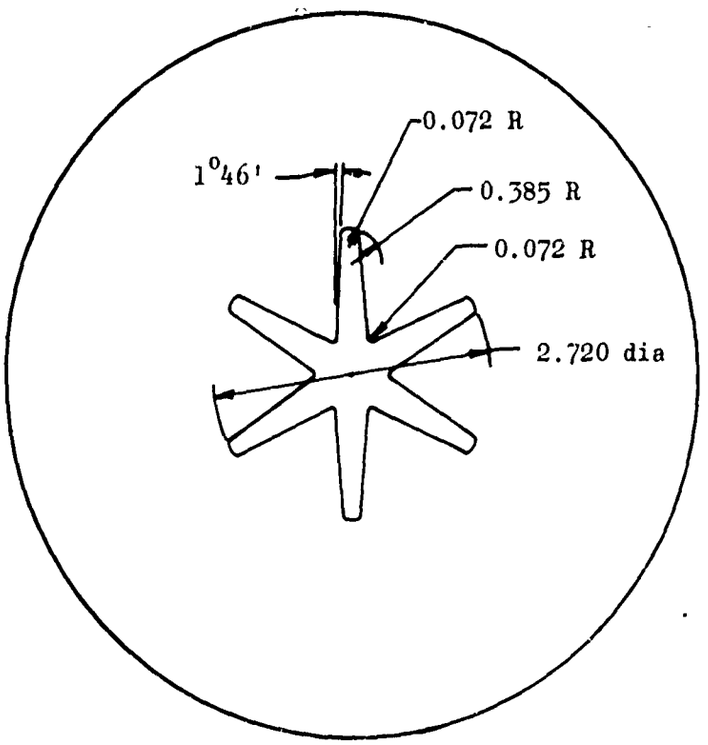

Figure 26. Star Port Biaxial Disc Cross Section

TABLE V

CRACK GROWTH INITIATION DATA FOR SOLITHANE DISC

SPECIMENS CONSTANT RATE TESTS

Specimen No.	Test No.	Initial Crack Depth, c_o in.	Failure Displacement δ_{cr} in.	Time to δ_{cr}, t_o, in.
Circular Port				
21	1	~ 0.015	0.131	45.0
	2	0.115	0.047	14.7
	3	0.296	0.027	5.0
22	1	--	0.164	55.7
26	1	--	0.146	49.8
Star Port				
23	1	--	0.077	20.0
	2	0.340	0.027	3.6
	3	0.600	0.018	1.8
24	1	--	0.098	30.8
	2	0.176	0.039	7.1
	3	0.550	0.025	5.8
25	1	--	0.087	24.5
	2	0.196	0.036	8.0

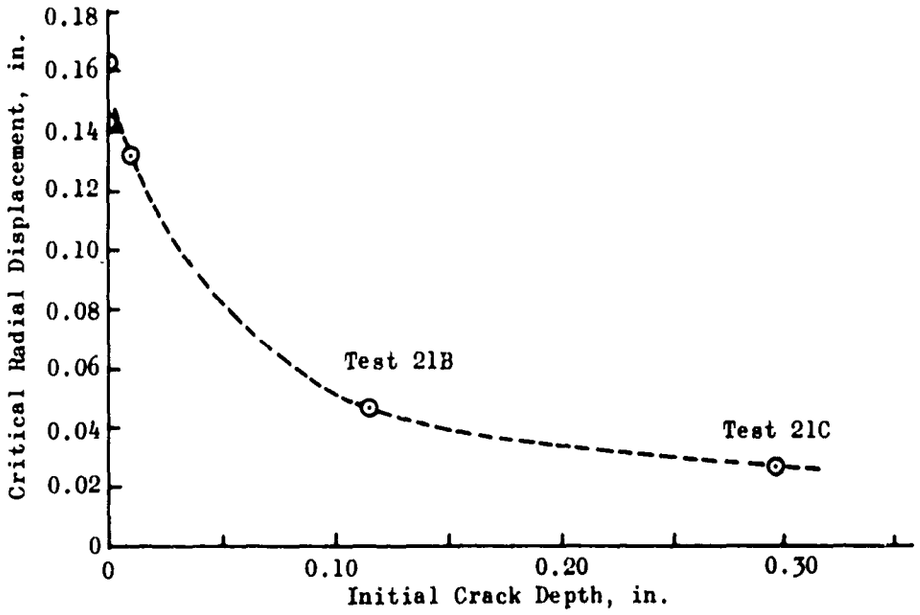

Figure 27. Critical Load vs Initial Depth Solithane Disc Specimens--Circular Port

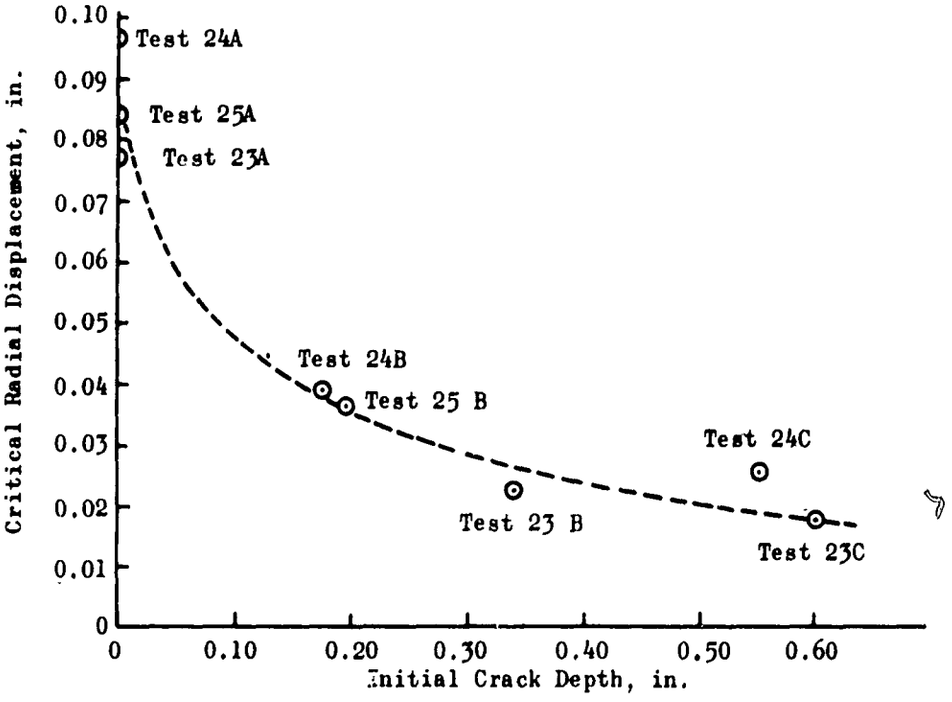

Figure 28. Critical Load vs Initial Crack Depth Solithane Disc Specimens--Star Port

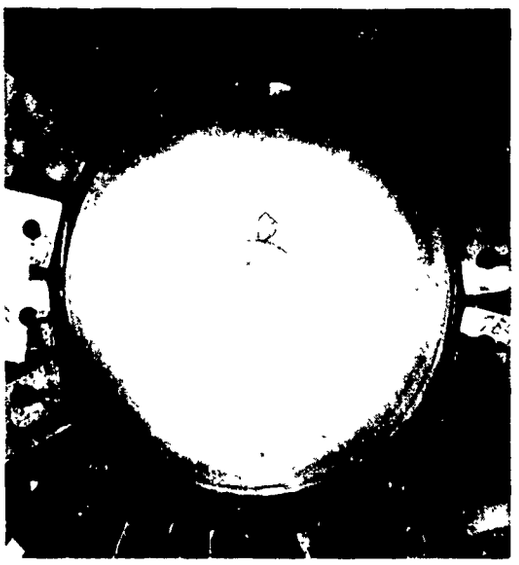

a. Time = 0

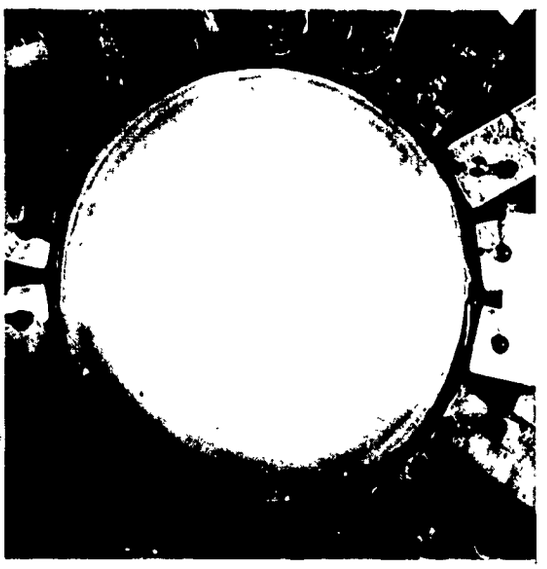

b. Time = 27 minutes

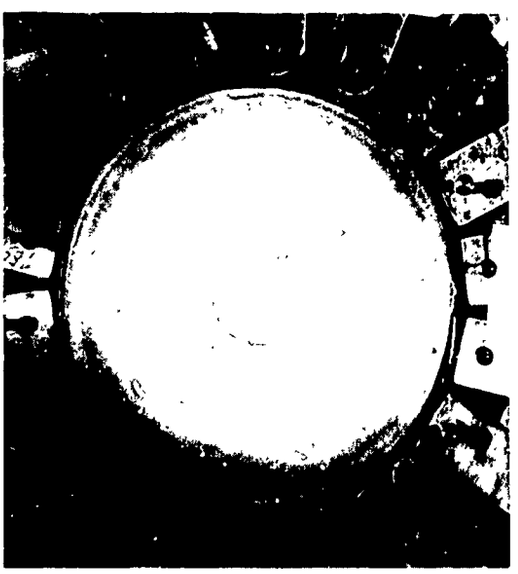

c. Second Test, Time = 0

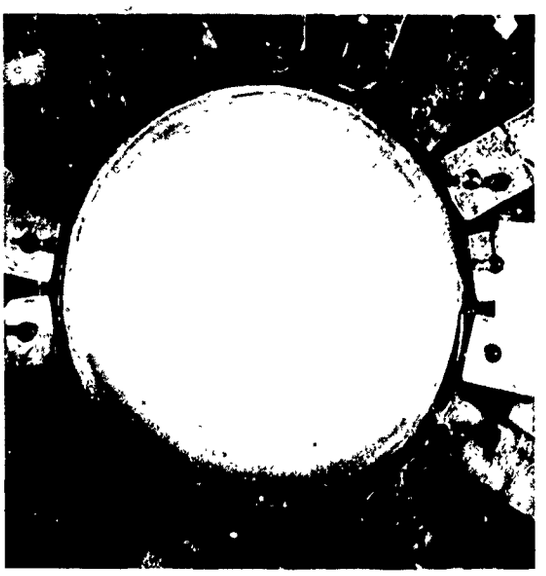

d. Second Test, Time = 17.6 minutes

Figure 29. Solithane As-Cast Circular Port RPL Disc Test, Constant Displacement Rate, Specimen No. 21

e. Second Test, Unloading

f. Third Test, Time = 0

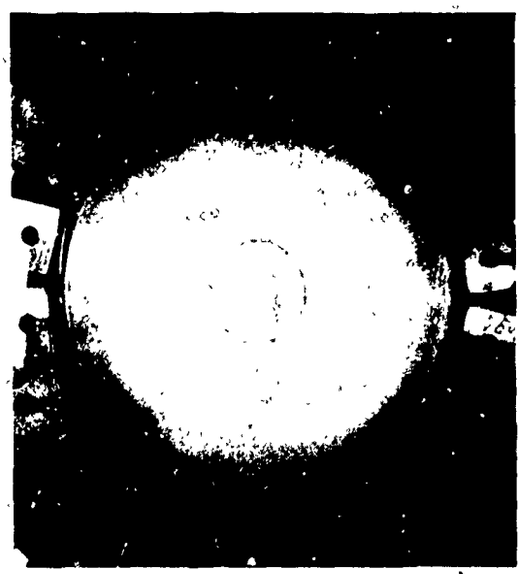

g. Third Test, Time = 8.1 minutes

h. Third Test, Unloading

Figure 29. Continued

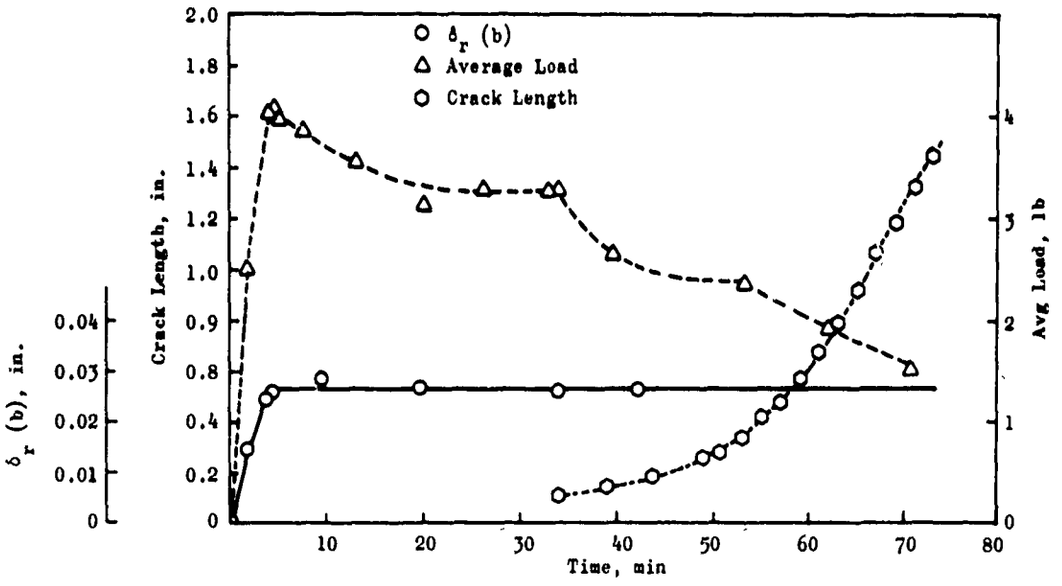

Figure 30. Solithane Circular Port Disc, Test 27

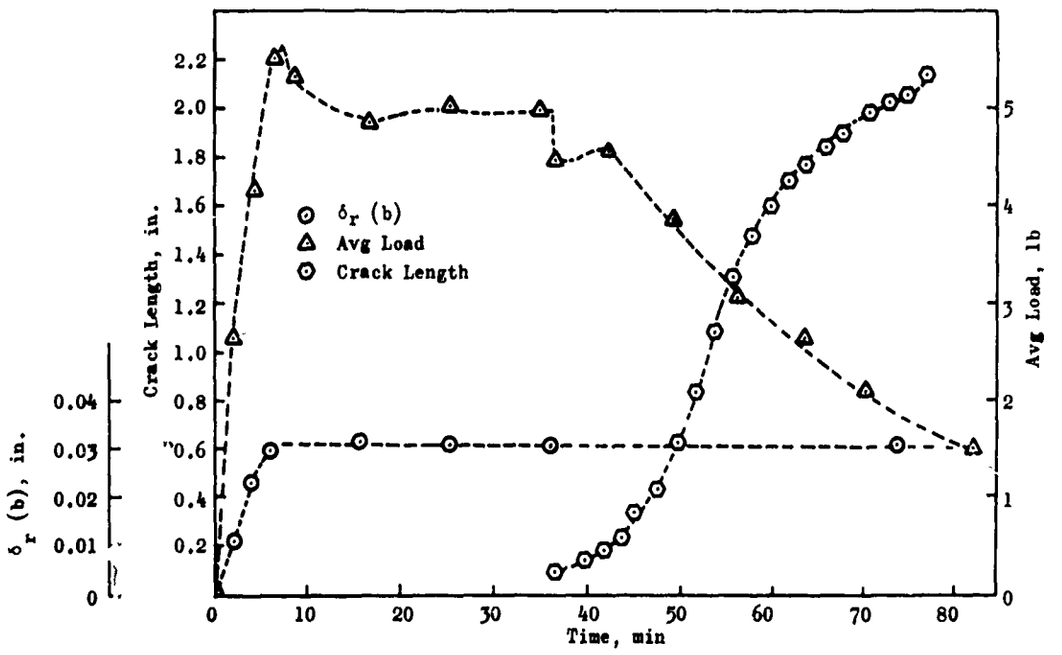

Figure 31. Solithane Constant Displacement Disc, Test 28

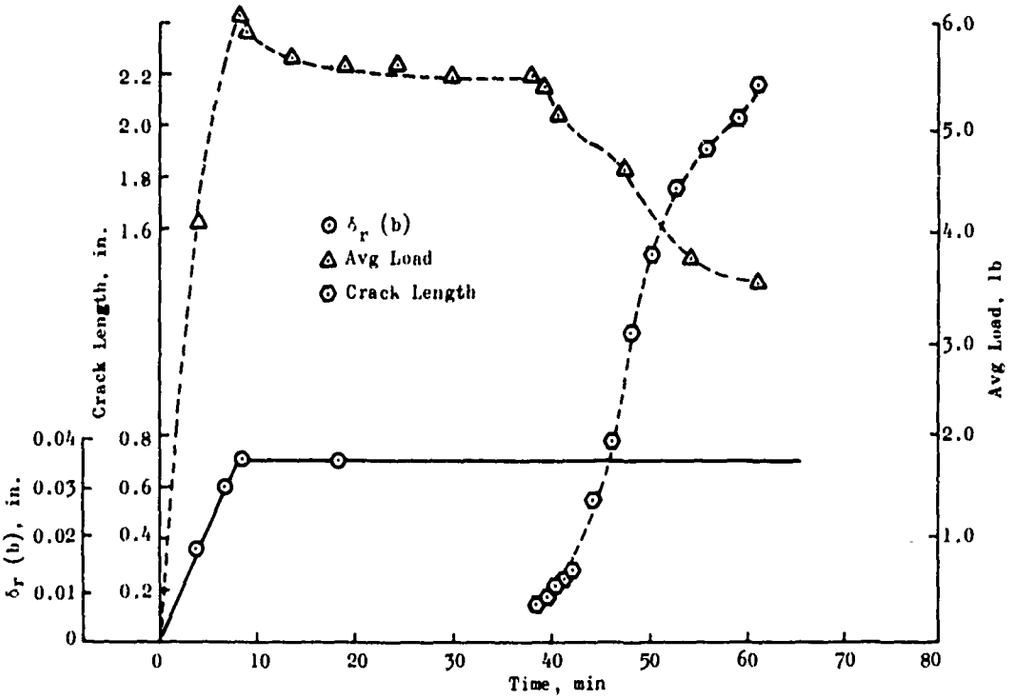

Figure 32. Solithane Circular Port Disc, Test 29, Data Summary

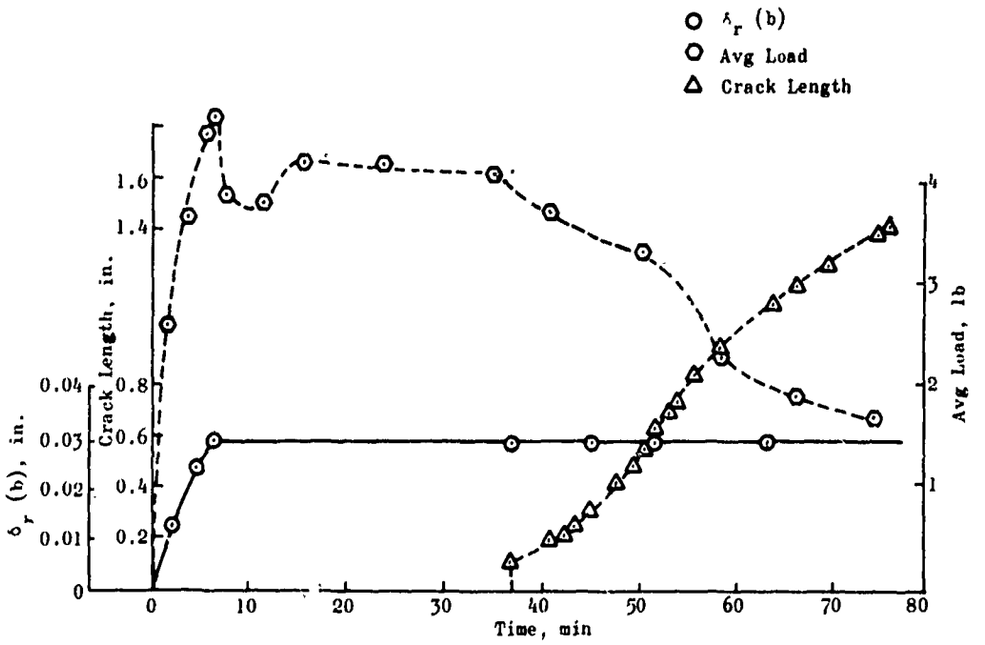

Figure 33. Solithane Star Port Disc, Test 30

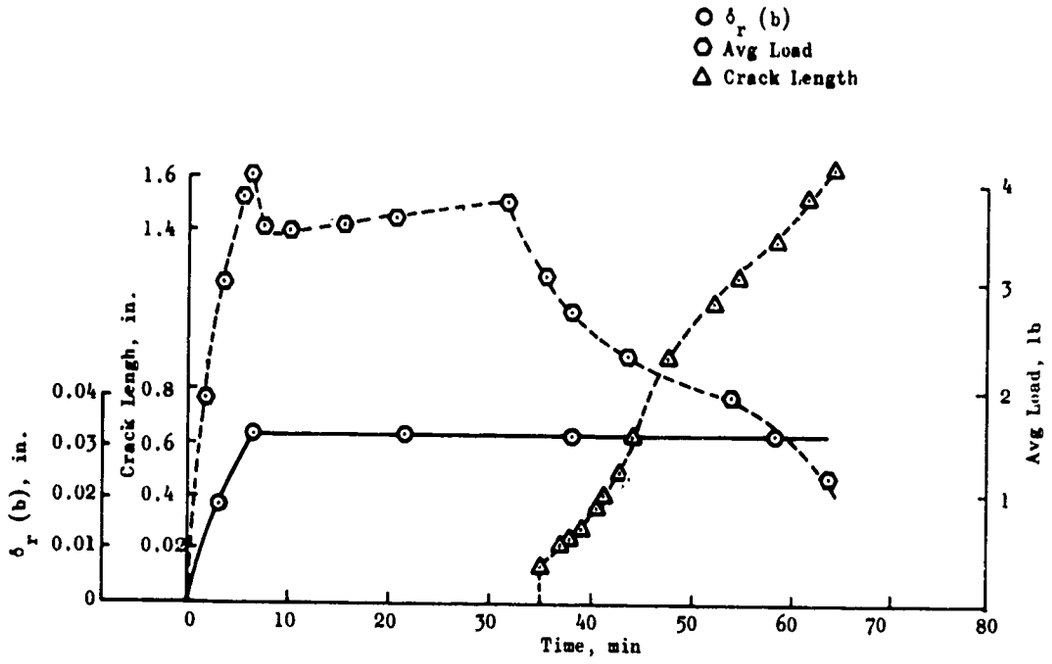

Figure 34. Solithane Star Port Disc Test 31

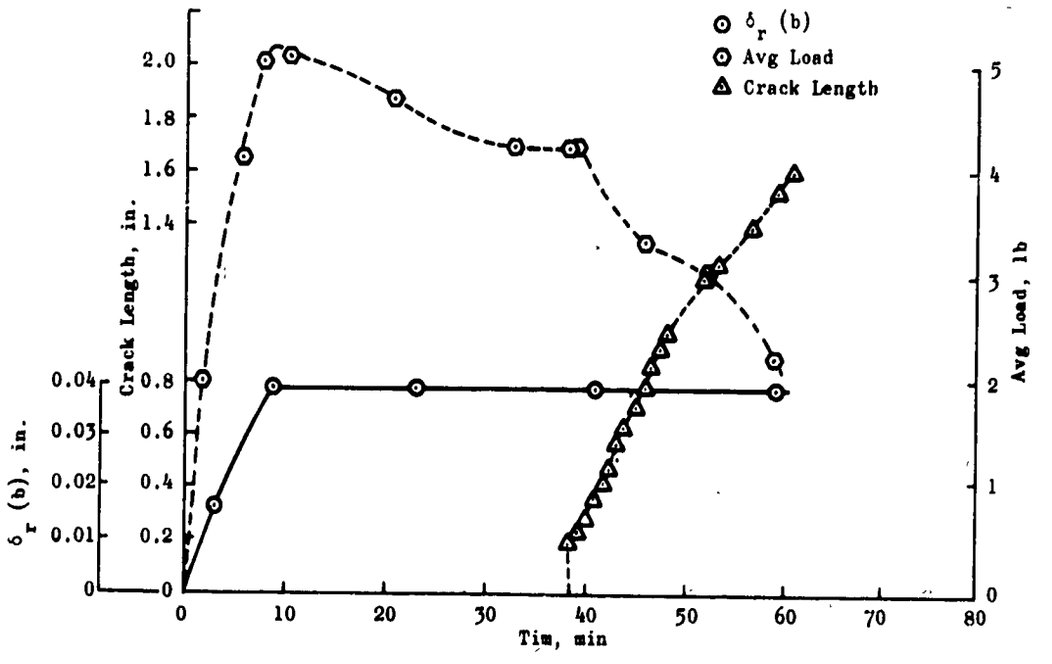

Figure 35. Solithane Star Port Disc Test 32

A second set of specimens, one of each configuration, was used with a photoelastic analysis to evaluate the load distribution arising from loading the discs at 18 discrete points. The stress field was evaluated at radial displacements ranging from 0 to 0.12 inch (Fig. 36). The expected symmetry of the stress field in the disc specimens was noted over the central 50% of the Solithane web at 0.02-inch radial displacement and over 75% at 0.04-inch displacement. At higher levels, the symmetry extended to near the collar edge.

It was concluded from these observations that the specimen analysis in which uniform loading at the boundary is assumed will be legitimate for the study of flaw behavior within the central (constant thickness) region of the specimen.

TPH-1011 PROPELLANT DISC TESTS

Chronologically, the RPL disc tests were first performed on the TPH-1011 propellant specimens prepared by Thiokol. Sixteen tests were conducted although experimental difficulties negated the usefulness of eight of these. Problems encountered were typical of initial effort on a new test concept of this type. The primary difficulty came from debonding of the propellant disc specimens from the load collars. Two tests were ruined when the aerial camera malfunctioned. The eight valid tests, however, provided an abundance of data including crack initiation, trajectory, and growth response.

The first set of tests performed involved deforming the disc specimens at a nearly constant rate of radial displacement and monitoring the load applied as well as the specimen geometric response. The upper surface of the propellant specimens was marked with static rubber beads to provide dimensional reference for the photographs. The first two tests were run on the circular port specimens, and multiple cracks were recorded as seen in Fig. 37 and 38. Data from these two tests are shown in Fig. 39 and 40. Similarly, two star port specimens were tested at an approximate constant radial displacement rate. Again, multiple cracks were noted at failure. Cracks appeared in all the star points, but they progressed toward the collar in only three. Photographs of these two specimens are shown in Fig. 41 and 42. The trajectory of the cracks was of particular interest on these tests. Analysis and prior experimental observations had indicated that the cracks would grow at some angle to a radius through the point of initiation then turn and grow radially toward the collar. Examination of Fig. 41 and 42 confirms this. Actual initial direction relative to the radius through the initiation point and depth to turning are listed in Table VI. The displacement boundary, load response, and crack length are shown as functions of time for these two tests in Fig. 43 and 44.

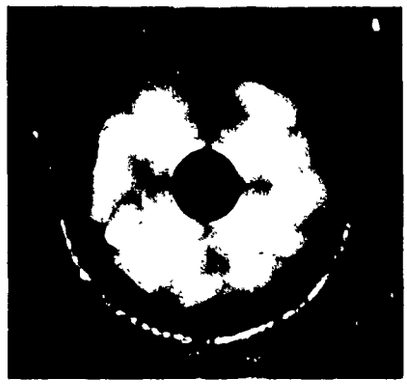

0.00-Inch Displacement
0-Degree Direction

0.02-Inch Radial
Displacement
0-Degree Direction

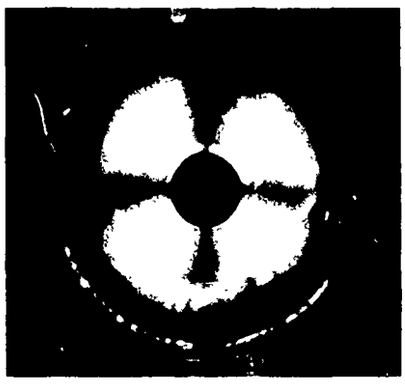

0.04-Inch Radial
Displacement
0-Degree Direction

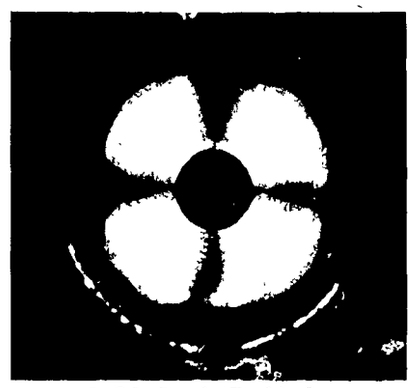

0.12-Inch Radial
Displacement
0-Degree Direction

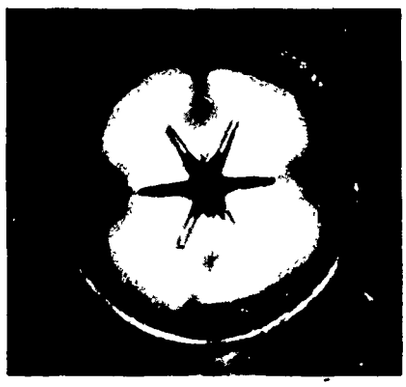

0.04-Inch Radial
Displacement
90-Degree Direction

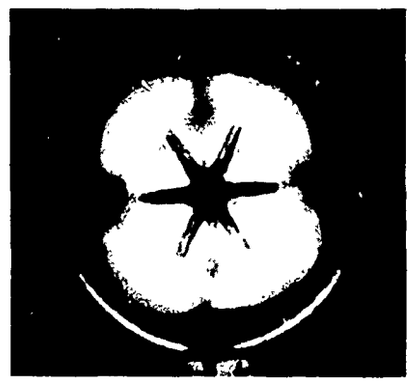

0.08-Inch Radial
Displacement
90-Degree Direction

Figure 36. Photoelastic Isoclonic Survey

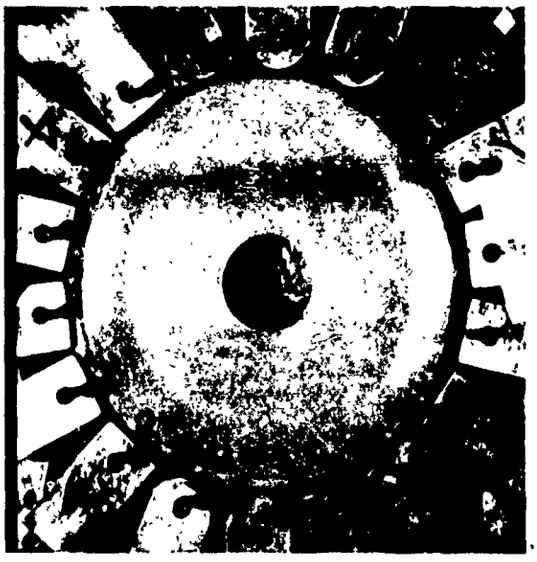

a. Time = 0

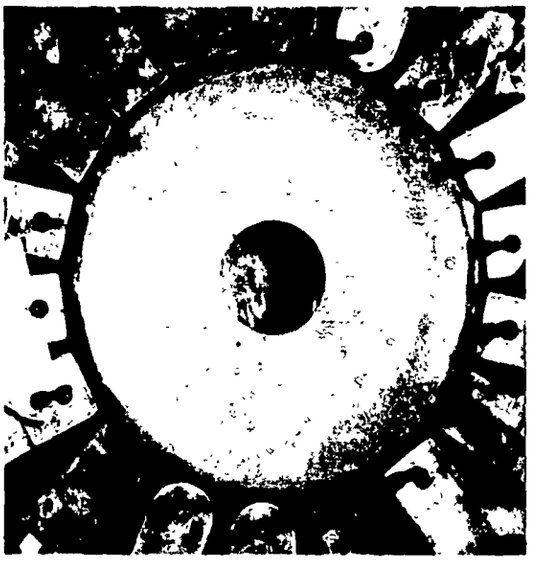

b. Time = 39 minutes

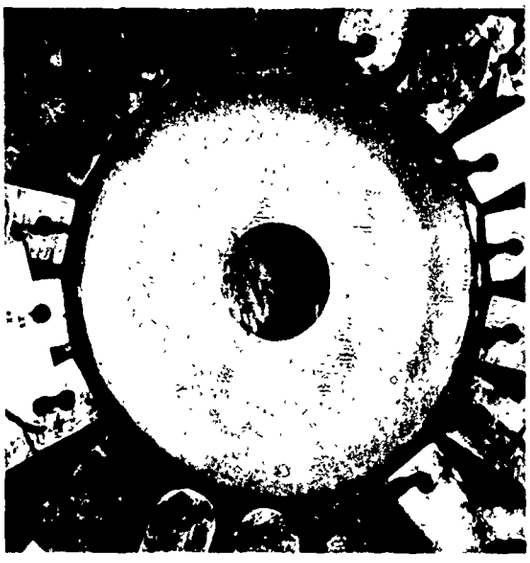

c. Time = 43.5 minutes

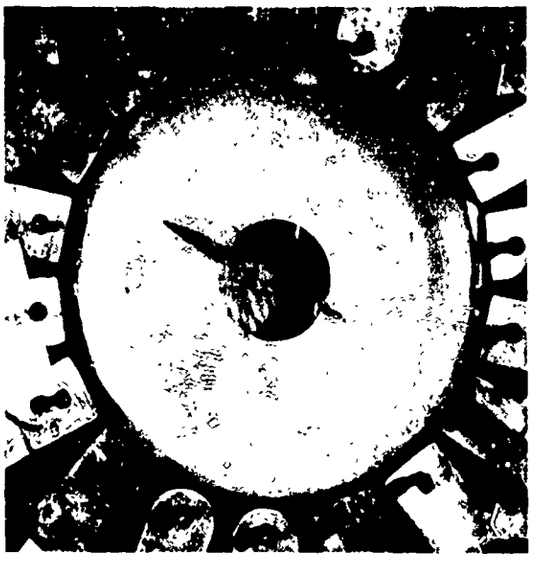

d. Time = 47 minutes

Figure 37. TPH-1011 Propellant As-Cast Circular Port RPL Disc Test, Constant Displacement Rate, Specimen No. 1

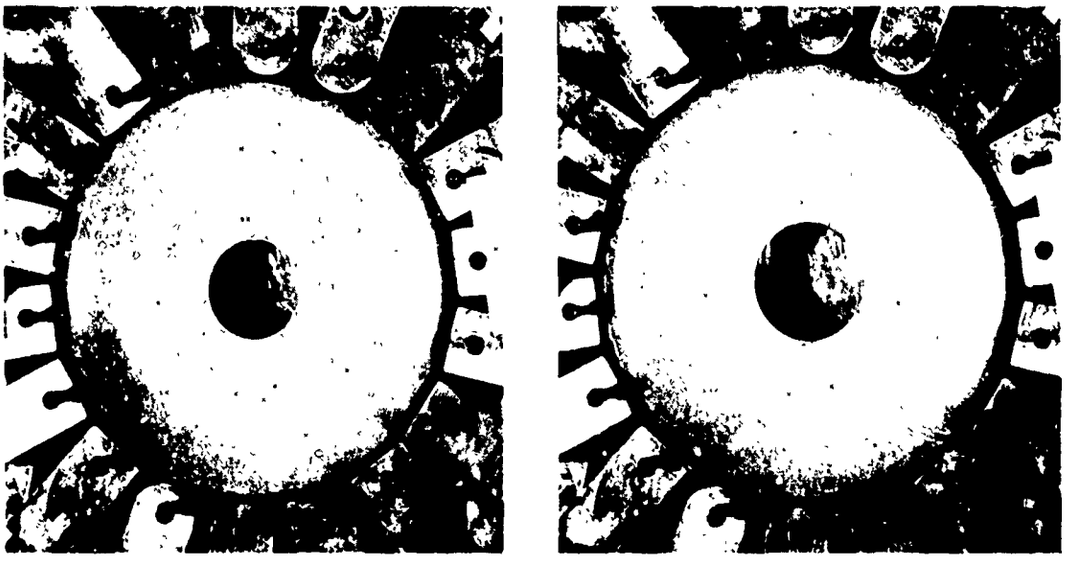

a. Time = 0

b. Time = 42.5 minutes

c. Time = 45.4 minutes

d. Time = 49.3 minutes

Figure 38. TPH-1011 Propellant As-Cast Circular Port RPL Disc Test, Constant Displacement Rate, Specimen No. 2

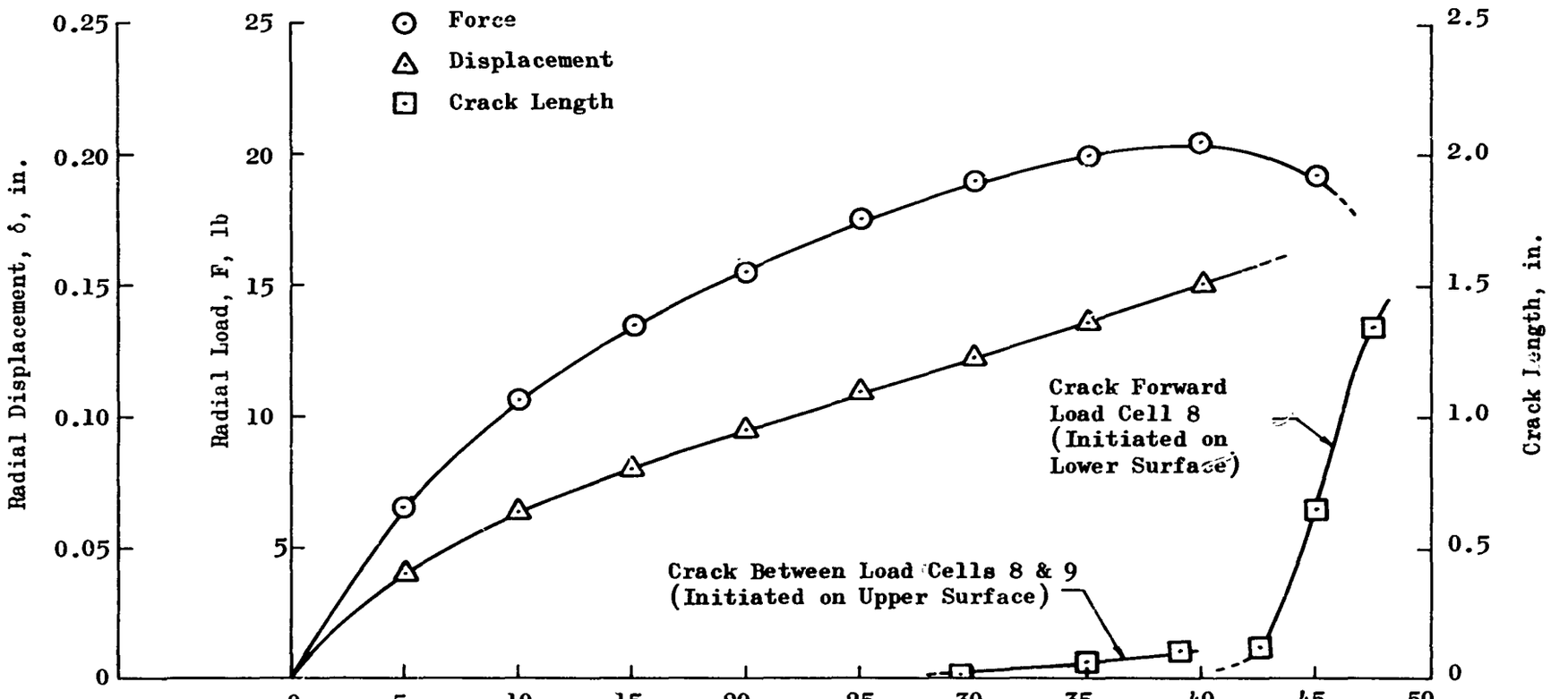

Figure 39. Crack Growth Data, Test 1

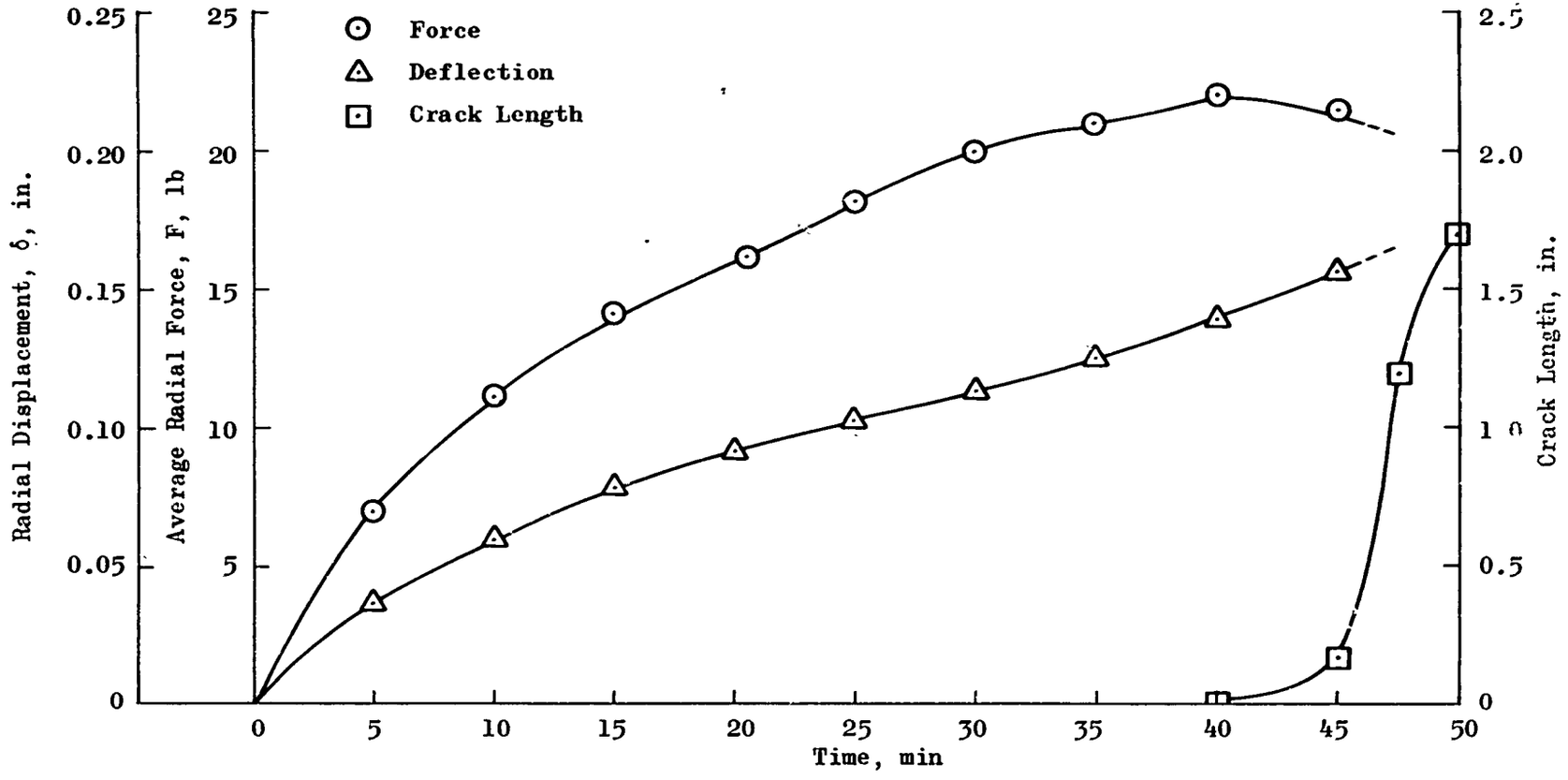

Figure 40. TPH-1011 Propellant Disc Data, Test 2

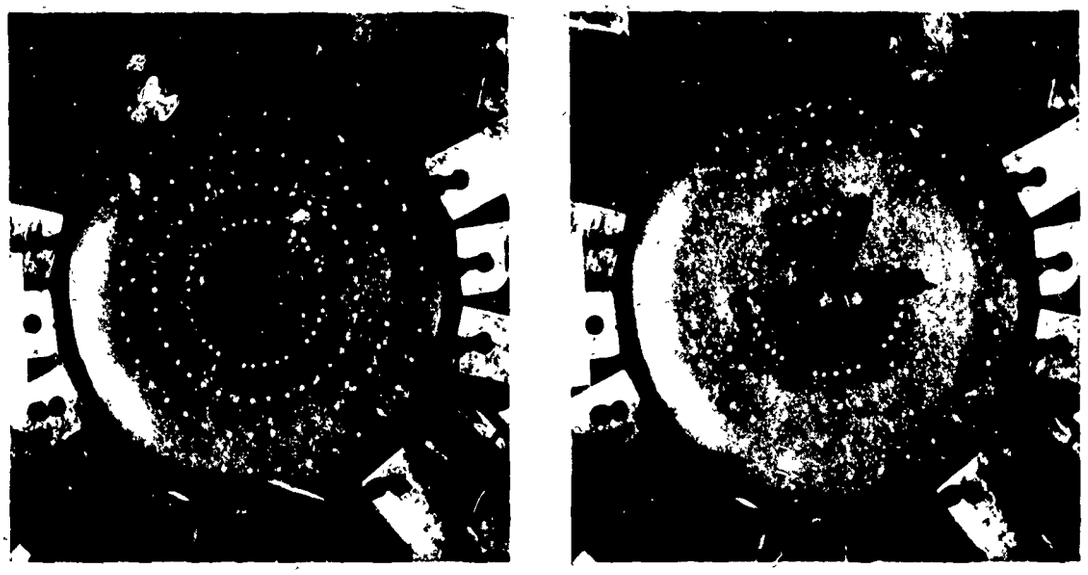

a. Time = 0

b. Time = 29.7 minutes

c. Time = 34.5 minutes

d. Time = 38.6 minutes

Figure 41. TPH-1011 Propellant As-Cast Star Port RPL Disc Test, Constant Displacement Rate, Specimen No. 7

a. Time = 0

b. Time = 26.5 minutes

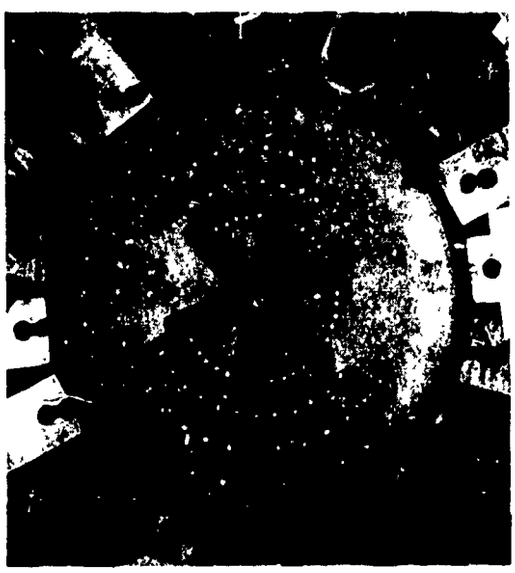

c. Time = 32.4 minutes

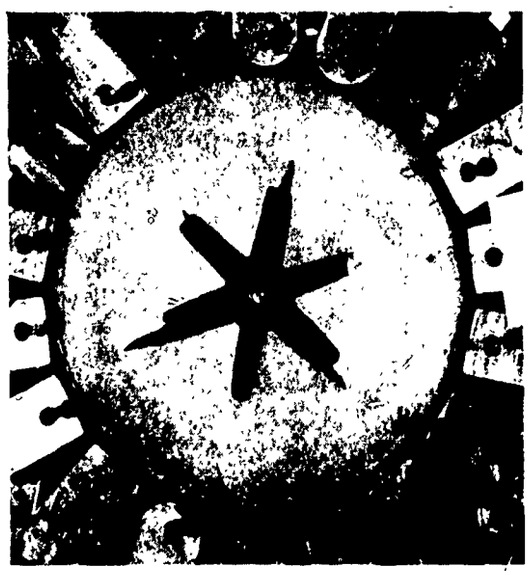

d. Unloading

Figure 42. TPH-1011 Propellant As-Cast Star Port RPL Disc Test, Constant Displacement Rate, Specimen No. 9

TABLE VI

TPH-1011 STAR POINT DISC SPECIMEN

INITIAL TRAJECTORY ANALYSIS

Test 7A1	Initial Trajectory, θ, deg	Depth of Initial Crack Portion, in.
Crack No. 1	~15	0.055
Crack No. 2	~15	0.065
Crack No. 3	~20	0.096
Test 9A		
Crack No. 1	~12	0.080
Crack No. 2	~20	0.090
Crack No. 3	~20	0.050

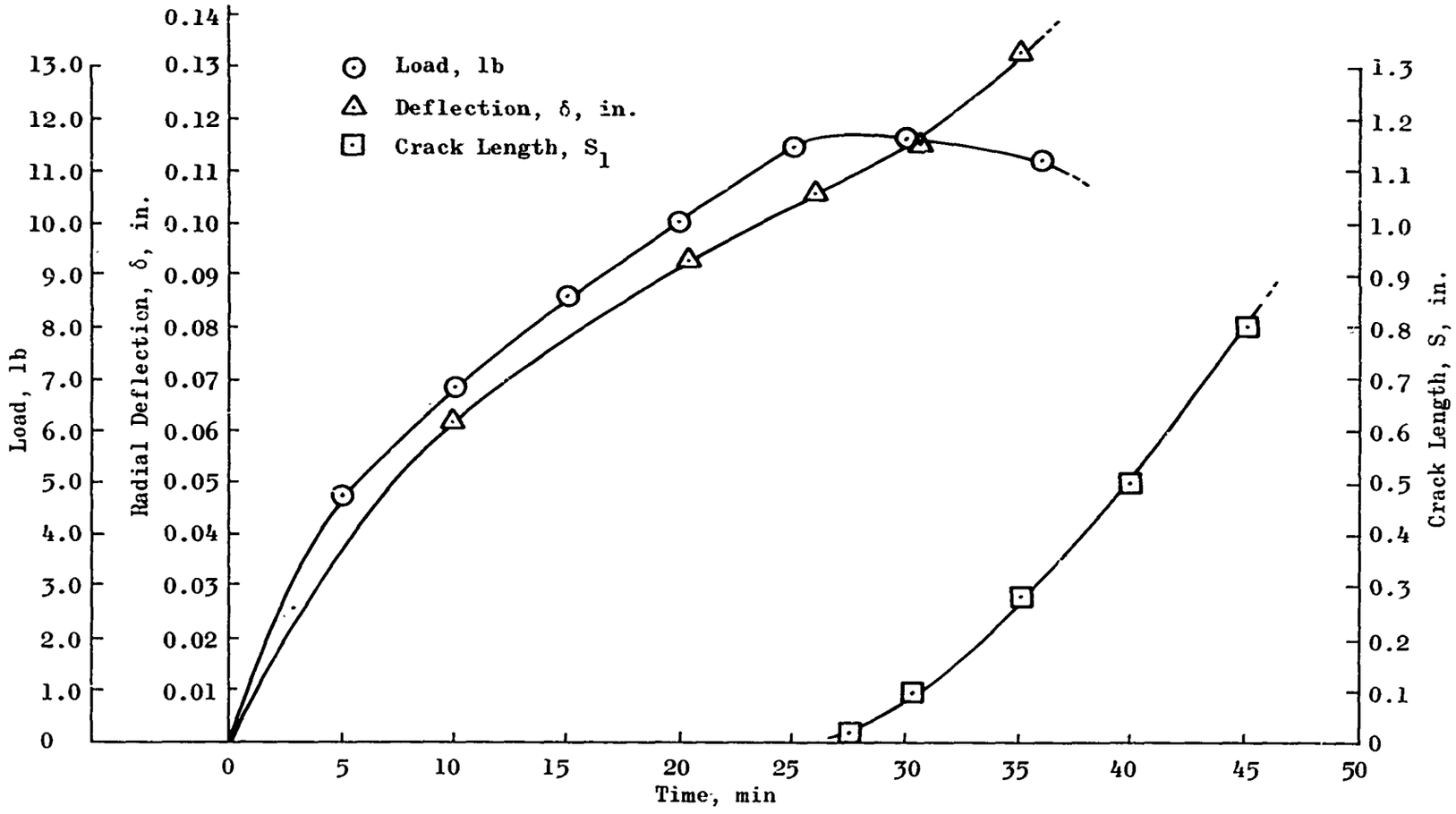

Figure 43. TPH-1011 Propellant Star Port RPL Disc Test Results, Test 7

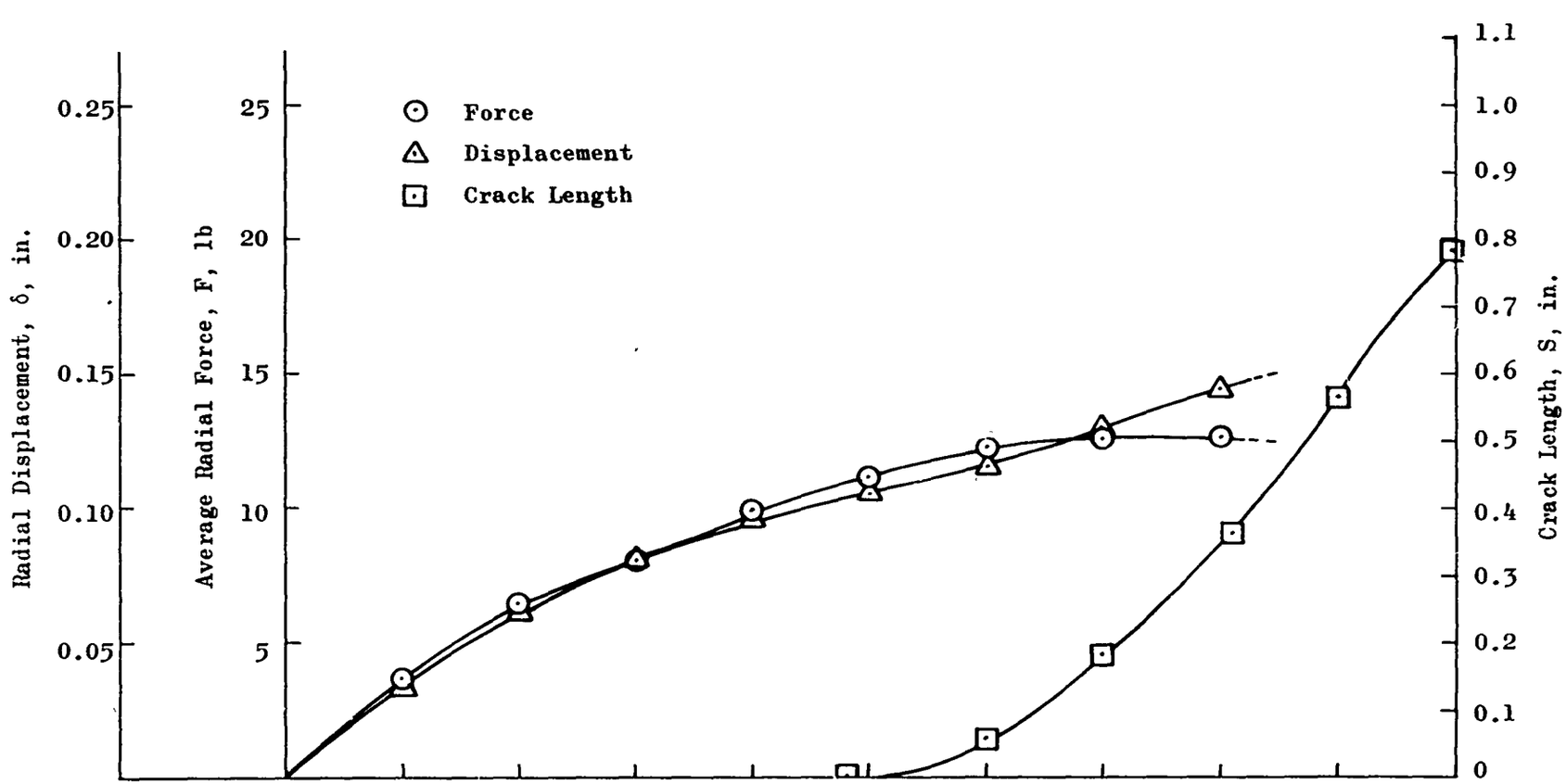

Figure 44. TPH-1011 Propellant Star Port RPL Disc Test Results, Test 9

The next four tests (1 star port, 3 circular port) were conducted with similar load histories to the first four tests, but the specimens were precracked in a controlled manner. These tests were conducted to obtain crack initiation data for a different initial crack depth and to evaluate growth rate. The circular port specimens were cut initially at two diametrically opposed points. The star port specimen was precracked in each star point. Photographs recording the crack growth are shown in Fig. 45 and 46 for one of the circular port specimens and the star port specimen, respectively. The displacement boundary and crack response are shown in Fig. 47--50. Crack initiation data for these eight TPH-1011 disc tests are summarized in Table VII.

The data package for the analytical study consists of the load input, material properties, and specimen responses as monitored in this experimental effort.

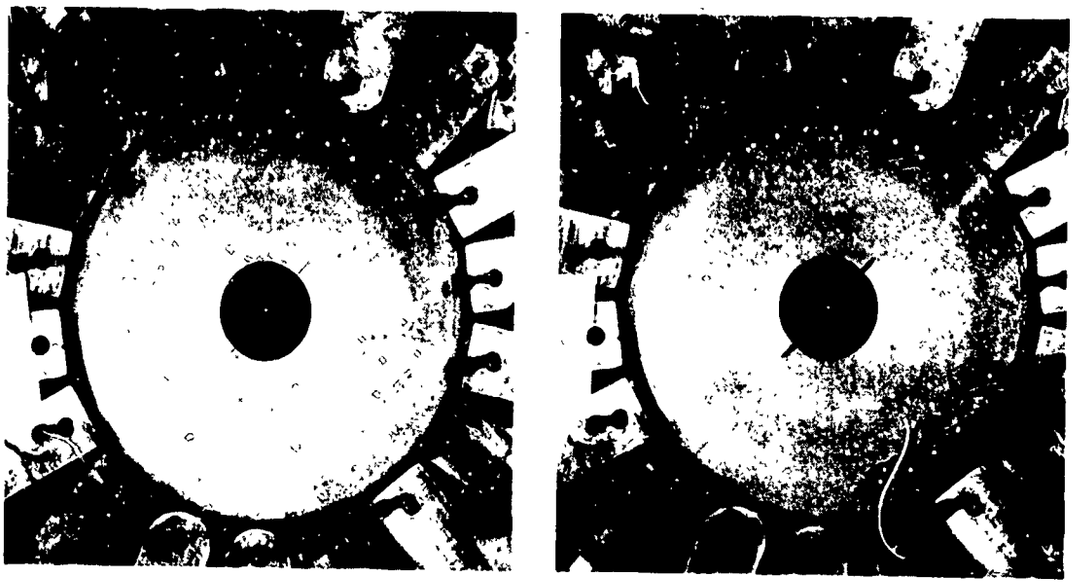

a. Time = 0

b. Time = 7.1 minutes

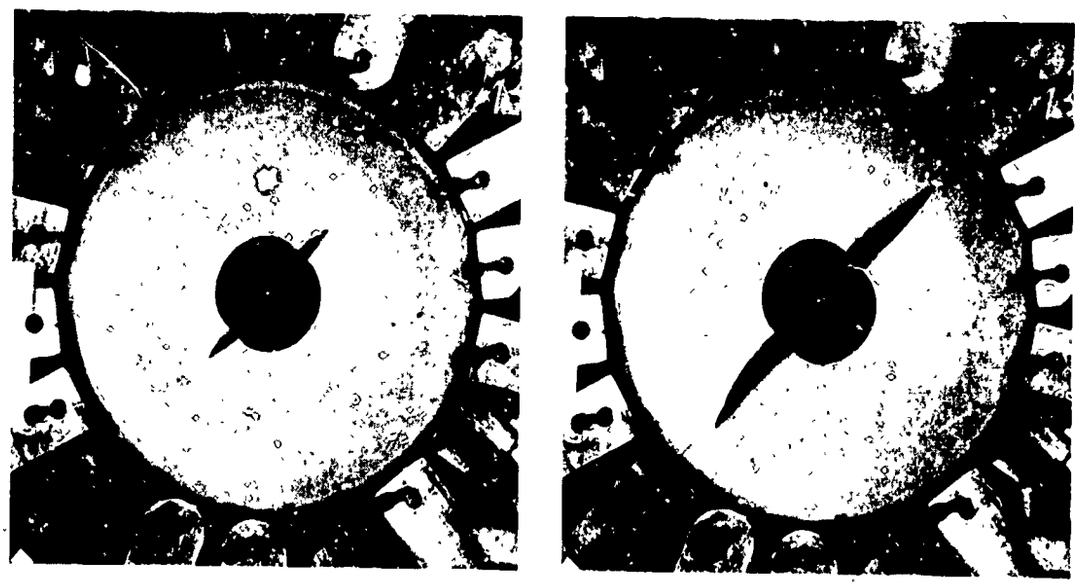

c. Time = 24.8 minutes

d. Time = 42.7 minutes

Figure 45. TPH-1011 Propellant Precracked Circular Port RPL Disc Test, Constant Displacement Rate, Specimen No. 10

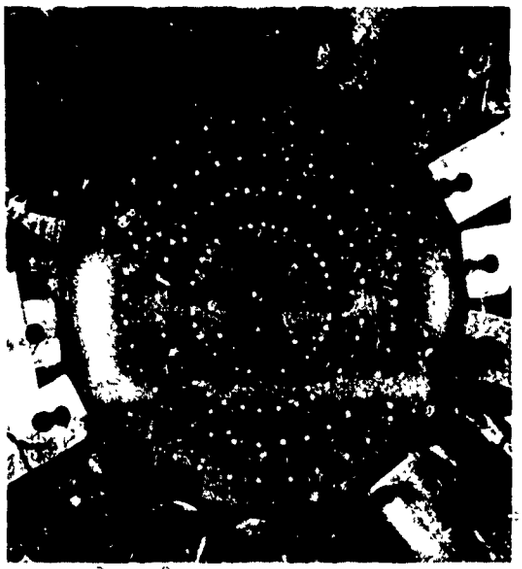

a. Time = 3.4 minutes

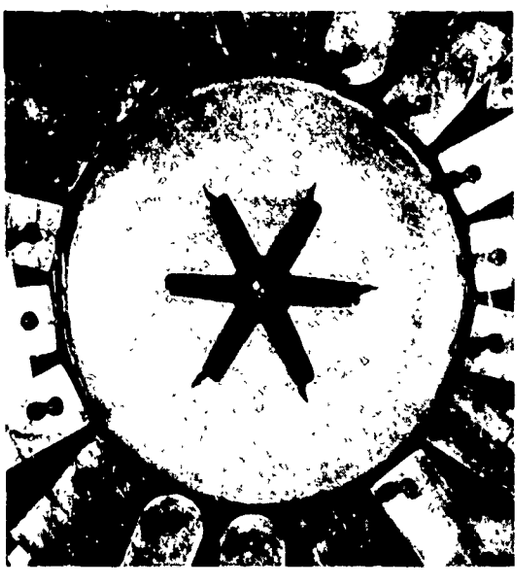

b. Time = 24 minutes

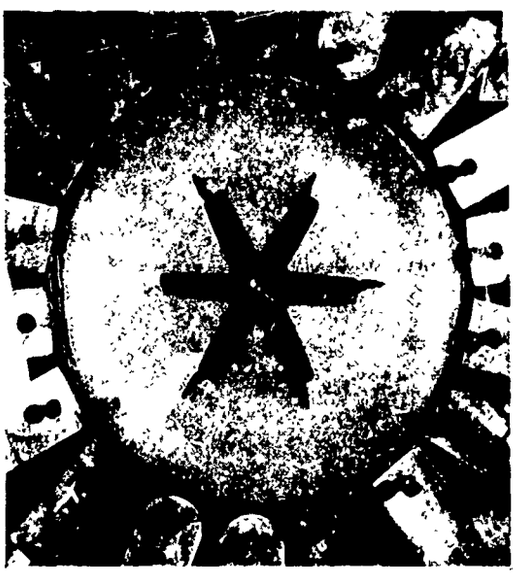

c. Time = 31.9 minutes

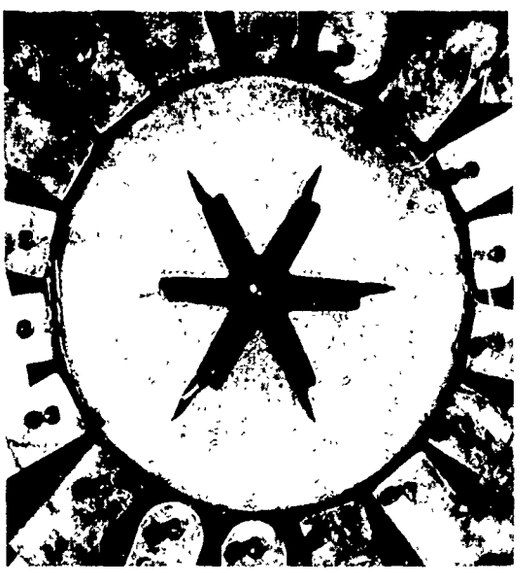

d. Time = 40 minutes

Figure 46. TPH-1011 Propellant Precracked Star Port RPL Disc Test, Constant Displacement Rate, Specimen No. 8

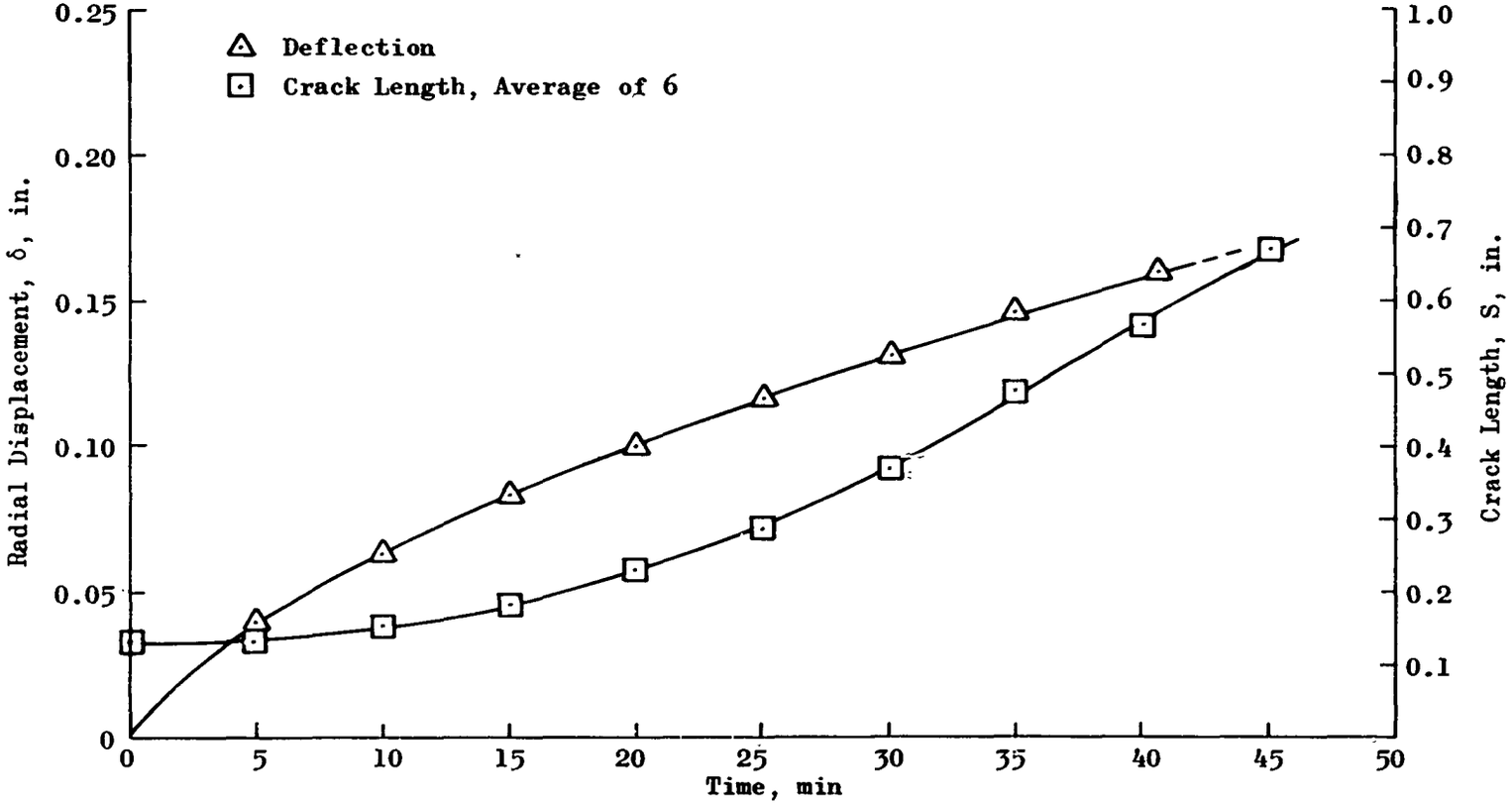

Figure 47. TPH-1011 Propellant Precracked Star Port RPL Disc Test Results, Test 8

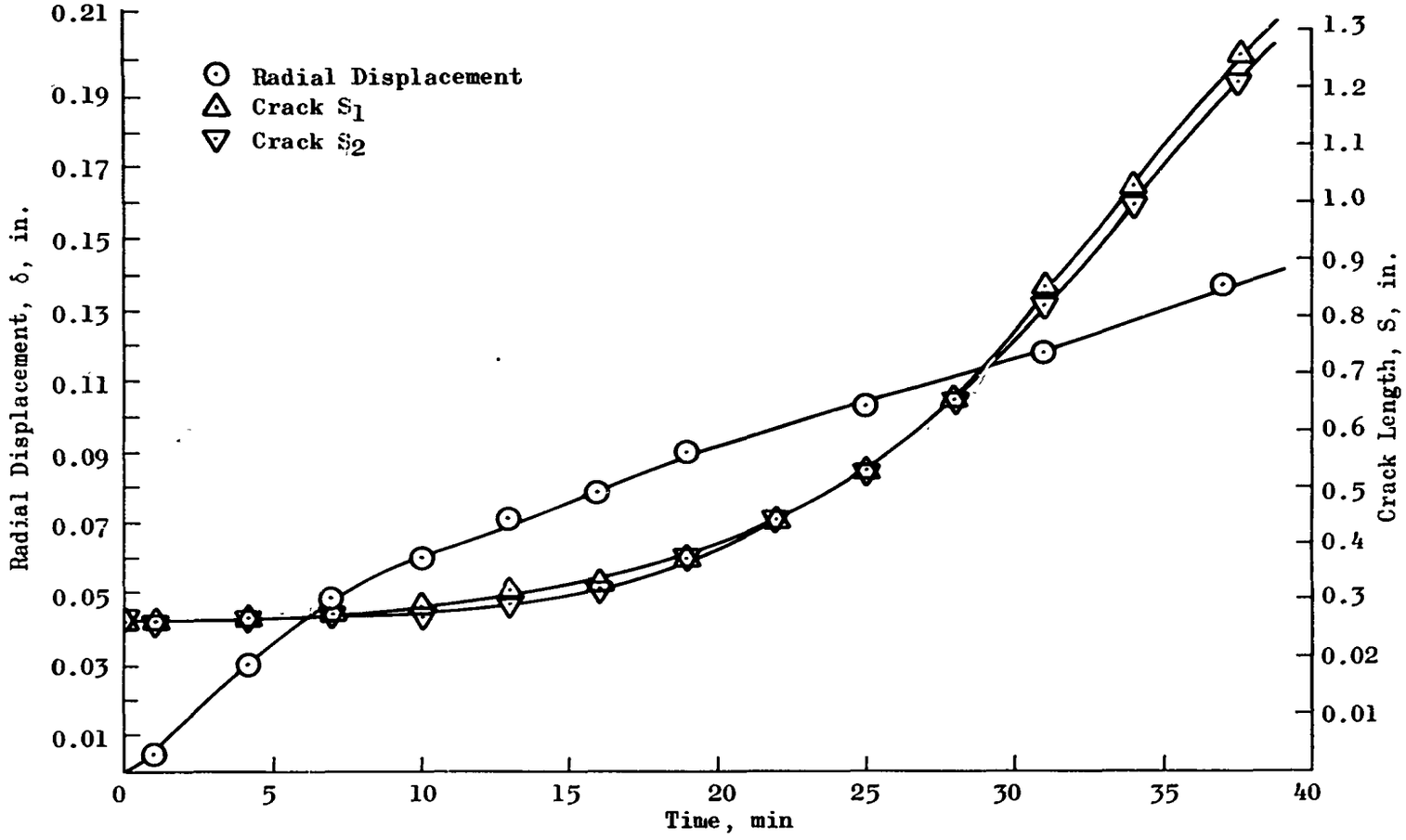

Figure 48. TPH-1011 Propellant Precracked Circular Port RPL Disc Test Results, Test 10

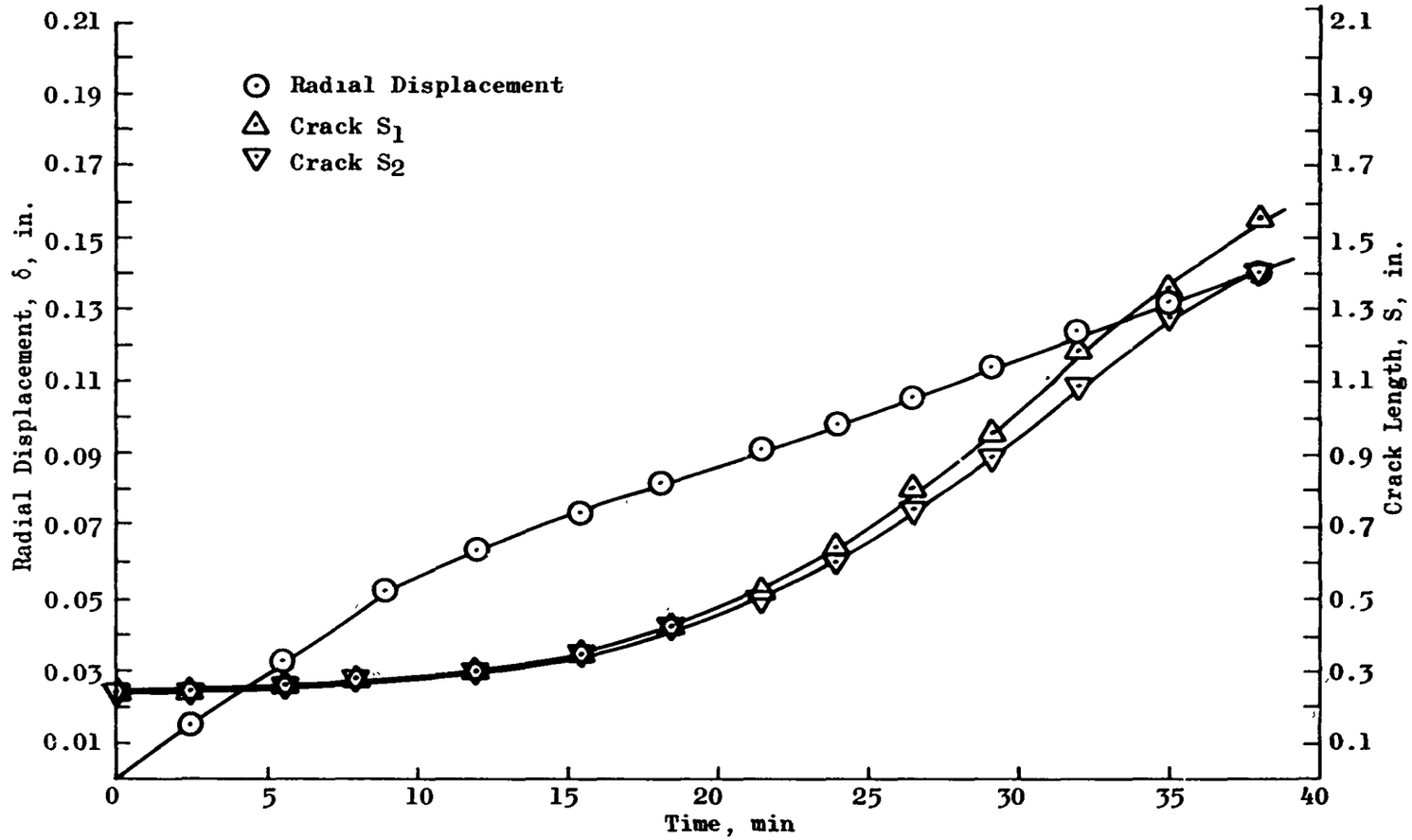

Figure 49. TPH-1011 Propellant Precracked Circular Port RPL Disc Test Results, Test 11

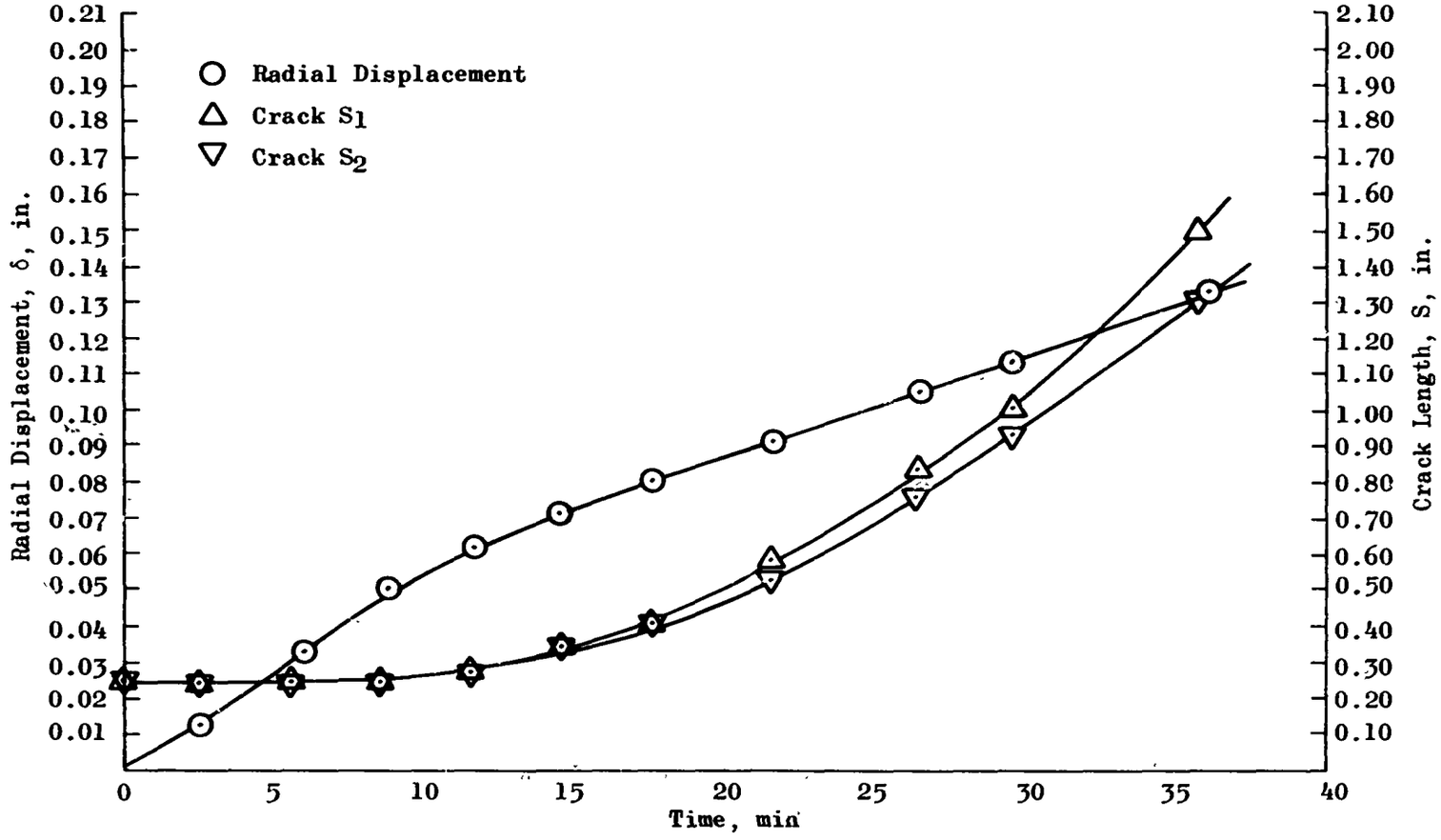

Figure 50. TPH-1011 Propellant Precracked Biaxial Circular Port RPL Disc Test Results, Test 12

TABLE VII

CRACK GROWTH INITIATION DATA FOR TPH-1011

DISC SPECIMEN CONSTANT RATE TESTS

Specimen No.	Initial Crack Depth, c_o, in.	Failure Displacement δ_{cr}[b], in.	Time to δ_{cr} t_o, min
Circular Port			
1A	--	0.119	28.7
2A	--	0.123	33.9
10A	0.262/0.265	0.031	4.1
11A	0.253/0.245	0.033	~ 4.3
12A	0.240/0.240	0.032	5.6
Star Port			
7A	--	0.106	25.6
8A*	0.128-0.156	~ 0.043	~ 6.0
9A	--	0.103	23.5

* All six star valleys were precracked.
Range of initial depths is indicated.

Page 64 is blank

SECTION IV. ANALYSIS OF TEST RESULTS

The analytical effort is directed toward interpretation of the data generated experimentally and evaluation of the validity of fracture mechanics concepts to the prediction of flaw growth initiation, propagation, and trajectory. Characterization of the materials being studied is essential to the analysis. Given the material properties and the test conditions, we shall examine, analytically, the response of the specimens to those conditions.

MATERIAL PROPERTIES (TPH-1011 PROPELLANT)

The propellant used on this program is TPH-1011, an 86% solids loaded PBAN composition, manufactured by Thiokol Chemical, Wasatch. Mechanical characterization data were obtained from Thiokol and verified in strip biaxial relaxation tests at Rocketdyne as described in the experimental section. The relaxation modulus as reported by Thiokol for uniaxial specimens is represented by Eq. 33 for 77 F behavior as

$$\log E_{rel} = 2.538 - 0.1232 \log (t) + 0.01292 \log^2(t) - 0.0006608 \log^3(t)$$

A modified power law of the form

$$E_{rel}(t) = E_e + \frac{E_g - E_e}{(1 + t/\tau_o)^n} \qquad (37)$$

was obtained to represent the modulus. The best fit was obtained with

Glassy modulus, E_g = 100,000 psi
Rubbery modulus, E_e = 100 psi
Log-log slope, n = 0.166
Relaxation characteristic, τ_o = 2.368×10^{-16} min

So that Eq. 3 becomes

$$E_{rel}(t) = 100 + 9.99 \times 10^4 \, (1 + 4.223 \, t \times 10^{15})^{-0.166} \qquad (38)$$

For comparison, Eq. 33 and 38 are plotted in Fig. 51.

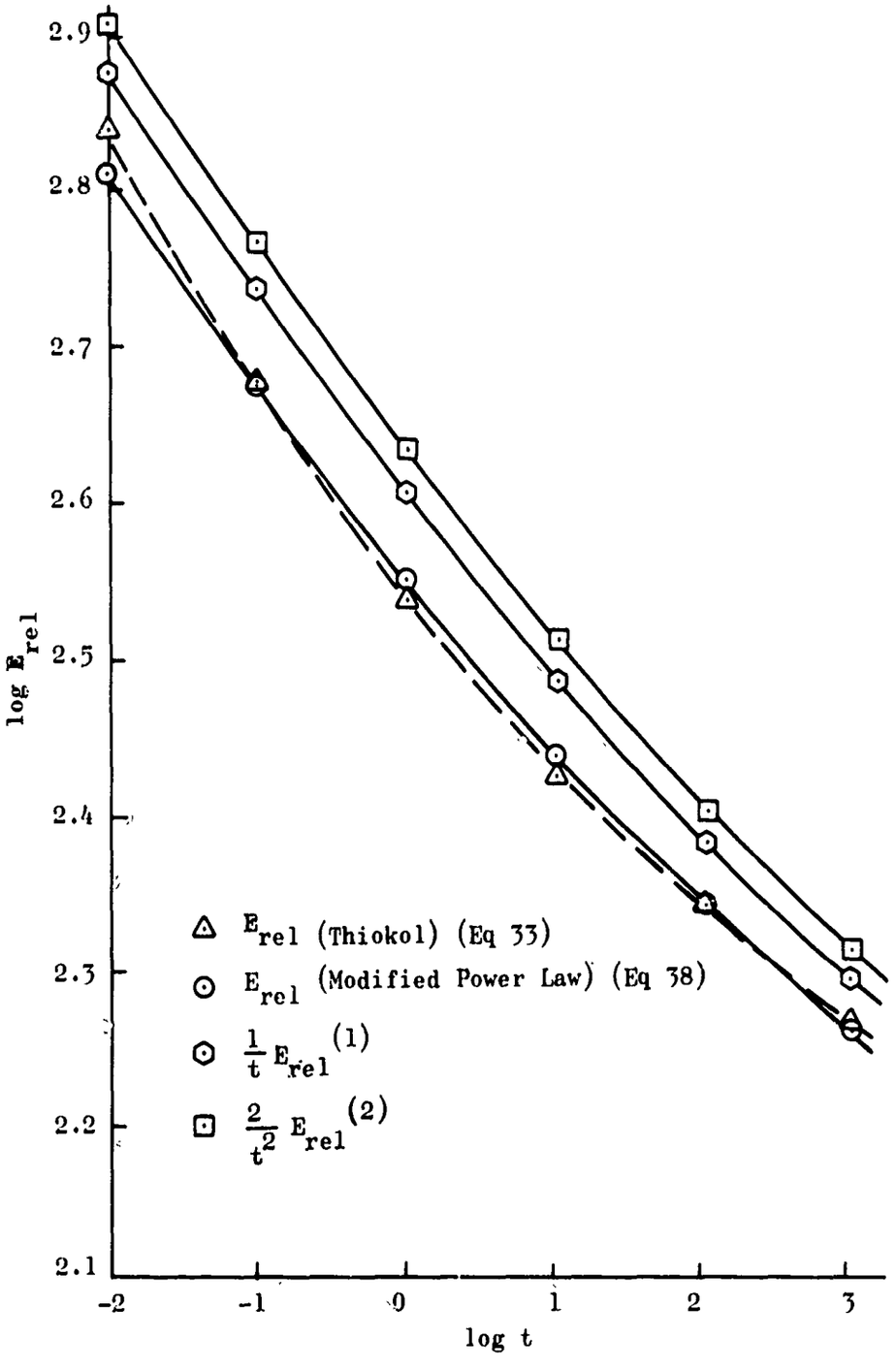

Figure 51. TPH-1011 Uniaxial Relaxation Behavior

A quantity of importance in the constant rate problem is the "second time-averaged" relaxation modulus, $\frac{2}{t^2} E^{(2)}_{rel}(t)$, where the superscript refers to the double time integral of the relaxation modulus. Using the modified power law representation we obtain

$$\frac{2}{t^2} E^{(2)}_{rel}(t) = E_e + \frac{2(E_g - E_e)}{(2-n)(1-n)} \left(\frac{\tau_o}{t}\right)^2 \left[\left(1 + \frac{t}{\tau_o}\right)^{2-n} - 1\right] - \frac{2(E_g - E_e)}{1-n} \left(\frac{\tau_o}{t}\right) \tag{39}$$

which gives, for TPH-1011 propellant,

$$\frac{2}{t^2} E^{(2)}_{rel}(t) = 100 + 7.324 \times 10^{-27} \left(\frac{1}{t}\right)^2 \left[\left(1 + 4.223t \times 10^{15}\right)^{1.834} - 1\right] - 5.673 \times 10^{-11} \left(\frac{1}{t}\right) \tag{40}$$

This quantity is also shown in Fig. 51.

Other properties of interest for the analysis include the uniaxial strain capability, shown in Fig. 52, taken from Ref. 27. For comparison and later reference, the uniaxial strain at corrected maximum stress (Ref. 28) is shown in Fig. 53. Characteristic energy release rates γ_c and γ_a (cohesive and adhesive) were discussed previously. The other quantity required for analytical investigation--the Poisson's ratio--was taken as 0.499 in the finite element analyses and 0.5 in the exact or closed-form analyses. This assumption has little effect on the disc specimen result due to the essentially plane-stress nature of the specimen.

Liner properties, including a modulus (elastic) of 150 psi and a Poisson's ratio of 0.4999, were assumed for the peel test.

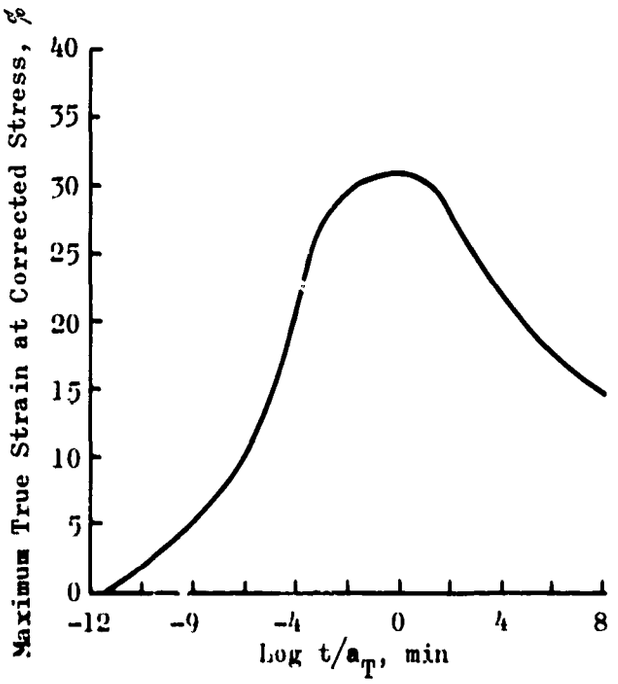

Figure 52. TPH-1011 Propellant Uniaxial Strain Capability

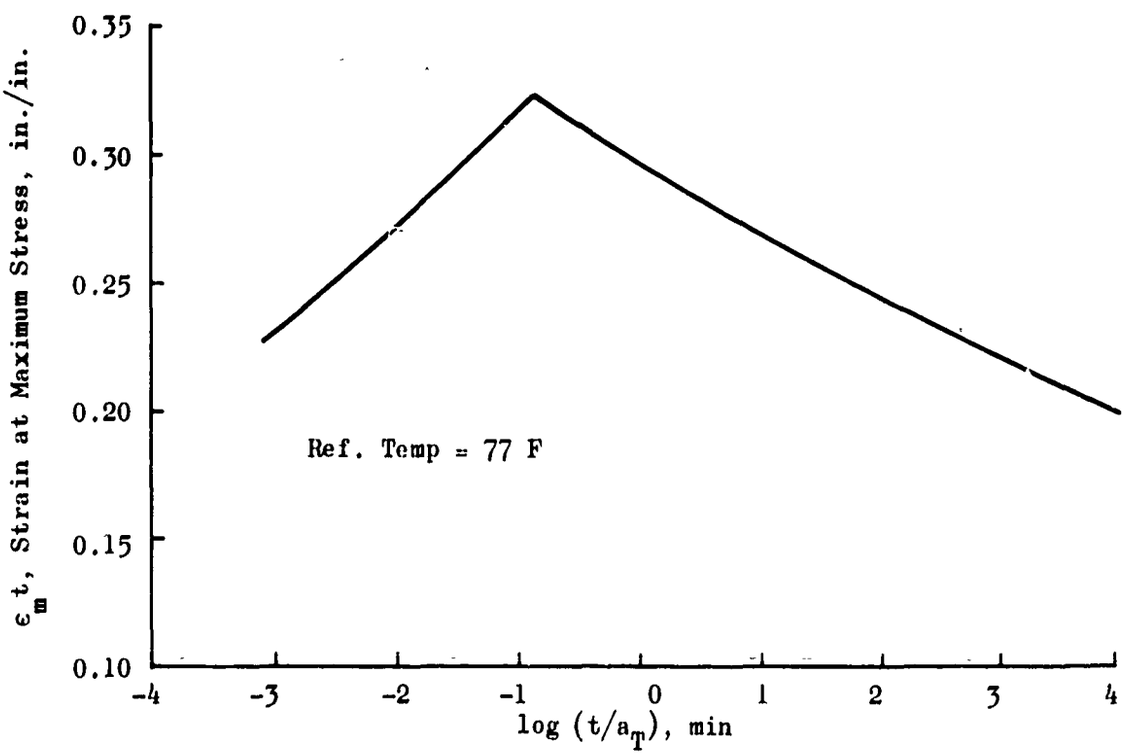

Figure 53. Uniaxial Strain at Maximum Stress, TPH-1011 Propellant (Ref. 28)

MATERIAL PROPERTIES (SOLITHANE 50/50)

Similar properties were obtained for Solithane 113 in a 50/50 (resin-hardener ratio) composition. Solithane 113 is a photoviscoelastic cross-linked polyurethane used as an interim standardized rubber for experimental and theoretical research purposes. The Solithane specimens were cast at UTC, Sunnyvale; but the material characteristics used in this analytical effort were those reported by Knauss and Mueller (Ref. 29). As for the TPH-1011 propellant, the Solithane relaxation data were shifted to 77 F and fitted to a modified power law, Eq. 33, by taking

$$E_g = 31{,}425 \text{ psi}, \; E_e = 425 \text{ psi}, \; n = 0.70, \; \tau_o = 1.635 \times 10^{-9} \text{ min}$$

which gives the curve shown in Fig. 54. The "second time-averaged" relaxation modulus was computed from the modified power law representation resulting in the representation also shown in Fig. 54. The creep compliance for Solithane 113 (50/50) from Ref. 29 is shown in Fig. 55. Also, for later reference, the uniaxial strain capability is presented in Fig. 56.

The fracture energy of Solithane 113 has been characterized by Mueller (Ref. 26) for the lower limit value using Toluene-swollen Solithane 113. He determined, for this lower limit, a value of $\gamma_c = 0.0321$ in.-lb/in.^{2}. Other values (quoted but unpublished) set a nominal range of γ_c for 50/50 Solithane as being between 0.7 and 1.2 in.-lb/in.^{2}.

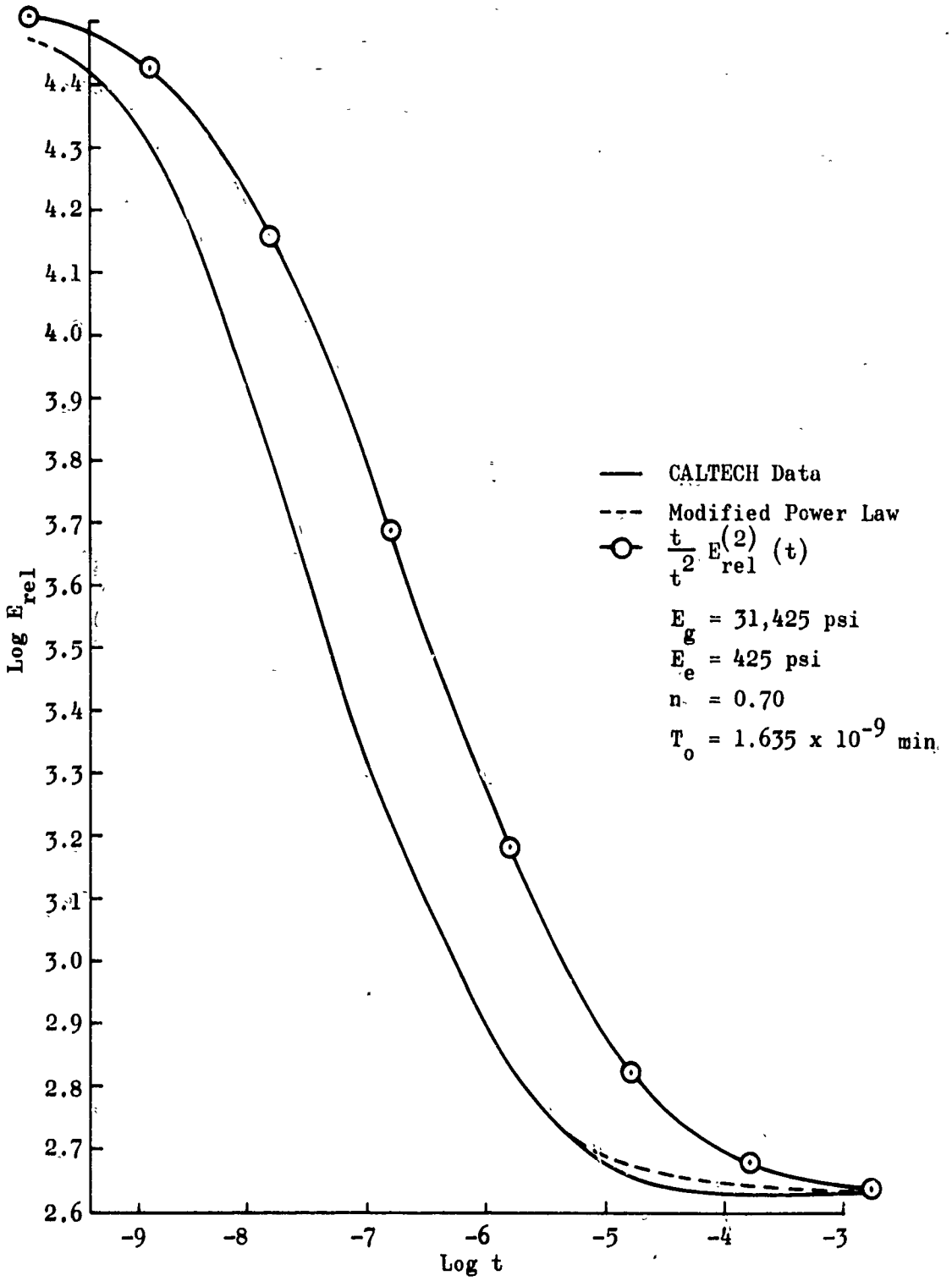

Figure 54. Solithane 113 50/50, 77 F Relaxation Modulus

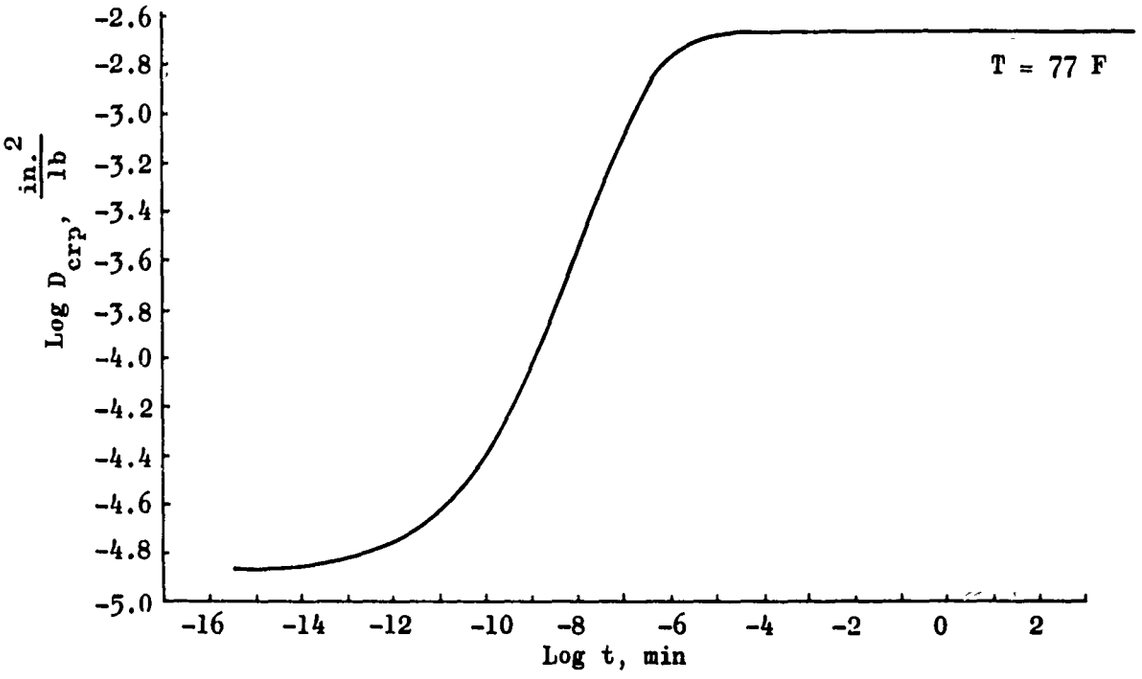

Figure 55. Creep Properties of Solithane 50/50

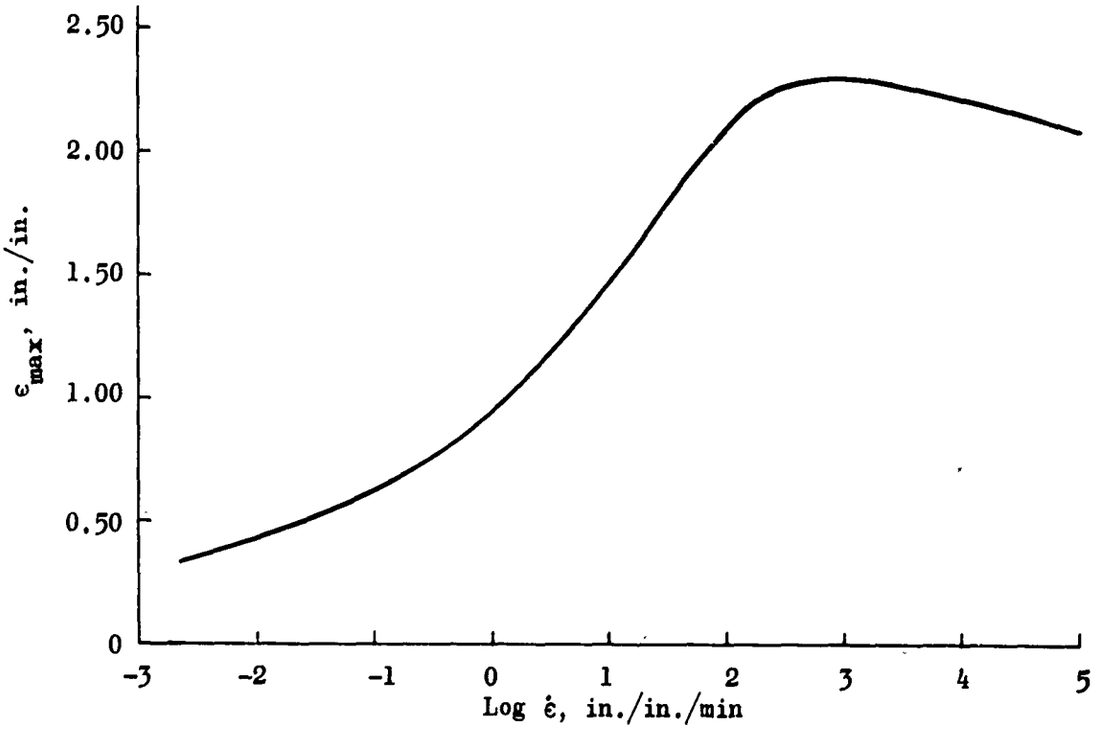

Figure 56. Solithane (50/50) Failure Strain, 77 F (Ref. 29)

MATERIAL PROPERTIES (DISC SPECIMEN LOAD COLLAR)

Interaction between the rubber load collar for the RPL test specimen and the propellant or Solithane disc merits calibration of the collar for use in analysis. The material used in the collar, a carbon-black filled ethylene propylene terpolymer (EPT) rubber used at Rocketdyne as a liner/restrictor material, was characterized in uniaxial tension at 77 F. The modulus (nearly time independent) at 100% strain was found to be 202 psi while the average modulus to approximately 500% strain was 378 psi. Since the strains will be less than 10%, the lower value of 202 psi is indicated. Verification testing was done on the load collar itself. A radial displacement rate of 0.00275 in./min was applied to the collar on the RPL device. The deflection vs load response was recorded. Figure 57 shows this relationship (load average for the nine load cells) for two consecutive tests on one collar. At the same time, a finite element elastic analysis was performed in which deflection resulting from applied loads was determined as a function of rubber modulus. The 200 psi modulus gave the best fit at 10-pound load (~0.45-inch radial deflection) as shown in Fig. 52. At the 6-pound load level (δ_r (b) ~0.20 inch) the elastic modulus is about 258 psi. The rubber material is taken to be incompressible under the conditions analyzed.

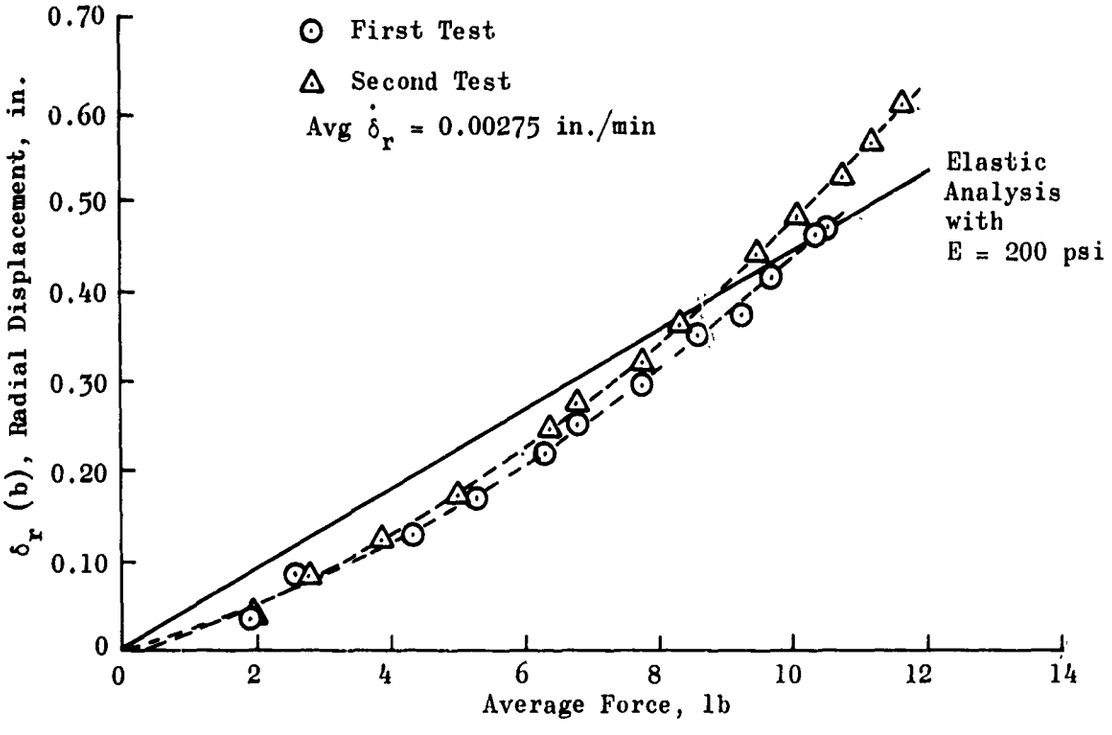

Figure 57. Collar Load-Deflection Measurement at 77 F

BLISTER PEEL TEST ANALYSIS

The initial data analysis of the blister peel test results was based on simplifying assumptions which neglected effects of finite propellant thickness and the pressure of the liner interlayer. For establishing feasibility of the experimental approach to bond failure characterization, this level of analysis is sufficient. To provide the basis for future development of the test technique, however, a detailed examination of the effects of propellant layer thickness and of the elastic interlayer (liner) is in order. A closed-form type analytical approach has been attacked by Jones and Williams (Ref. 24, 25, and 30). A finite element elastic computer solution was obtained for the specific geometry tested at SRD on this program. These analyses are summarized in the following paragraphs.

Consider a circular rod of incompressible elastic material bonded to a rigid plate with air injected through a hole in the rigid plate into a circular unbond between the rod and plate. From an energy analysis, the pressure at which the unbond will begin to grow is given by (Ref. 31):

$$P_{cr} = \sqrt{\frac{2\pi E \gamma_a}{3c}} \tag{41}$$

where c is the radius of the unbond. As the length of the rod decreases (and is referred to as a plate of thickness, h) the condition for criticality is given by

$$P_{cr} = \sqrt{\frac{32 h^3 E \gamma_a}{3(1-\nu^2) c^4}} \tag{42}$$

These criticality conditions (Eq. 41 and 42) are plotted in Fig. 58. In Ref 30, experimental results from Solithane or glass tests indicated that Eq. 41 was valid for $(h/c) > \sim 2.0$. Assuming the simplified analysis to be valid for $c \sim 0.5$ inch for the tests conducted on TPH-1011 propellant, the values of γ_a determined initially are used to evaluate $P^2 c/E\gamma$ for the larger initial unbond radii (h/c smaller). This experimental result is superposed on Fig. 58 along with the experimentally determined transition for Solithane/glass determined by Jones. This transition is important when considering the range of validity of test data reduced using Eq. 41.

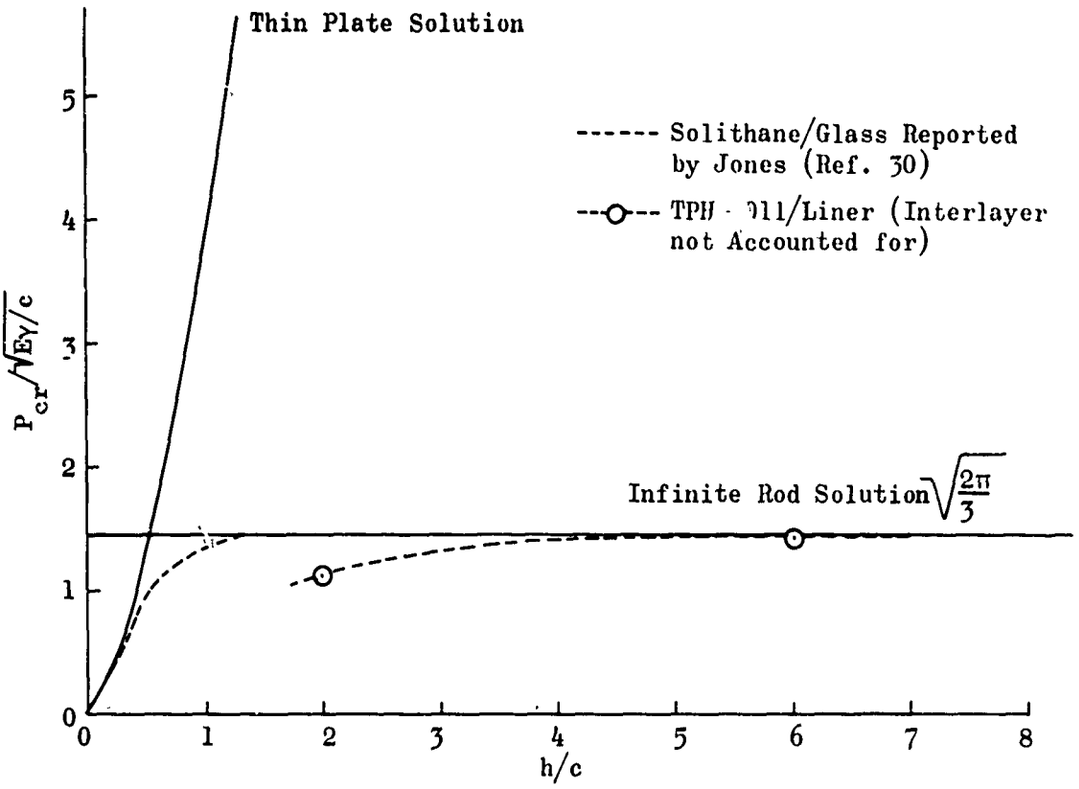

Figure 58. Limit Solutions for Two-Material Blister Test

The problem of the adhesive interlayer is quite complicated. Williams (Ref. 25) approached the problem of considering the interlayer by treating it as an elastic foundation supporting a long plate as in Fig. 59. The field equations for the region inside the unbond are (Ref. 26):

$$D\nabla^4 w = P \tag{43}$$

while outside the unbond,

$$D\nabla^4 w + \lambda^4 w = 0 \tag{44}$$

where w is the deflection of the upper plate; k, the interlayer stiffness; and D, the plate flexural rigidity. From Fig. 59 we have

$$D = \frac{E h^3}{12(1 - \nu^2)} \tag{45}$$

and

$$k = \frac{1 - \nu'}{(1-2\nu')(1+\nu')} \frac{E'}{h'} \tag{46}$$

while λ is defined through

$$k = 4D\lambda^4 \tag{47}$$

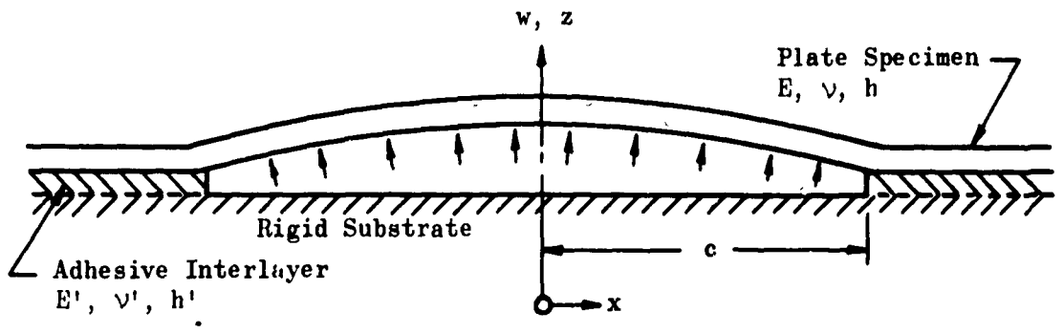

Figure 59. Sketch of Adhesive Interlayer Geometry

At the intersection of the regions represented by Eq. 43 and 44, namely at x = c, deflection, slope, moment, and shear must be equal. Imposing these conditions, the deflections are determined throughout the body. Applying an energy balance, the condition for criticality is found to be

$$P_{cr} = \sqrt{\frac{32E\gamma_a}{3(1-\nu^2)c}\left(\frac{h}{c}\right)^3}\left[1 - g(\lambda c)\right] \tag{48}$$

where $g(\lambda c)$ is a complex combination of Kelvin functions and their derivatives as functions of λc. The bracketed term in Eq. 48 is the correction due to the interlayer. This factor is plotted in Fig. 60. Note that as $k \rightarrow \infty$ (interlayer thickness $\rightarrow 0$) the correction $g(\lambda c) \rightarrow 0$. For most cases, the liner will be nearly incompressible ($\nu \sim 0.5$) which also gives $k \rightarrow \infty$ so that the correction will be quite small.

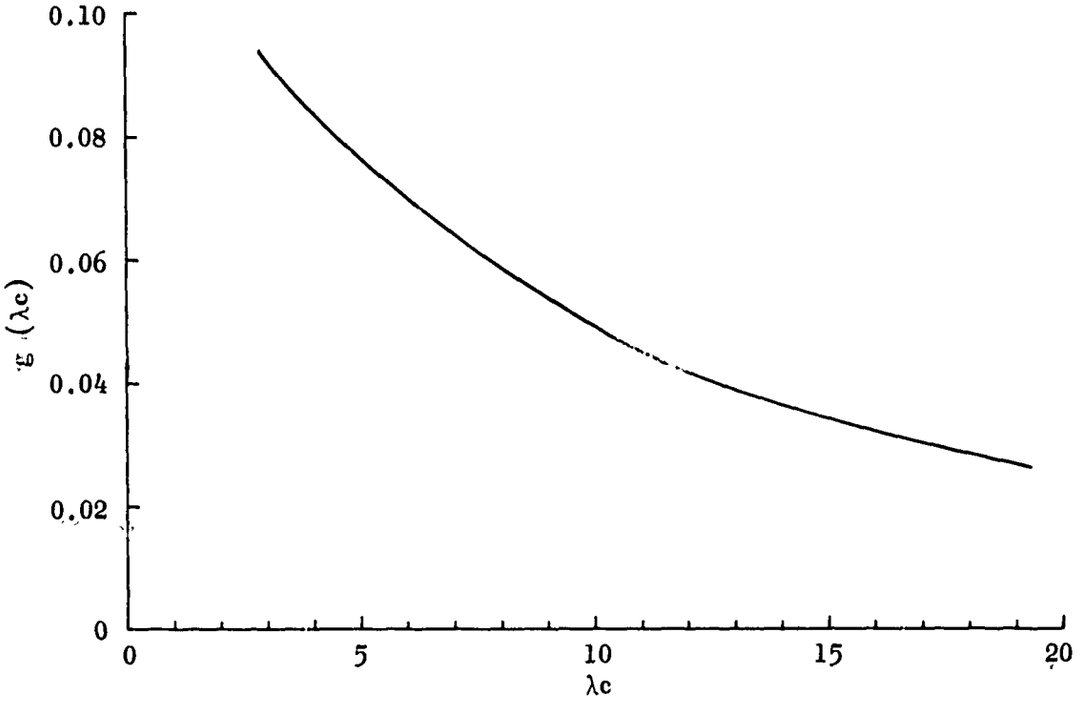

Figure 60. Adhesive Interlayer Correction Factor, $g(\lambda c)$ (from Ref. 25)

Since the direct solution is not available for axisymmetric cases where (h/c) is large (as in the experiments conducted on this program) a finite element computer solution was obtained. Since only one liner thickness and modulus was evaluated, the generalized effect cannot be determined. For the specific case at hand, however, the presence of the liner reduces the critical pressure on the order of 3% so that the γ_a determined using Eq. 41 is high by about 6%. Within the overall accuracy of the test measurements, this 6% error is not particularly bad.

SOLITHANE DISC TESTS

Much of the analysis performed in support of the RPL test is equally applicable to the Solithane and TPH-1011 propellant specimens. The conditions for which analytical-experimental correlation is evaluated are crack initiation, crack growth rate, and crack trajectory. Supportive analyses in the last two areas were conducted at Thiokol (for the TPH-1011 propellant) and UTC (for the Solithane). Here, the basic interest is in

evaluating the test results against the theoretical foundations of fracture of viscoelastic materials. Because of analytical simplicity, the bulk of the interpretation is directed toward the circular port specimen. The star configuration is of special interest in the trajectory study at Thiokol and it is this configuration which exemplifies the possibilities for the RPL test as a "plane stress analogue motor."

CRACK INITIATION

The initiation of crack growth is the first problem of interest to a solid rocket motor grain stress analyst. This initiation may occur at a surface with very tiny flaws (beyond the range detectable by the unaided eye) or by growth of a finite crack in a grain. Conventional analysis techniques are unable to treat the latter problem because of the mathematical stress singularity at the crack tip. For the first case, that of an apparently flawless surface, a typical approach is to apply a maximum principal strain criterion for failure. The geometry of the RPL disc specimen is amenable to comparing uniaxial tensile specimen strain capabilities (on which most strain criteria are based) with the uniaxial failure strain at the port of the disc. For the circular port Solithane disc specimens tested as cast, the tangential strain at the inner port at failure was found to lie between 0.19 and 0.21 in./in. The time to failure for these tests (conducted at 77 F) was in the range of 50 minutes. From Ref. 29, the uniaxial failure strain for this condition is on the order of 0.35 in./in. As will be shown later, this discrepancy is roughly the same as that noted for the TPH-1011 propellant tests.

An alternate approach to predicting the crack initiation at the inner port was attempted. This technique relied on direct application of cylindrical flaw theory (as discussed in Section I) to the circular port disc geometry. From Ref. 5, for a plane stress cylindrical flaw subjected to constant rate displacement at the boundary, the condition for criticality is given by:

$$\frac{1}{8}\left(1 + 3\,k^2\right)^2 \left(\gamma_c/a_o\right) = \left(\frac{U_o t}{b}\right)^2 \left[\frac{2}{t^2} E^{(2)}(t)\right] \qquad (49)$$

where $k = (a_o/b)$ and the radial displacement, $\delta(t) = U_o t$. For the circular port Solithane specimens, we have $a_o = 0.681$ inch, $b = 2.934$ inches, and $U_o = 0.0031$ in./min. The criticality may be expressed by writing γ_c as a function of time from Eq. 49 then intersecting the resulting curve at t_o (time of failure) to determine γ_c or at the given γ_c to predict t_o. Using the relaxation modulus shown in Fig. 55, the γ_c vs t relationship implied by Eq. 49 is shown in Fig. 61. The times to failure for the two Solithane specimens with no apparent initial flaw were 49 and 55 minutes. From Fig. 44, this would infer a γ_c of about 4.3 in.-lb/sq in. or about 2 orders of magnitude greater than that reported by Mueller as a lower limit (long-time) value. Taking the frequently quoted value, $\gamma_c = 1$, for

Solithane, the predicted time to failure would be ~ 26 minutes. Thus, in terms of predicted critical applied displacement, we are conservative by a factor of 2 using the cylindrical flaw approach and on the opposite side by a factor of 2 using the strain criterion. Discussion of the significance of this observation is given in Section V where the corollary results for TPH-1011 propellant are also discussed.

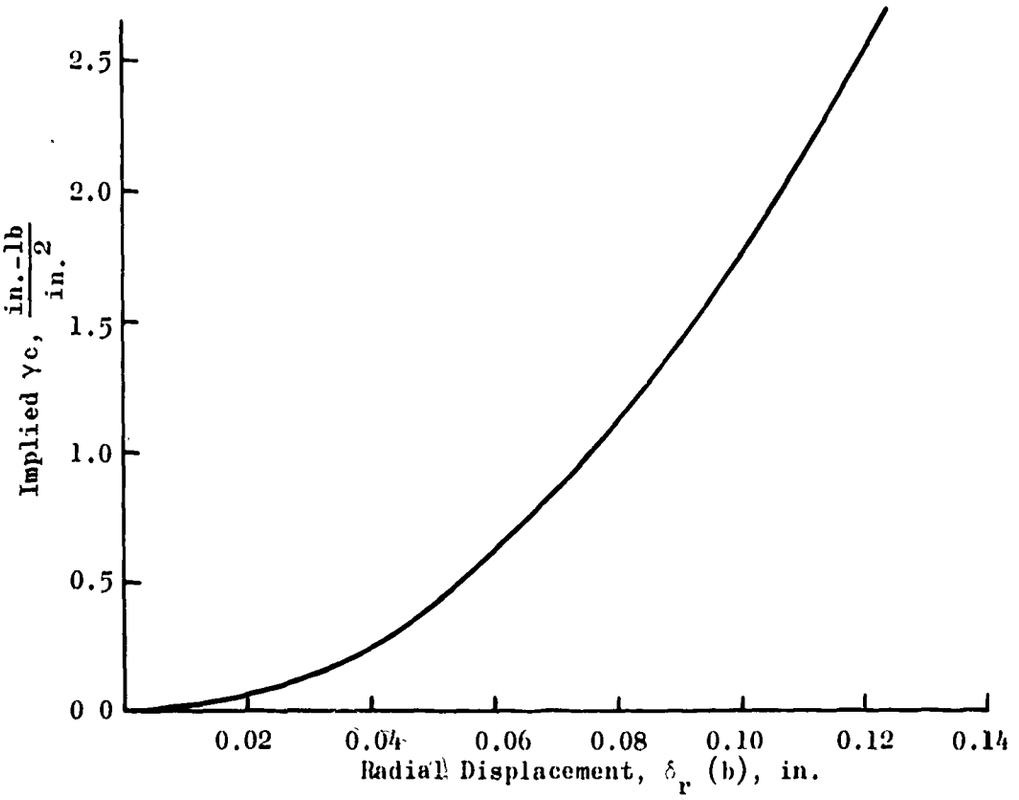

Figure 61. γ_c vs δ_{cr} Solithane Circular Port Disc Specimen; 77 F, Time > 1 Sec

Initiation of crack growth at a pre-existing crack is not amenable to analysis by either of the methods described above. The fracture mechanics approach formulated by Griffith is addressed specifically to this problem. The analysis discussed here is based on Bowie's study of a crack in a sheet with a central hole (Ref. 6). For the star port geometry, a direct computation of the rate-of-change of energy with increase in crack length using finite-element computer techniques is indicated. These computations for this specific geometry were conducted at Thiokol. The evaluation of the test and the results are based on the circular port specimens.

Bowie, in Ref. 6, considered the case of an infinite plane plate of elastic material with a circular hole. He derived the criticality conditions, based on the Griffith hypothesis, for one and two (symmetrical,

equal-length) cracks radiating from the central hole when the plate is subjected to simple or uniform tension at infinity. For the case of uniform tension at infinity,

$$\sigma_{cr} = \sqrt{\frac{k\,E\,\gamma_c}{\pi\,-f'(L)}} \tag{50}$$

where $f'(L)$ is a crack length parameter and L is the crack length expressed in units of the center port radius, a. For the elastic problem, with $b \gg a$,

$$\sigma_{cr} = \frac{E\,\delta_{cr}}{b(1-\nu)} \tag{51}$$

Modifying the result to represent the displacement boundary, we have as a first approximation

$$\frac{\delta_{cr}}{b} = \sqrt{\frac{k\,\gamma_c(1-\nu)}{-\pi\,E\,f'(L)}} \tag{52}$$

The parameter k is the number of cracks. The value of $f'(L)$ is shown for various values of L in Table VIII. For the case of a single crack in an incompressible material, and replacing E by $\frac{2}{t^2}E^{(2)}(t)$ we have for the test data as shown in Fig. 27,

$$\frac{\delta_{cr}}{b} = \sqrt{\frac{\gamma_c}{2\pi\,E\left[-f'(L)\right]}} \tag{53}$$

The energy release rate γ_c, was determined from Eq. 53 and is shown, as a function of time in Fig. 62. The range of values (0.4 - 0.25 in.-lb/sq in.) is compatible with the quoted value of ~ 1 in.-lb/sq in. and the lower limit of 0.03 in.-lb/sq in. established by Mueller. These results, while not conclusive in terms of verification of the theoretical approach, indicate the feasibility of expanding the study in this area.

TABLE VIII

$f'(L)$ FOR RADIAL CRACKS IN PLANE STRESS SHEET

WITH CENTRAL HOLE, UNIFORM TENSION

L	$-f'(L)$ for k = 1	$-f'(L)$ for k = 2
0.0	0.000	0.000
0.1	0.203	0.406
0.2	0.334	0.668
0.3	0.433	0.877
0.4	0.503	1.073
0.5	0.565	1.230
0.6	0.610	1.539
0.8	0.694	1.653
1.0	0.756	1.885
1.2	0.819	2.002
1.4	0.857	2.337
1.6	0.952	2.497
1.8	0.994	2.704
2.0	1.020	2.974
2.4	1.169	3.287
2.8	1.237	3.753
3.2	1.352	4.082
3.6	1.469	4.455
4.0	1.547	4.883
5.0	1.709	5.649

a. Time = 0

b. Time = 21 minutes

c. Test No. 1, Unloading

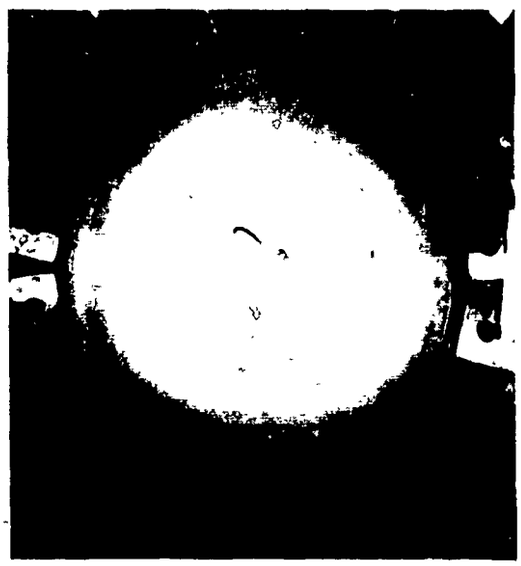

d. End of Test No. 2

Figure 62. Solithane As-Cast Star Port RPL Disc Test, Constant Displacement Rate, Test 23

CRACK GROWTH

The problem of crack growth is of equal importance to that of the initiation of growth. The rate at which a crack can be expected to grow under a given set of conditions may determine the usefulness of a motor with a pre-existing crack. The trajectory of the growing crack may also be a determining factor. For the circular port geometry, the crack path for a symmetric boundary loading would be expected to be radially outward. For the star port, however, the stress field in the local area of the initiating crack is influenced by the configuration of the port. As seen in Fig. 62, the initial direction of the crack is at an angle away from a radius through the point of initiation. This angle was on the order of 15-20^0 in the specimens tested. This phenomena is primarily a function of specimen geometry and can be evaluated by means of finite element elastic computer energy variation calculations. Similar observations are found for the TPH-1011 propellant tests as shown later.

The rate of growth for the crack has been studied by Mueller as discussed in Section II. His approach, to consider the energy balance in the local area of the advancing crack tip, requires a knowledge of the stresses in the vicinity of the crack tip and of the geometry of the crack opening near the tip. The viscous dissipation of energy enters through the crack geometry enter the problem through the "stress intensity factor," k_n. The criticality condition for stable crack propagation is of the same form as that obtained from spherical flaw theory using a global energy approach but with the geometrical characteristics being expressed in terms of the stress intensity factor. Computation of the stress intensity factor is accomplished via a finite element computer approach and is being carried out at UTC as a part of the Fracture Mechanics Program.

The test performed to evaluate propagation rate in the lease complicated manner consisted of starting a crack in a specimen with a constant displacement applied. As a first order evaluation of the result, the criticality criterion established by Mueller was applied in a relative manner. For two tests on the same geometrical configuration, differing only in applied load, we find

$$\frac{\delta_2^{cr}}{\delta_1^{cr}} = \sqrt{\frac{D_{cr}\left(\frac{\Delta c}{\dot{a}_1 a_T}\right)}{D_{cr}\left(\frac{\Delta c}{\dot{a}_2 a_T}\right)}} \qquad (54)$$

where Δc is the width of the region failing immediately in front of the advancing crack tip. After Mueller, the value of Δc was taken to be 10^{-8} inch. The results from comparing applied displacements and resultant velocities for the six Solithane tests conducted at constant displacement are shown in Table IX. The favorable comparison is indicative of the validity of the test method and the relationship between applied load and crack velocity as given in Eq. 50.

TABLE IX

RELATIVE CRACK VELOCITY COMPARISONS

SOLITHANE DISC SPECIMENS

Parameters	Test No.					
	Circular Port			Star Port		
	27	28	29	30	31	32
$\delta_r(b)$, in.	0.026	0.031	0.035	0.029	0.032	0.039
$\dot{a}$, in./min	0.069	0.119	0.181	0.058	0.082	0.121
$D_{cr}\left(\frac{10^{-8}}{\dot{c}\ a_T}\right)$, $in.^2/lb$	1.073×10^{-3}	7.795×10^{-4}	6.110×10^{-4}	1.167×10^{-3}	9.150×10^{-4}	6.755×10^{-4}

$$\left\{\frac{\left(\frac{\delta_{27}}{\delta_{28}}\right)^2 = 0.703 \qquad \frac{D_{cr}^{28}}{D_{cr}^{27}} = 0.726}{\left(\frac{\delta_{28}}{\delta_{29}}\right)^2 = 0.784 \qquad \frac{D_{cr}^{29}}{D_{cr}^{28}} = 0.784}\right\} \qquad \left\{\frac{\left(\frac{\delta_{30}}{\delta_{31}}\right)^2 = 0.821 \qquad \frac{D_{cr}^{31}}{D_{cr}^{30}} = 0.785}{\left(\frac{\delta_{31}}{\delta_{32}}\right)^2 = 0.673 \qquad \frac{D_{cr}^{32}}{D_{cr}^{31}} = 0.738}\right\}$$

PROPELLANT DISC TESTS

The RPL tests conducted on the TPH-1011 propellant specimens were less varied and subject to the difficulties of developing a new test. Phenomenologically, the test results were quite similar. The greatest single observed difference was that the TPH-1011 propellant specimens which were tested as-cast exhibited multiple cracks at failure while the Solithane specimens failed with single cracks. This is attributed to the higher density of initial flaws provided by the presence of filler particles in the propellant. The same categories of interest--initiation, propagation, and trajectory--apply for the propellant data analysis.

CRACK INITIATION

Of the five circular port specimens tested, two were with the as-cast surface, three with double precracks. The two as-cast specimens failed at strain levels of 0.134 and 0.172 in./in. This compares with the reported strain capability (Fig. 42) of about 0.27 in./in. Treating the failure with plane stress cylindrical flaw theory, we have the result shown in Fig. 63. The implied γ_c as a function of test time intersected with the γ_c measured in biaxial strips at SRD, Fig. 10, predicts failures at 29 and 32 minutes, respectively. The observed failures occurred at approximately 28 and 34 minutes. While this comparison is encouraging, the result is tempered by the observation on Solithane and the lack of additional comparable test data on the propellant.

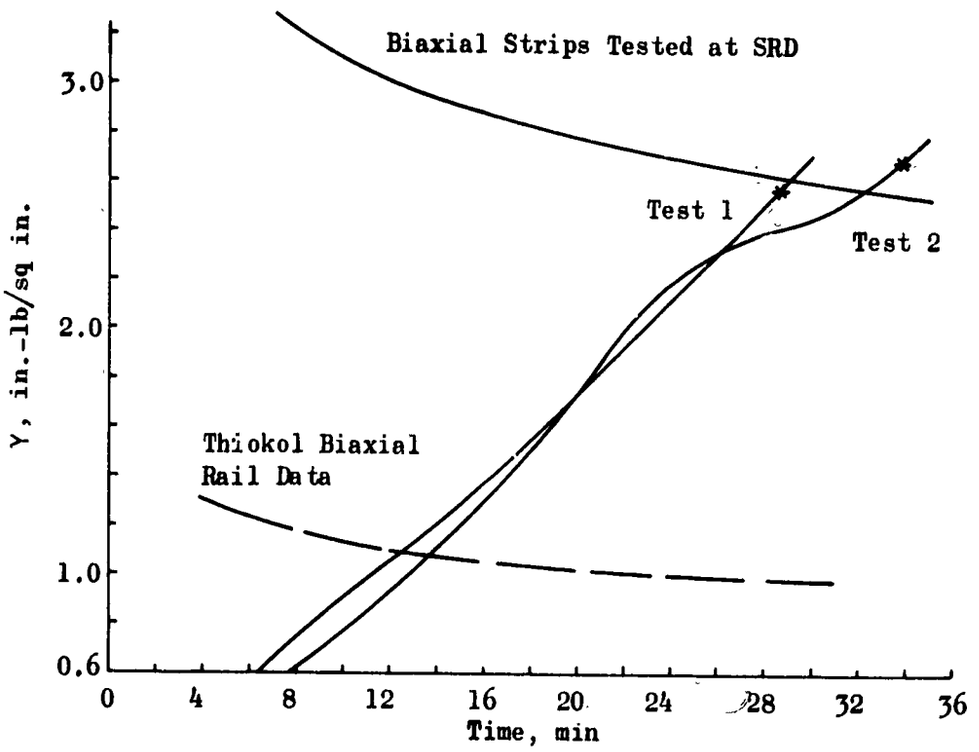

Figure 63. Circular Port RPL Disc Test Failure Data, TPH-1011 Propellant

The precracked specimens may be viewed in terms of the Bowie problem. These specimens were precracked with two diametrally opposed cracks approximately 0.24 inch in length. From the data in Fig. 48--50, however, the Bowie results, as applied to the Solithane tests, give γ_c for the TPH-1011 propellant on the order of 1.0 in.-lb/sq in.--about the same order of magnitude as that measured on biaxial strips. This result will be discussed in the following section. A finite element computer calculation for circular port geometry was made, and the result is shown in Fig. 64. The values for γ_c computed from the above data using Fig. 64 agree with the Bowie result and, again, are on the order of 1.0 in.-lb/sq in.

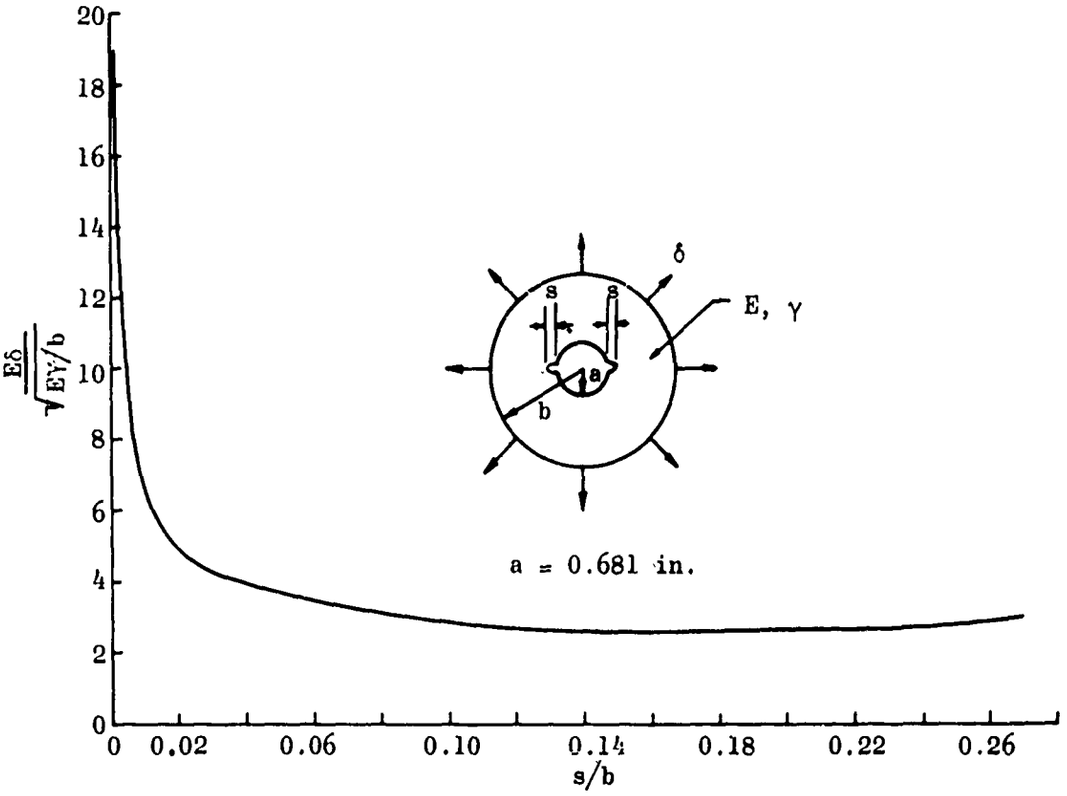

Figure 64. Finite Element Criticality Computation

CRACK GROWTH

The growth rate problem on the TPH-1011 propellant tests is complicated by the method of testing used--the continuously varying displacement boundary. The observed crack trajectory on the star port specimens (Fig. 41 and 42), as discussed previously, exhibited the initial away-from-the-radial direction as given in Table VII. Again, as in the Solithane specimens, the initial crack direction is $\sim 20^0$ away from the radial line through the point of initiation. Lacking the characteristic Δc for TPH-1011 propellant and the stress intensity factor, being evaluated for these test geometries by UTC, no attempt is made to correlate an analysis with the crack velocity measurements. The added problem of the changing boundary was recognized and corrected before the Solithane tests were run.

Page 86 is blank

SECTION V. DISCUSSION OF RESULTS AND CONCLUSIONS

The primary objectives of the Fracture Mechanics program at Rocketdyne were accomplished. The feasibility of the blister peel test for propellant/liner systems was demonstrated, and the development of the Radial Planar Loading disc test was completed. Comparison of test results with the theories of fracture mechanics as applied to viscoelastic materials was encouraging, but it revealed problems with major impact. The following paragraphs discuss the technical observations and summarize inferences drawn from these observations.

BLISTER PEEL TEST

Results from the blister peel tests were most encouraging. The observed data spread, $\pm$ 20%, is not particularly good, but with the limited number of tests performed it is not surprising. The ability to obtain multiple data points from a single specimen is encouraging from the standpoint of maintaining reasonable test costs and of having repetitive data on a given system. Evaluation of specimen geometry, a study of the effects of the pressurizing agent, and characterization of several systems over a range of rates and temperatures are still needed in development of this test method. Application of the results to failure prediction of bond lines loaded in tension (as in poker chip tests or motors) is needed to determine the validity of the fracture concept to flaw growth in bimaterial systems.

DISC TESTS

Disc test results indicate (1) a difference in the fracture response of Solithane and filled propellant and (2) an area of difficulty in predicting the initiation of crack growth from initial as-cast surfaces. A basic difference in fracture initiation was recorded between the as-cast Solithane and as-cast TPH-1011 propellant specimens in that the Solithane specimens all failed with single cracks; while the propellant failed with multiple cracks.

Prediction of crack initiation at the disc bore surface was an unrewarding endeavor. Presupposition had been that uniaxial tensile strain capability would provide an accurate indicator for this mode of crack initiation. Results, however, indicate that failure initiated at strain levels on the order of 50% of uniaxial strain capability. One question that arises concerns the validity of making such a comparison. Uniaxial failure data reflect strain to catastrophic failure; while disc failures are reported for flaw growth to a size visible to the unaided eye. Another often used indicator for uniaxial capability is strain at maximum stress as shown in Fig. 53 for TPH-1011 propellant. At a log reduced strain rate of about 1.0 in./in./min the reduction in implied strain capability over maximum strain is only slight. however, the crack initiation, speciment load (as exemplified in Fig. 65) vs applied

deflection, indication on the disc specimen is not a peak stress but rather a change in slope. One may conclude from these observations that standard uniaxial failure strain interpretation is less conservative than the interpretation of failure at a grain surface in motor-like geometries.

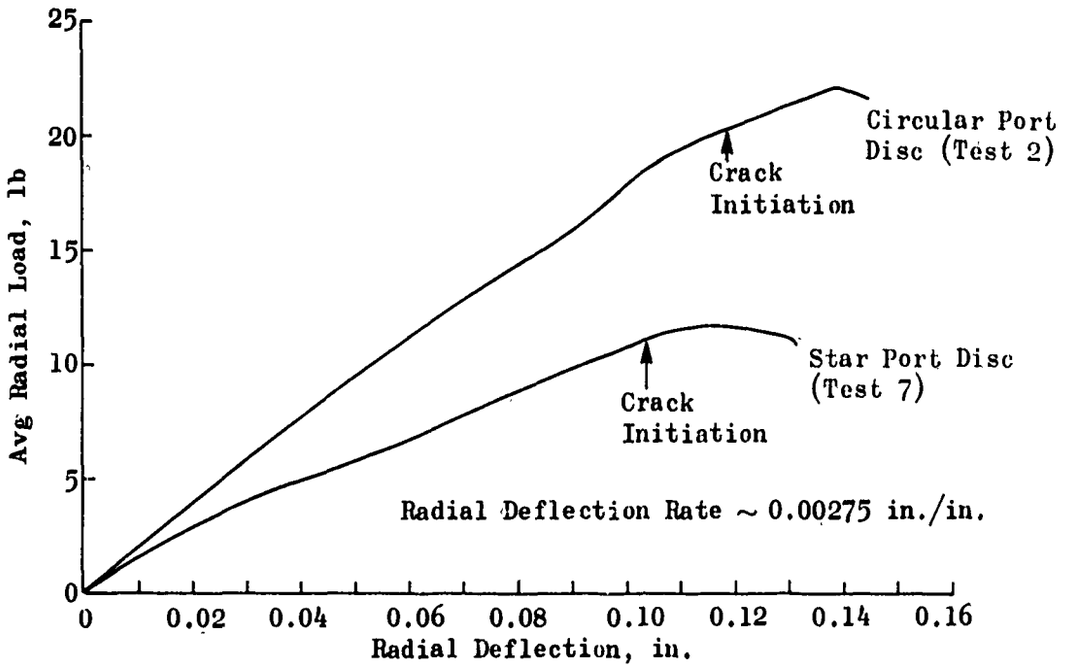

Figure 65. Load Deflection Relationship, TPH-1011 Propellant Disc Tests

The apparent correlation between the cylindrical plane stress fracture computation and the TPH-1011 propellant circular port specimen results as discussed in the previous section and the equal lack of correlation with the Solithane data lead to two possible viewpoints. The first is that the TPH-1011 propellant correlation is a coincidence. The second rests on the phenomenological observation of the mode of failure initiation and the assumption inherent in the analysis. The key factor in the cylindrical flaw solution is flaw growth by "ablation" or disintegration of the inner surface. TPH-1011 propellant specimens exhibited failure through initiation of multiple cracks (at least 10 in both cases) although only two or three continued beyond the surface layer. This mode of initiation may thus be viewed as an eroding of the surface analagous to the theoretical assumption. The Solithane mode of failure, single crack opening, is quite different from the ablating surface analogy.

RPL TEST APPARATUS

The RPL test apparatus worked reasonably well in the role for which it was intended. Problem areas encountered with the test were (1) non-uniform rate of loading and (2) imperfect circular symmetry of the boundary loading. Neither of these problems proved detrimental to the testing or analysis but should be corrected for future work devoted to more precise study of fracture in this type specimen.

The loading history programmed into the MTS system controller for the RPL apparatus was not duplicated at the bolt circle on the load collar. For the intended linear displacement rate tests, the collar responded with a displacement rate which was initially three times the final rate of displacement as shown in Fig. 66. The explanation for this phenomenon rests in locating fabrication errors in the mechanical linkage between the hydraulic lift and the attachment to the load collar. The most likely source of error is a slight mismachining of the runners in the cam which forces the load arms outward. The cylindrical flaw fracture analysis was performed using the final loading rate, the average loading rate, and a bi-linear rate loading history with no apparent difference in the results. Thus, we may conclude that this history variation did not adversely affect the tests performed on this program.

The other area of potential difficulty deals with the symmetry of the applied loading. The problem here is traced back to the initial set-up of the bolt circle where the load collar is attached. It is best reflected in the load measured on the nine load arms. Figure 67 shows the load as measured at the nine load cells around the specimen. The initial diameter (as measured from test specimen photos) across the specimen at the nine load-arm sets and the radial displacements corresponding to the loads in Fig. 67 are shown in Fig. 68. That the loads and displacements are uniformly distributed throughout the inner portion of the specimen web was confirmed in the photoelastic study of the Solithane specimens. At displacement of 0.02 inch (radial) load symmetry exists over the inner 30% of the web and at 0.04 inch, over the central 60%. The setup of this bolt-circle diameter is correctable without additional fabrication and can be readily accomplished after the loading rate problem is resolved.

The temperature capability of the RPL apparatus was not utilized on this program although all necessary equipment is available. One potential area of difficulty was uncovered while checking out the operation of the thermal environmental chamber. The stiffness of the load collar and propellant increases by greater than an order of magnitude between room temperature and -80 F. The load cells mounted on the arms have a capacity of 1000 pounds to accommodate the expected load response at the lower temperatures. U-joints between the arms which transmit load from the cam to the rods and the rod attachment to the load collar insure radial loading of the collar. These U-joints were designed as weak links to protect

the load cells and were chosen to break at loads of about 750 pounds. In the check-out testing, however, these U-joints began to fail at about 500 pounds. They were replaced with available stock to permit testing, but future work which utilizes the temperature capability of the apparatus will require connectors that are able to carry greater loads.

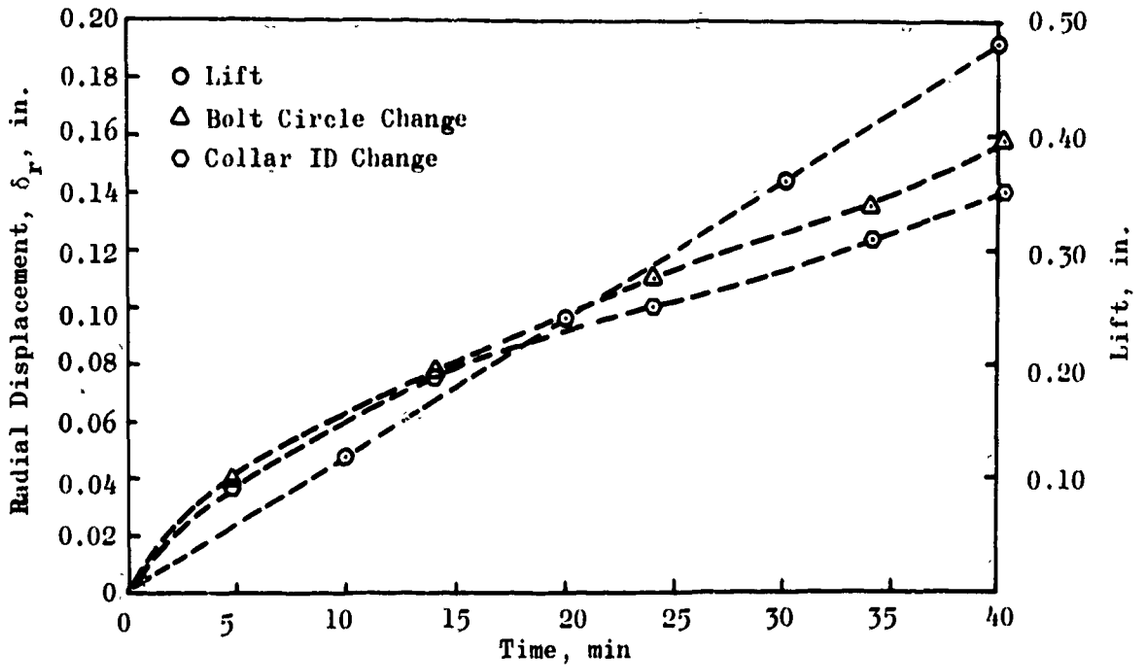

Figure 66. Displacement Boundary at Lift, Bolt Circle, Collar ID

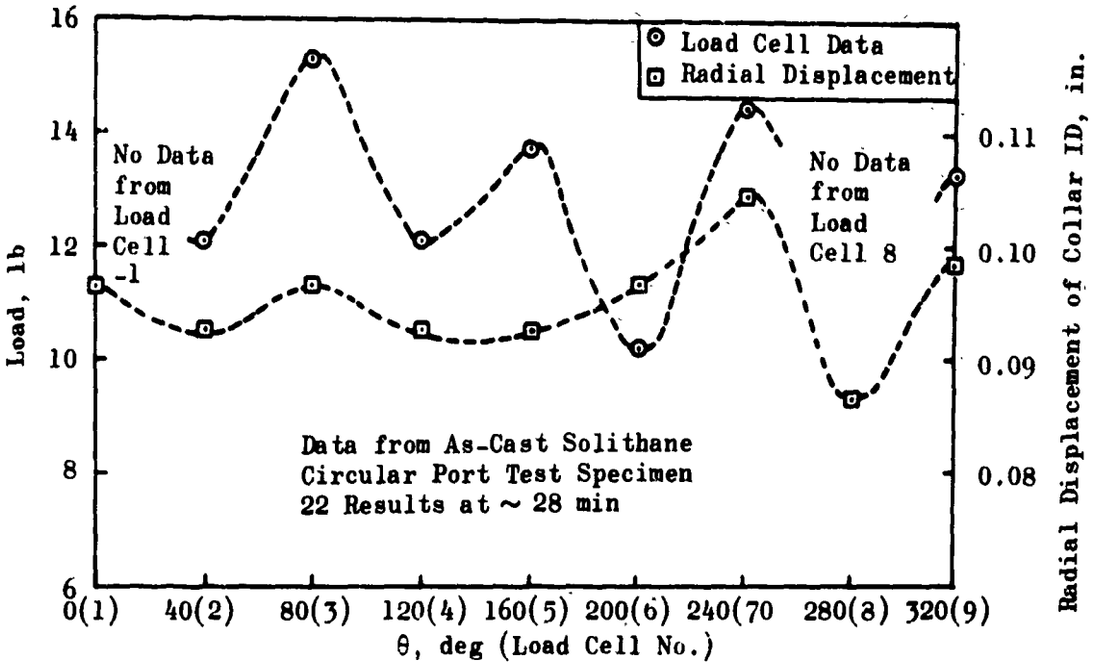

Figure 67. Load-Deflection Around Disc Specimen

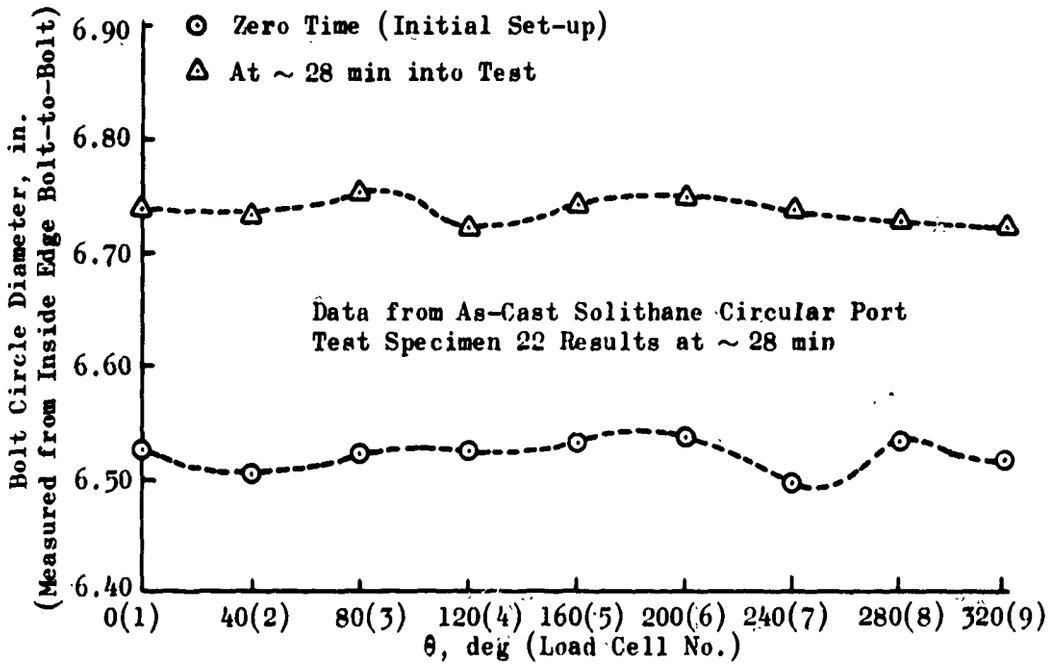

Figure 68. Bolt Circle Diameter Variation, RPL Disc Specimen

CONCLUSIONS

The test feasibility and development effort provided positive results in attacking the problem of applying fracture mechanics to solid propellant rocket motor grain failure analyses. The limited results obtained from the testing and corollary analytical studies attest to the applicability of these concepts to grain analysis. Exploitation of these experimental tools to define the parameters associated with crack or unbond initiation and growth and relating of the results to actual motor response are discussed in the following recommendations.

SECTION VI. RECOMMENDATIONS

The Fracture Mechanics Program has provided two promising experimental methods for applying fracture concepts to propellant analysis and had indicated applicability of these concepts. The following paragraphs contain recommendations for extending the present results to motor configuration evaluation. The needed effort is experimental and analytical in each phase. The first part of the recommended study applies to single loading problems. The second part extends into the area of cumulative damage effects of repeated loadings and behavior of other materials in uniform tension. The recommendations cover four specific areas:

1. Blister peel test development and application
2. RPL disc test extended testing
3. Subscale motor analysis and testing
4. Applications studies utilizing RPL disc test

Specific problems which need to be attacked in these four areas are summarized below.

BLISTER PEEL TEST

There are three particularly important questions to be answered concerning the blister peel test. One involves test technique; another combines test technique with implications to fracture behavior in general, and the third concerns the applicability of test results to motor situations. The first area of interest centers on specimen geometry. The configuration used on this program was steel base/thin liner/thick propellant layer. An alternate configuration for which the analysis is available would be steel base/thin propellant layer/thin liner. This alternate overcomes the problem of inaccessibility of the unbond during testing and might provide more reliable results.

The second area is concerned with the pressurizing agent used to propagate the debond. Nitrogen (N_2) was used in the tests to date. In a motor unbond, however, nitrogen is an unlikely substance to be found in significant quantity. A more likely agent might be chemicals from an uncured binder material. In a study of the effects of pressurizing agents, other gases and liquids should be considered. The results would have implications for cohesive fracture testing as well as the peel test work. Change in the physical/chemical microstructure of materials undergoing fracture is plausible and has been monitored. The presence of an extraneous substance--whether N_2, air, oxygen, ozone, freon, or binder material--will give rise to interaction between energy released by excited or separated molecules and the atmosphere in the vicinity of the crack tip. To ensure obtaining representative release rate characteristics from lab tests, it may prove necessary to conduct those tests in an atmosphere analogous to those existing inside motors.

The third subject of the recommended study of the blister peel test deals with correlative experimental effort. While it has been demonstrated that the basic analysis of the blister specimen is adequate for data reduction, no tests in alternate specimens have been made to demonstrate applicability of the blister test results to motor-scale geometries. Three different tests, in their order of increasing complexity, are bimaterial tests of circular disc specimens of the RPL device, poker chip testing, and thermally cooled analogue motors. A test matrix including these types of tests will have bifocal objectives—one toward direct application to grain stress analysis, the other toward advancing technology in the understanding of dewetting (particle-to-binder debonding). This latter area is discussed under RPL device applications.

RPL DISC TEST EXTENDED TESTING

Correlation of the RPL disc test results with subscale (and finally full-scale) motor response requires a full matrix characterization of the parameters which influence crack initiation and growth. This will require testing of two or more geometries over a range of loading rates and temperatures to establish functional dependency on boundary conditions and environment. Other considerations might include simultaneous cooling and boundary displacements to simulate motor history during thermal cycling. Not only does this type testing provide the broad base necessary for extension of the results to motor geometries, but it is also more definitive of limitations in the analytic capabilities. Applicability of quasi-viscoelasticity in the techniques of fracture mechanics, an approach which is state of the art in motor analysis, has yet to be verified through testing. In motor experiments, the results (in the form of predicted stress as a function of temperature) have been found (Ref. 32, 33) to have significant errors at colder temperatures (below 0 F). A basic test such as that available with the RPL device provides a meaningful approach for resolving the difficulties in analyzing grains at critical cold temperatures.

SUBSCALE MOTOR ANALYSIS AND TESTING

The culmination of an analytic or experimental study of the behavior of solid propellants must be the correlation of the results to motor grain response. As the end-point of the two discussed endeavors in the characterization of propellant fracture (adhesive and cohesive) a test program incorporating subscale (e.g., 4-inch ID) motors is recommended. This test vehicle provides the transition between basic lab specimens (such as the RPL disc) and the complex full-scale motor geometry. A series of cylindrical bore and solid grain subscale motors, instrumented with bondline stress transducers and corollary in geometry to specimens tested on the RPL device should be failed in a slow-cooling experiment to establish validity of the disc test results and peel test characterization and to evaluate the analytic predictions of stress-state and failure response.

APPLICATIONS STUDIES UTILIZING THE RPL DISC TEST

The RPL disc test is amenable to experimental investigation of material behavior in a wider scope than characterization of fracture parameters. In a solid disc specimen, the stress state, up to failure, is one of uniform biaxial tension, analogous to the port surface of a cylindrical bore rocket. The solid disc test is half way between the biaxial strip test and an analog motor test. The biaxial strip test is simple, but the specimen is not in equal biaxial tension; the analog motor test is difficult to conduct with close controls. Failure characterization by individual or combined straining and cooling should correlate well with failure characterization in analog motors. If so, a better controlled and less expensive test for this type propellant characterization will have been defined.

As mentioned previously, the RPL device shows promise in the study of bimaterial interface debond studies. Analytic solutions for the debonding of concentric cylinders of dissimilar materials (one rigid) are available. By casting propellant with appropriately controlled initial unbonds against a core of liner material (or steel coated with liner) an alternate to the blister peel test for characterizing debond at the propellant-liner interface is available. Equally important, this geometry is analogous to the oxidizer particle/binder state in solid propellant. If the test proves feasible, a core of oxidizer material in a web of binder material would be a logical specimen for investigating dewetting through propellant/oxidizer bond strength characterization.

Other materials than propellant and propellant/liner would be of interest for experimental studies in geometries compatible with the RPL machine. One material of particular interest in the solid rocket field is fiberglass-reinforced epoxy such as that used in lightweight motor cases. The RPL apparatus should have sufficient load capability to test thin rings of these case materials in controlled tension-simulating loadings experienced in service life.

Another area in which the RPL device is potentially applicable is in the study of cyclic loading effects on propellant characteristics. While cyclic capability was not originally included in the design of the RPL test machine, only slight modification would be required to produce low frequency loading boundaries. This modification would provide a unique test for the extension of studies into cumulative damage effects on solid propellants.

Page 96 is blank

REFERENCES

1. Griffith, A. A.: "The Theory of Rupture," Proceedings of the First International Congress of Applied Mechanics, Delft, 1925, pp 55-63.
2. Williams, M. L.: "The Fracture of Viscoelastic Material," Fracture of Solids, Interscience Publishers, New York, 1963.
3. Williams, M. L.: "Initiation and Growth of Viscoelastic Fracture," International Journal of Fracture Mechanics, Vol. 1, No. 4, 1965.
4. Burton, J. D., and J. S. Noel. "Viscoelastic Fracture in Plane Stress and Plane Strain Fields," Bulletin of the 6th Meeting, ICRPG Mechanical Behavior Working Group, 1967.
5. Noel, J. S, J. D. Burton, and B. C. Harbert: Fracture Mechanics Approach to Cumulative Damage, AFRPL-TR-68-132, Final Report, Rocketdyne, McGregor, Texas, 1968.
6. Bowie, O. L.: "Analysis of an Infinite Plate Containing Radial Cracks Originating at the Boundary of an Internal Circular Hole," Journal of Mathematics and Physics, Vol. 25, 1956, pp 60-71.
7. Becker, E. B., and J. J. Brisbane: Application of the Finite Element Method to Stress Analysis of Solid Propellant Rocket Grains, Rohm & Haas Co., Report No. S-76, Vol. I and II, 1966.
8. Dickson, E. C., and D. H. Lee: IBM 360 Computer Program for Plane Strain Analysis, and IBM 360 Computer Program for Axisymmetric Stress Analysis, Thiokol Chemical Corp., Controller Division Reports, Jan 1969 and Mar 1968.
9. Jones, W. B.: A Simple Test for Certain Cases of Adhesion, University of Utah, College of Engineering Report No. UTEC-DO-69-088, 1969.
10. Fracture of Solids, Interscience Publ., John Wiley & Sons, N. Y., 1963.
11. Rosen, B. (Editor): Fracture Processes in Polymeric Solids, Interscience Publishers, John Wiley & Sons, N. Y., 1964.
12. Black, B. L., et al: A Study of the Mechanics of Solid Rocket Grain Fracture, Proposal R-4507P to AFRPL, Rocketdyne, McGregor, Texas, July 1968.
13. Fundamentals of Viscoelastic Fracture Mechanics, Proposal 68-40, Appendix I, United Technology Center, Sunnyvale, California, July 1968.
14. Williams, M. L., P. J. Blatz, and R. A. Schapery: Fundamental Studies Relating to Systems Analysis of Solid Propellants, GALCIT SM 61-5, California Institute of Technology, Feb 1961.
15. Biot, M. A.: "Theory of Stress-Strain Relations in Anisotropic Viscoelasticity and Relaxation Phenomena," Journal of Applied Physics, Vol. 25, 1954, p. 1385.

16. Schapery, R. A.: "Approximate Methods of Transform Inversion for Viscoelastic Stress Analysis," Proceedings of the Fourth U.S. National Congress on Applied Mechanics, Vol. 2, p 1075, 1962

17. Bennet, S. J., G. P. Anderson, and M. L. Williams: The Time Dependence of Surface Energy in Cohesive Fracture, UTEC-DO-69-072, College of Engineering, University of Utah, Salt Lake City, July 1969.

18. Williams, M. L.: The Kinetic Energy Contribution to Fracture Propogation in a Linearly Viscoelastic Material, UTEC-DO-67-038A, College of Engineering, University of Utah, Salt Lake City, August 1967.

19. Blatz, P. J.: An Elastodynamic Theory of Fracture, Polymer Science Report, North American Aviation Science Center, Thousand Oaks, California, April 1967.

20. Jones, W. B., F. R. Wagner, and M. L. Williams: "Cumulative Damage in the Mechanical Viscoelastic Fracture," JCRPG Mechanical Behavior Working Group, 6th Meeting, CPIA Pub. No. 158, Vol. I, October 1967.

21. Mossakovski, V. I. and M. J. Ryhka: "Generalization of the Griffith-Sneddon Criterion for the Case of a Nonhomogeneous Body," PMM, Vol. 28, 1964, pp 1061--1069.

22. Dannenberg, H.: "Measurement of Adhesion," Journal of Applied Polymer Science, Vol. 5, 1961, pp 125--134.

23. Malyshev, B. M. and R. L. Salganik: "The Strength of Adhesive Joints Using the Theory of Cracks," International Journal of Fracture Mechanics, Vol. 1, 1965, pp 114--128.

24. Williams, M. L.: The Fracture Threshold for an Adhesive Interlayer, UTEC-DO-69-061, College of Engineering, University of Utah, Salt Lake City, Utah, June 1969 (Revised November 1969).

25. Burton, J. D., W. B. Jones, and M. L. Williams: Theoretical and Experimental Treatment of Fracture in an Adhesive Interlayer, UTEC-DO-69-143, College of Engineering, University of Utah, Salt Lake City, Utah, February 1970.

26. Mueller, Hans-Karl: Stable Crack Propagation in a Viscoelastic Strip, NASA CR-1279, California Institute of Technology, Pasadena, California, March 1969.

27. Service Life Improvement Program, Task 2, Monthly Report, Thiokol Chemical Corp., Wasatch Div., Brigham City, Utah, October 1968.

28. Garrison, U. E.: Service Life Improvement Program, Task 5, Final Report, TWR-2984, Thiokol Chemical Corp., Wasatch Div., Brigham City, Utah, 20 August 1968.

29. Knauss, W. G. and H. K. Mueller: The Mechanical Characterization of Solithane 113 in the Swollen and Unswollen State, AFRPL-TR-68-125 (GALCIT SM 67-8), California Institute of Technology, Pasadena, California, December 1967.

30. Jones, W. B. and M. L. Williams: Some Recent Advances in Adhesive Fracture Analysis, UTEC-DO-69-088, College of Engineering, University of Utah, Salt Lake City, Utah, July 1969.

31. Williams, M. L.: "The Continuum Interpretation for Fracture and Adhesion," Journal of Applied Polymer Science, Vol. 13, 1969, pp 29—40.

32. Leeming, H.: Structural Test Vehicle Final Report, AFRPL-TR-70-10, Lockheed Propulsion Company, Redlands, Calif., 1970.

33. Burton, J. D.: "Solid Propellant Grain-to-Case Bond Stress Measurement," SESA Paper No. 1385, Experimental Mechanics, (To be published mid 1970).

UNCLASSIFIED
Security Classification

DOCUMENT CONTROL DATA - R & D

(Security classification of title, body of abstract and indexing annotation must be entered when the overall report is classified)

1. ORIGINATING ACTIVITY *(Corporate author)* North American Rockwell Corp., Rocketdyne, Solid Rocket Division P. O. Box 548, McGregor, Texas	2a. REPORT SECURITY CLASSIFICATION UNCLASSIFIED 2b. GROUP

3. REPORT TITLE
Application of Fracture Mechanics to Predicting Failures in Solid Propellants

4. DESCRIPTIVE NOTES *(Type of report and inclusive dates)*
Final Report

5. AUTHOR(S) *(First name, middle initial, last name)*
J. D. Burton
B. C. Harbert

6. REPORT DATE	7a. TOTAL NO. OF PAGES	7b. NO. OF REFS
May 1970	99 + x	33

8a. CONTRACT OR GRANT NO.	9a. ORIGINATOR'S REPORT NUMBER(S)
F04611-69-C-0035	R-4608
b. PROJECT NO.	
c.	9b. OTHER REPORT NO(S) *(Any other numbers that may be assigned this report)*
d.	

10. DISTRIBUTION STATEMENT
This document is subject to special export controls and each transmittal to foreign governments or foreign nationals may be made only with prior approval of AFRPL (RPORT/STINFO).

11. SUPPLEMENTARY NOTES	12. SPONSORING MILITARY ACTIVITY
	Air Force Rocket Propulsion Laboratory Edwards, California

13. ABSTRACT

Report documents a 14-month program conducted at Rocketdyne, Solid Rocket Division, to study the parameters of crack growth in viscoelastic materials. Tests conducted on Solithane and a filled propellant are described, and results of the experimental effort are presented. Analysis of data through the concepts of viscoelastic fracture mechanics is discussed. The behavior of cracks in solid rocket motor geometries and of propellant/liner unbonds was monitored in unique test situations. Basic analytic concepts were compared with test data and found to show promise of applicability. Recommendations for expansion of the study are presented.

DD FORM 1 NOV 65 1473

UNCLASSIFIED
Security Classification

14. KEY WORDS	LINK A		LINK B		LINK C	
	ROLE	WT	ROLE	WT	ROLE	WT
Fracture mechanics						
Flaw initiation						
Energy balance						
Solid Propellant						
Viscoelastic materials						
Adhesive failure						
Cohesive failure						
Radial Planar Loading device						
Blister Peel Test						